INFORMATION TO USERS

This reproduction was made from a copy of a document sent to us for microfilming. While the most advanced technology has been used to photograph and reproduce this document, the quality of the reproduction is heavily dependent upon the quality of the material submitted.

The following explanation of techniques is provided to help clarify markings or notations which may appear on this reproduction.

1. The sign or "target" for pages apparently lacking from the document photographed is "Missing Page(s)". If it was possible to obtain the missing page(s) or section, they are spliced into the film along with adjacent pages. This may have necessitated cutting through an image and duplicating adjacent pages to assure complete continuity.

2. When an image on the film is obliterated with a round black mark, it is an indication of either blurred copy because of movement during exposure, duplicate copy, or copyrighted materials that should not have been filmed. For blurred pages, a good image of the page can be found in the adjacent frame. If copyrighted materials were deleted, a target note will appear listing the pages in the adjacent frame.

3. When a map, drawing or chart, etc., is part of the material being photographed, a definite method of "sectioning" the material has been followed. It is customary to begin filming at the upper left hand corner of a large sheet and to continue from left to right in equal sections with small overlaps. If necessary, sectioning is continued again—beginning below the first row and continuing on until complete.

4. For illustrations that cannot be satisfactorily reproduced by xerographic means, photographic prints can be purchased at additional cost and inserted into your xerographic copy. These prints are available upon request from the Dissertations Customer Services Department.

5. Some pages in any document may have indistinct print. In all cases the best available copy has been filmed.

University Microfilms International
300 N. Zeeb Road
Ann Arbor, MI 48106

Das, Purna Chandra

ELECTROMAGNETIC PROPERTIES OF SMALL SOLID STATE PARTICLES AND REALISTIC SURFACES

City University of New York PH.D. 1983

ELECTROMAGNETIC PROPERTIES OF SMALL SOLID STATE PARTICLES AND REALISTIC SURFACES

by

PURNA CHANDRA DAS

A dissertation submitted to the Graduate Faculty
in Physics in partial fulfillment of the
requirements for the degree of
Doctor of Philosophy,
The City University of New York.

1982

This manuscript has been read and accepted for the Graduate Faculty in Physics in satisfaction of the dissertation requirement for the degree of Doctor of Philosophy.

9/29/82
date

Chairman of Examining Committee

9/29/82
date

Executive Officer

Supervisory Committee

The City University of New York

Abstract

ELECTROMAGNETIC PROPERTIES OF SMALL SOLID STATE PARTICLES AND REALISTIC SURFACES

by

PURNA CHANDRA DAS

Advisor: Professor Joel I. Gersten

We study the electromagnetic properties of small solid state particles. In particular the origin and consequences of spontaneous electric dipole moments in small particles of diameter ranging from 10-1000 Å are considered. Theoretical analysis of such particles with or without nearby molecules is done and their surface effects are extracted. Various mechanisms promoting the dipole moments are considered (dispersion dipole due to nearby molecules, binary composite structures, and asymmetric homogeneous structures). The study is basically divided into two parts - homogeneous systems and inhomogeneous systems. Under homogeneous systems we evaluate the dipole moment of a hemispherical jellium shape. Under inhomogeneous systems we evaluate the dipole moment of an atom near a spheroid and the dipole moment of a bimetallic spheroid.

Realistic surfaces have invariably some roughness present on them. Such rough surfaces have unusual optical properties. We model roughness as a spheroidal bump

protruding out of a flat plane surface and study the surface shape (electromagnetic) resonances of such a bumpy surface. The shape resonances are based on the fact that there are localized states associated with the (vibrating) bumps, which can couple to the delocalized collective (electronic or ionic) excitations of the underlying substrate. Our goal is to study, and determine the frequencies and widths of these surface shape resonances.

The study of a rough surface and its neighborhood in various experimental situations by electron loss spectroscopy is a rapidly growing field. An accurate interpretation of experimental data depends up on detailed theoretical analysis of the problem of electrons scattering from a rough surface. However, the problem is complicated as can be imagined. So we consider inelastic electron scattering from isolated metal spheres. This, in itself, is an important problem, because it facilitates the investigation of small particles and their surfaces. The electron energy loss to be considered arises from the excitation of plasmons associated with the sphere. Expressions for the scattering cross section and for the radiative scattering are derived.

Finally we use the fact, that there exists a set of shape resonances for a bumpy surface to investigate the effects of the presence of a substrate on a molecule undergoing photochemical reaction. Photochemistry involves a

certain accumulation of energy in the molecule before it undergoes photochemical reaction. The energy accumulation would be hindered if there were damping mechanisms such as are associated with the shape resonances. However, nothing could be predicted in the absence of a theoretical study of the situation. We therefore investigate the effects of the substrate on photochemical reaction taking into account the surface shape resonances. Expressions of the cross section for photochemistry and radiative cross section of the molecule are derived. We shall see if the enhancement of photochemical reactions occurs due to the enhanced local field near a rough surface.

DEDICATION

To
My Beloved Parents

ACKNOWLEDGEMENT

First and foremost, I extend my heartiest gratitude and thanks to my advisor Professor Joel I. Gersten for his guidance, encouragements, and for being a constant source of inspiration throughout the course of this work. I was initiated into the study of surface physics by him and have learnt a great deal from discussions with him and from his timely criticisms. I have a deep sense of admiration for his valuable advices, outstanding personality, and his keen interest in my work. The completion of this research has left me indebted to him.

I wish to acknowledge the advice of Professor V. Sahni as to the most desirable content of part of this thesis. The timely advices of various faculty members of the Physics Department of the City College of New York is gratefully appreciated. I also wish to acknowledge the considerable help given by the staff of the Physics Department and the Computer Center of the City College.

The final tribute must go to my friend Dr. Ashok Das whose continuing encouragement and understanding have been the most helpful solace at difficult times.

TABLE OF CONTENTS

APPENDICES

LIST OF TABLES

LIST OF FIGURES

Fig. II.4 Magnitude of the electric dipole moment as a function of the aspect ratio for a given value of a. The ground state is labeled (0) and the first excited state (1).

Fig. II.5 Magnitude of the electric dipole moment as a function of semimajor axis, a, for fixed aspect ratio. Data for the three most low-lying states are shown. They are labeled (0), (1), and (2). Here a/b=2.0. The resonance energies are 2.71, 3.39, and 3.62 eV, respectively. The dielectric constants are from ref. 11.

Fig. II.6 Ratio of decay rate to resonance frequency for three branches of decay: e stands for inelastic electron scattering, sp stands for surface plasmon decay, and rad stands for photon decay. The data is plotted as a function of aspect ratio

Fig. II.7 Same as Fig. II.6 but plotted as a function of semimajor axis size, a. Note that Γ_{rad}/ω_r^0 is magnified by a factor of 10. Here a/b=2.0 and the resonance frequency for the lowest state is 2.71 eV.

Fig. II.8 Radiative yield as a function of semimajor axis for the ground (0) and first excited states (1). Here a/b=2.0. The resonance energies are 2.71 eV ($\hbar\omega_r^0$) and 3.39 eV ($\hbar\omega_r^1$).

Fig. II.9 Radiative yield versus aspect ratio for fixed a.

Table 1

$a(a_0)$	ϵ (a.u)	$\mu_z(ea_0)$
1	-0.394	-0.0043
2	-0.312	-0.0015
4	-0.218	0.045
6	-0.168	0.125
8	-0.137	0.226
10	-0.116	0.341
12	-0.101	0.477
14	-0.0889	0.625
16	-0.0797	0.779
18	-0.0723	0.939
20	-0.0662	1.113

Table 2

a/b	ϵ_r^o	ϵ_r^1	ϵ_r^2
1.2	-4.29	-1.80	-1.36
1.5	-5.64	-2.85	-1.80
1.8	-6.64	-2.86	-1.92
2.0	-7.35	-2.97	-2.04
2.5	-9.25	-3.30	-2.33
3.0	-11.30	-3.72	-2.61
3.5	-13.60	-4.20	-2.89
4.0	-15.90	-4.75	-3.18

INTRODUCTION

Over the years people have primarily been interested in bulk properties of solids. One of the reasons for it is the simplified idealization that a solid has an infinite extent in all directions. The justification for this is however understandable. Out of the 10^{24} atoms in a macroscopic crystal of typically 10^{8} atoms on a side, only about one in 10^{8} reside near the surface. Although such an idealization is valid for understanding bulk properties of a macroscopic crystal, surface properties such as crystal growth, catalysis, corrosion, photoemission, transport along a surface, adsorption, desorption etc. have to be understood in the realm of surface physics. The conventional use of periodic boundary conditions, along with the idealized model of an infinitely extended solid with lattice constant translational invariance imparts Bloch character to the electrons in the solid. Independent electrons, each of which obeys a one electron Schrodinger equation with a periodic potential, which is an effective one-electron potential representing the interactions of the electrons with the massive atomic nuclei and the electron-electron interactions, are known as Bloch electrons. Lattice symmetry and its influence on the form of the eigenvalues and the eigenfunctions of the Schrodinger equation produce the division of the energy spectrum of one electron states into bands separated by forbidden gaps. The electrical as well as

most other transport properties are determined by the band structure of the crystalline solid, and to the extent to which these bands are filled. In bringing free atoms together to form a crystal, the discrete levels of these atoms split up into groups of levels which then form an energy band. The valence band is composed of low-energy bonding states and the conduction band is composed of high energy anti-bonding states. Alternatively, lattice symmetry produces breaks in the continuous energy spectrum of free electrons at certain energies, where those electrons undergo Bragg reflections from the lattice, on their passage through the crystal.

In a perfectly periodic crystal corresponding to a set of rigid ions, a free carrier will propagate without scattering. The electronic wave function is a Bloch wave of the form $\psi_{n\vec{k}}(\vec{r}) = u_{n\vec{k}}(\vec{r}) \exp(i\vec{k}\cdot\vec{r})$, which for a given $\vec{k}$-direction has a quadratic energy dispersion, $E(k) = \frac{\hbar^2}{2}\vec{k}\cdot\frac{1}{\overleftrightarrow{m}^*}\cdot\vec{k}$, valid near a band minimum. The electron behaves as if it were free, except that its wave function is modulated by a spatial factor $u_{n\vec{k}}(\vec{r})$ that has the periodicity of the lattice and is charaterised by an effective mass $\overleftrightarrow{m}^*$, which can be quite anisotropic.

In real crystals, however, electrons travel freely only very short distances. This is because the perfect periodicity of the lattice is broken up by imperfections. Besides impurities and phonons, causing electrons to scatter

from one k-vector to another, the presence of crystal surfaces forms two dimensional imperfections.

The complexities of surface physics lies in the fact that the surface region is one of extreme spatial inhomogeneity. The presence of the surface breaks the symmetry perpendicular to it, while the symmetry parallel to it is preserved. This leads to the conversion of Bloch waves into non-current carrying (in a direction perpendicular to the surface), standing waves near the surface. On the other hand the charge distribution in surface cells of a finite crystal differs from the charge distribution of cells in the interior. This is partly due to the breaking of the periodicity of the bulk lattice and partly due to relaxation and reconstruction of the lattice near the surface. Due to the consequent loss of symmetry in charge distribution, surface cells have a nonvanishing electric dipole moment. Sometimes such asymmetric charge distributions lead to a surface dipole layer. Moreover the surface charge distribution depends on the morphology of the surface (whether plane or rough). The determination of such a charge distribution and its consequences is a very difficult problem in surface physics.

As in the case of impurities, the imperfection introduced by the presence of the surface requires the occurrence of localized states near it. Such excitations are localized to a narrow region in the direction normal to the surface, but extend parallel to the surface. This is

because, in addition to the Bloch solutions to the one-electron Schrodinger equation for the periodically extended crystal, there are solutions with complex wave vectors describing electronic levels that are localized in the neighborhood of a real crystal. To describe the spatial and energy distribution of such states, we use the concept of a Local Density of States (LDS) ρ_i [1], given by

$$\rho_i(\epsilon, n) = \sum_a |\langle \varphi_{in} | \psi_a \rangle|^2 \, \delta(\epsilon - \epsilon_a) . \qquad (1)$$

Here ψ_a is an eigenfunction with eigenvalue ϵ_a and φ_{in} is a localized (atom-like) basis function of symmetry type i and centered on the nth lattice site.

Besides these geometrical and analytical complexities, which had slowed the progress in surface studies, the difficulties in carrying out experiments for real as well as model surfaces were sufficient enough to persuade researchers to confine themselves to the study of bulk properties of solids. It should be noted that as a first step in understanding the physics of phenomena occuring near a surface, we must characterize the static surface. This means that we have to know the morphology of the surface, the chemical identity of atoms or molecules present at the surface, the geometrical arrangement of these species and their electronic distribution. Only then one can proceed to devise techniques to probe the dynamical

interaction of the surface with its environment, such as atoms, molecules, ions, photons, electrons or other surfaces. Surface studies are so complex that often the surface responses observed in an experiment can not be interpreted simply. There comes the need for a closer relationship between theoretical as well as experimental studies in surface physics. Hence the surge in the study of surfaces during the last decade has been mainly due to the following three reasons:

(i) surface phenomena are responsible for the existence and control the performance of the many technologies, such as energy and communication;

(ii) there is now available a great many number of high resolution, surface sensitive spectroscopic techniques capable of providing analytical and structural data on surfaces; and

(iii) theoreticians in recent years have worked closely with experimentalists to provide reasonable interpretation of data and this has pushed forward the research on material surfaces a great deal.

Some recent advances made in the application of Raman spectroscopy to the molecular characterization of surfaces, have enhanced the need for studying morphology dependent (local as well as nonlocal) surface properties. There had been a consistent effort to overcome the limitations of the conventional Ultra High Vacuum (UHV) spectroscopies [2].

The most widely used UHV spectroscopies are Electron Loss Spectroscopy, Auger Electron Spectroscopy (AES), Ultraviolet and X-ray photoelectron spectroscopy (UPS and XPS), and Secondary Ion Mass Spectroscopy (SIMS). Their disadvantage, however, lies in molecular surface characterization (detection, identification and a quantitative analysis of individual molecules adsorbed on a surface). UHV techniques are also not universal in the sense that they can't be applied to solid-liquid interfaces. Surface electronic X-ray absorption spectroscopy (SEXAFS) [3] and surface vibrational spectroscopy remedied these limitations encountered in UHV techniques. The former, however, lacks molecular specificity and is less surface sensitive due to large penetration depths (10^2 - 10^4 Å depending on photon energy) of optical photons. On the other hand surface vibrational spectroscopy [4] scores high marks in the area of molecular surface characterization. Among other techniques, Surface Raman Spectroscopy (SRS) [5] is universal in being applicable to most surface environments, although the normal Raman scattering process lacks sensitivity. SRS has obtained new life during the last decade and assumed the name Surface Enhanced Raman Scattering (SERS) [4,6], after the discovery that when a molecule is appropriately adsorbed on a metal surface, its Raman scattering efficiency can be increased by factors of 10^3 to 10^6 [7].

The phenomenon of SERS alone has created a new group of surface physicists who are dedicated to understanding the microscopic mechanisms involved in it. It clearly is a classic example of how certain vital experimental results open up a completely new area of physics. Physically interesting and technologically important, the potential of SERS in becoming the surface spectroscopic technique of the future is so great that scientists all over the world are currently analysing the phenomena from various angles. As it often happens, the investigation of one anomalous phenomenon, namely SERS, has given birth to several other anomalous observations, both experimentally and theoretically. In addition, a few other anomalous solid state phenomena that existed prior to the discovery of SERS, have received renewed attention in terms of research in recent years, because of their apparent relation to SERS. It is hoped that an understanding of each of these anomalies will be a step forward toward a fuller understanding of SERS. Therefore it is worthwhile to give a brief account of each of these anomalies here, in an attempt to make possible conclusions from their similarities as well as differences. It would also help us motivate the research undertaken here.

The so called surface anomalies are discussed under the following headings:

1. Surface Enhanced Raman Scattering
2. Nonlinear Optical Phenomena

3. Enhanced Fluorescence of Molecules

4. Enhanced Photoemission and Infrared Absorption Anomalies

5. Photochemistry

Surface Enhanced Raman Scattering

SERS, as has been pointed out earlier, is an unusual phenomenon in which the Raman intensity of molecules adsorbed on or near a metal (Ag, Au, and Cu) surface is enhanced by about six orders of magnitude. One might wonder, why the phenomenon be called anomalous, where a resonant Raman scattering mechanism might be operative. It should be noted that for Pyridine/Ag system, in which the original observation of SERS [8] was possible, it occurs at 514 nm whereas pyridine absorbs at 280 nm. Hence is the anomaly. The effect has various aspects to it so that a serious theoretical effort to explain the phenomena, might need an understanding of these aspects. The conclusive experiments of Van Duyne et al [4,7] were performed for Ag/pyridine system in an electrochemical environment. Since then SERS has been observed for polycrystalline Ag wire or foil [9]. Polycrystalline Ag thin film electrode, obtained by vacuum deposition on a glass substrate, has also been reported [10] to give rise to SERS. Pettinger [11] has reported observation of SERS on Ag(100) and Ag(111) single crystal surfaces. Results for SERS in the case of Ag(111) single crystal, epitaxial thin films [11] are also in existence in literature. Thin film results are less by a factor of two

than those for polycrystalline wire, suggesting the association of SERS with perhaps surface roughness. Also increase in SERS intensity is related to some combination of cleaning and roughening.

It has been shown that SERS can be observed under non-electrochemical conditions including surfaces under vacuum conditions [12], those exposed to air [13], and in tunnelling junctions [14].

SERS has been found to have a linear response in the sense that the relative intensity of Raman scattered light grows linearly with respect to laser power. It should be pointed out that in the green SERS has been substantial for Ag, less substantial for Cu and Au. Towards the red, Cu and Au give strong SERS signals. Trials with other materials have not produced encouraging results, although some reports do exist.

In the light of these observations several theories have been proposed to explain the effect, both from a macroscopic as well as from a microscopic point of view.

The image dipole mechanism [15] assumes that the polarizability of the adsorbed molecule is modulated due to the presence of the metal surface. The molecule considered as a point dipole sees itself in a field environment which consists of a superposition of two fields: the field due to the image dipole in the metal, and that due to the incident laser light. The effective dipole moment of the adsorbate is

then enhanced at very small molecule-surface separation. The Raman enhancement factor $\sim(\alpha_{eff}/\alpha)^4$, where α is the polarizability of the free molecule and α_{eff} is the effective polarizability of the molecule in the presence of the surface. This model, being dependent on a critical adsorbate surface separation at which the assumption of point dipole would break down, has been criticized, among others, by Oxtoby and Hilton [16]. Furthermore the observation of SERS from multilayer adsorbates on metal surface [17] adds a long range component to it, which can hardly be explained by the image enhancement mechanism. However, it is believed to contribute at small surface-adsorbate separation.

A modulated reflectance theory [18] has been reported along with the charge transfer theory due to McCall and Platzman [19]. These models may explain some of the short range (chemical) aspects of SERS but the models have not yet been adequately tested. They do not account for the long range characteristics of SERS nor the role of surface roughness.

Resonant Raman scattering from the molecule in the presence of coupling between the molecule and the metal via surface plasmons is another mechanism [20], that was investigated by Philpott. Philpott has quantum mechanically shown that there is significant shortening of life time of an electronically excited molecule, when it is coupled to

delocalized surface plasma oscillations of the substrate. The coulomb interaction between the molecule and the metal substrate shifts and broadens the energy levels of individual electronic states, and the molecule which is able to undergo normal Raman scattering in the absence of the metal can now give rise to resonant Raman scattering [20]. However, the predictions of this model have not been in accord with experimental observations.

Some models [21], which are microscopic in nature and which have stood up to the experimental tests of certain aspects of SERS, have been based on the suggestion of Moskovits [22]. It involves the absorption of radiation by the collective modes of the ensemble of microscopic bumps on a metal surface, which is coupled to the vibrational modes of the molecule. This model implicitly requires the presence of surface roughness. Although the requirement of surface roughness for observing enhanced Raman scattering is not yet fully agreed upon, it is worthwhile to point out that experiments where surfaces were deliberately prepared smooth, did not show appreciable enhancement [23]. So it should be kept in mind for the present that surface roughness adds significantly to the enhancement.

More recently Gersten and Nitzan have proposed an electromagnetic theory of SERS [24] in the presence of a rough surface. The rough surface has been modelled as a set of hemispheroidal protrusions sticking out of a base plane.

The idea is that there is an increase in the local elctric field at the surface due to resonant absorption of radiation by the collective modes of the bumps. This in turn gives rise to enhanced Raman scattering. In addition the effect of the interaction between the molecule and a small spheroidal particle or roughness feature on the Raman scattering was treated. One of the important conclusions of their study is that the discrete plasmon frequencies of the bump is a very sensitive function of the aspect ratio of the spheroid, which models it. A laser would then select spheroids of a given aspect ratio to be in resonance with. Near such a resonance the dipole moment of the system is strongly enhanced, giving rise to enhanced Raman scattering. Another interesting conclusion is that enhanced Raman scattering is related to the proximity of the molecule to a small metal particle. There have been some experimental support for the theory, coming from the observation of low frequency ($\sim$ 10 cm^{-1}) Raman side bands by Weitz et al [25] and from the SERS experiment by Liao and coworkers [26] on microlithographic Ag-particle surfaces.

Non-linear Optical Phenomena:

Since the discovery of the laser in 1960, it has been put to much use to probe the properties of matter, both because of its high intensity and near perfect monochromaticity.The demonstration of second harmonic generation in 1961 by Peter Franken opened up a whole

new field of non-linear optics. Bloembergen and his coworkers have developed a general formalism to describe a large number of non-linear optical phenomena, applicable almost universally. The starting point is the expansion of the electric polarization $\vec{P}$ in a power series in $\vec{E}$, the electric field amplitude.

$$\vec{P} = \overleftrightarrow{\chi}^{(1)} \cdot \vec{E} + \overleftrightarrow{\chi}^{(2)} : \vec{E}\,\vec{E} + \overleftrightarrow{\chi}^{(3)} \vdots \vec{E}\,\vec{E}\,\vec{E} + \ldots\ldots\ldots \qquad (2)$$

$\overleftrightarrow{\chi}^{(1)}$ is the linear susceptibility tensor and $\overleftrightarrow{\chi}^{(2)}$ is the lowest order non-linear susceptibility tensor of rank three. An inspection of Eq.(2) suggests that at weak electric field strength non-linear terms would be negligible. On the other hand, high intensity light would make the non-linear terms significant. Since the study of optical properties of rough surfaces has become all the more important with the advent of SERS, one would like to make some general predictions about the behavior of rough surfaces. Such studies, although directly unrelated to but arising out of the attempts to explain SERS, may provide us with such tools that are required in surface characterization and surface specificity determination. As we shall see surface enhanced non-linear optical properties may already have provided us with such a tool. It can be seen that the various interpretations of SERS can be divided into two groups : Namely, the Chemical and Electromagnetic

effects. It is the latter which has been successful in predicting the experimentally observed enhancement of 10^4-10^6 [27]. It is based on a local field enhancement picture. The electric field induced by a metal particle at the position of the adsorbed molecule in a SERS geometry was shown [28] to be 10^2-10^3 times stronger than the incident field. This therefore implies that non-linear optical processes and molecular ionization may occur at weak incident field intensities. This prediction indeed has been confirmed recently by Chen et al [29]. They have been able to demonstrate second harmonic generation (2ω at 0.53 μm), enhanced by a factor of 10^4 by surface roughness, at a silver-air interface. This roughened silver surface was also shown to produce surface Raman enhancement of $\sim 10^6$ for .05 M pyridine. The second harmonic and background signals were shown to be substantially dependent on surface roughness. Clearly it has been demonstrated, beyond doubt, that a local field on rough surface structure can lead to a large enhancement in the strength of a non-linear optical process.

As indicated earlier, surface enhanced non-linear optical process has been used to detect adsorbed molecular monolayers on a silver surface by Chen et al [30]. Adsorption of AgCl and pyridine on silver were observed. Adsorption of pyridine molecules were found to be neccessary for a second harmonic signal from pyridine.

More recently Heinz et al [31] have used resonant second harmonic generation to measure spectra of transitions in molecules of Rhodamine 6G and 110 dye samples adsorbed at a surface at submonolayer coverage. The method has the potential for identifying the nature and quantity of adsorbates. Some amount of information regarding the structural properties of adsorbates and surfaces may be obtained from the polarization dependence of the signal.

Hence non-linear phenomena at a rough surface are observable and an understanding of the mechanism giving rise to such phenomena may prove to be of enormous importance to surface science. Some amount of work has been done [32,33] in this direction. However, a more detailed theoretical analysis of the above experiments is needed. Before one makes an attempt in this direction it is probably essential to understand the properties of rough surfaces and related phenomena.

Enhanced Fluorescence of Molecules :

Spectroscopic properties, such as fluorescence and Raman scattering, of isolated molecules are well understood. However, the inelastic scattering properties of molecules situated near a metal surface are of current interest. Emission of radiation from molecules close to a planar surface is basically understood[34]. It is now well known that surface roughness influences optical properties of metal surfaces [35], and hence those of molecules situated

near it. Such effects have become apparent with our knowledge of SERS and its relation to surface roughness.

There are many ways of surface roughening. Surface anodization [7] sometimes causes the formation of spheres on the surface and these act as roughness. Even single silver atoms lying on top of a flat silver surface may perform the same role [36]. Inherent roughness through the formation of metal-island films by vapor deposition [37] seem to be sufficient for the appearance of SERS. Both island films and colloidal particles should be considered as rough systems, due to the small size of these systems.

Owen et al [38] have observed enhancements of fluorescence induced by microstructure resonances, such as the resonance between the natural modes of a dielectric fiber and molecular vibrational modes. Here the cylindrical fiber acts as roughness. Although the microstructure shapes and separations are uncontrollable, theoretical models [39] based on electromagnetics predict that the intensity of the incident field (wavelength λ_i) at or near the surface is greatly enhanced when λ_i is resonant with the surface plasmon modes of the metallic microstructure. Such enhancements also occur in the inelastic emission from molecules on or near a surface, when the emission wavelength, λ_f , is in resonance with the surface plasmon modes. Thus the metallic microstructures act as efficient receiving and transmitting antennas for wavelengths in

resonance with the plasmon modes.

Weitz et al [40] have observed such interaction between the molecule and Ag-islands giving rise to a dramatic shortening of the fluorescent lifetime of the molecule and on enhancement of fluorescence. Despite the fact that the life time is shortened, the amount of light emitted remains virtually unchanged. Thus instead of quenching the excited molecule, the island assists in the radiation process. The fluorescence decay rate is seen to increase by three orders of magnitude. This is believed to be due to the electromagnetic interaction between the molecule and the localized electronic plasma resonances. It should be pointed out that fluorescent decay rates of molecules can be a probe of the interaction of a molecule with its environment.

These experiments indicate a definite correlation between the existence of SERS and/or enhanced fluorescence emission and the presence of metallic microstructures. It is therefore hoped that an understanding of the fluorescence phenomenon may aid our attempts to analyse the phenomenon of SERS theoretically and to investigate the shape and size effects for such phenomena.

In passing, it is worthwhile to recognize that other unusual optical properties of adsorbed molecules [41] have been observed.

Enhanced Photoemission and Infrared Absorption Anomalies:

By now we are familiar with the relation between small particles and rough surfaces. An understanding of properties of small particles may ultimately facilitate our knowledge about rough surfaces. the correspondence between sizes and shapes of small particles and roughness features implies that properties of such small particles would be dependent on their shapes and sizes.

Indeed Schmidt-Ott et al [42] have observed increased photoyields from small particles (diameter $\lesssim 50$ Å). The results are for Ag and WO_3 particles and the enhancement in photoyield is by about two orders of magnitude. Although Fowler-Nordheim law, $Y(h\nu)=C(h\nu - \phi)$, is obeyed near the threshold, it still is not sufficient to explain the anomaly. In the above expression for photoyield $Y(h\nu)$, at energy $h\nu$, C is the Photoemission constant and ϕ is the work function. Typically $C \approx 7.5\times10^{-5}$ for a plane surface. This constant drastically increases with decreasing radius of particles and becomes typically between 10^{-2} to 10^{-3} for particle diameter around 30 Å. It is conjectured that the understanding of this enormous photoyield may enable us to ultimately understand SERS.

Recently Penn and Rendell [43] have reported calculations of the photoabsorption and photoyield of small particles (metal spheres) for photon energies below the

plasmon energy. The calculation is based on nonlocal dielectric function and inclusion of electron-hole (e-h) pair excitations in the small particles. The excitation of e-h pairs is shown to have a far greater effect on the yield of a sphere than on the yield of a plane surface. This is directly related to the existence of a resonance behavior [44] in the sphere absorption for $\omega > \omega_p$ due to the existence of plasmons. Below ω_p, however, e-h pair excitations involve a range of wave vectors, some of which will satisfy the conditions of resonance.

Although the results of Penn and Rendell are in fair agreement with the experimental values, the approximations incorporated in the calculation require a more detailed and microscopic look at the whole subject. Dasgupta and Fuchs[45] have derived expressions for a small spherical particle including nonlocal nature of the dielectric response. It is hoped that these results can be applied to photoabsorption and photoyield anomalies, as well as to infrared anomalies [46]. Some modifications of theories of SERS may be incorporated by considering the adsorbed molecule as a small dielectric sphere, rather than a point dipole.

Far infrared absorption anomalies for small particles are also in existence in literature. Tanner et al [47] have observed that samples of Cu, Al, Sn, and Pb having diameters ranged from 65 to 350 Å showed absorption which

was very small at low frequencies and which increased more or less linearly as the frequency increased. These observations have not yet been fully understood. An explanation based on classical dielectric theory, coupled with the quantum mechanical ensemble theory of Gorkov and Eliashberg [48] failed to account for the experimental data. The far infrared absorption spectrum for these above samples of small particles depends mostly upon their sizes and very little on the elements of which they are composed. For smaller size particles Gorkov and Eliashberg's theory predicts quite well the observed data. But it fails for larger size particles (energy level spacing $\Delta \sim \frac{1}{\Omega}$, Ω being the volume of the particle). Since all these optical properties of small particles are related to a special process of absorption and since these systems are very important industrially, a fresh look at the anomalous behavior presented in this section is in order. It should be noted that enhancement of infrared absorption from molecular monolayers with thin metal overlayers has been obseved by Hartstein et al [49]. The enhancement is by a factor of 20 and is consistent with an electric field enhancemnet due to collective electron resonances associated with the island nature of thin metal films.

Photochemistry:

It is expected that since the local electric field is enhanced near a surface, there would be an enhancement in

the rate of a photochemical reaction occuring close to a surface. A substantial enhancement is expected if the surface is rough. It was shown by Gersten and Nitzan [50] that spectroscopic properties of molecules near small scale structures are modified significantly. On the same footing Nitzan and Brus [51] have shown that photochemical reactions occuring near a small sphere would be enhanced.

SERS is a nonresonant scattering as far as the molecule is concerned, but photochemistry involves resonant absorption and energy flow within the molecule. Photochemistry often requires a finite accumulation of energy in the molecule or in a colliding molecular system before the desired process can take place. Hence unfavorable damping processes for molecules very near a surface may hamper the chemical process. At the same time since the incident field has to be in resonance with molecular excitations and surface resonances, sometimes broader resonances are helpful and this may be obtained by a suitable choice of the substrate.

The substrate effect on photochemistry has not really been investigated so far and it would be worthwhile looking into those effects.

We have outlined briefly the various theoretical and experimental studies aimed at understanding the anomalous, but interesting, properties of small particles and rough

surfaces. Each of these anomalies discussed above is special in its own right and is important academically and industrially. It is also clear from the discussion that the local environments of small particles and rough surfaces are not much different. Properties of small particles and rough surfaces are quite similar except for substrate effects that arise in case of rough surfaces. Our study is confined to these systems, namely small particles and rough surfaces.

We have seen above that small scale structures play an important role in surface spectroscopic experiments. They give rise to enhanced Raman intensity in case of SERS and their presence changes substantially the optical properties of molecules, including radiative and non-radiative decay rates and quantum yields. Small metallic particles were also pointed out to possess anomalous optical properties in the far infra-red region.

In this context, leaving aside the phenomena where rough surfaces are involved, we consider isolated small particles, and we are concerned here with the understanding of various mechanisms that give rise to spontaneous dipole moments in such particles.

Since the phenomenon of SERS occurs when a molecule is sitting in front of a bump, in the presence of an external photon field, it is worthwhile to determine the dipole moments of such systems as an atom near a spheroid. It is also helpful in determining the infra-red activity of a solid with an adsorbate on it.

In the case of an atom near a smooth saurface the dipole falls off asymptotically as D^{-4}, D being the atom-surface distance. Here we shall attempt to generalize this to the determination of the dipole moment of an atom near a small spheroidal particle and compare it with the atom near a flat surface result. The case of bimetallic spheroidal particle will also be studied. All these above subjects form the content of Chapter I.

Enhanced local optical fields are believed to be responsible for a large part of the SERS. Importance of the enhancement of the local optical fields is also sensed in the observation of fluorescence anomalies and even in non-linear phenomena at weak field strengths. We would argue in Chapter II that the discrete resonant states of a bump, giving rise to surface shape resonances, by their coupling to continuum states on the substrate surface, give rise to strong local fields and our goal will be to study the widths of such resonances.

An interesting problem of the scattering of fast moving electrons and ions from small dielectric spheres is treated in Chapter III. Here we are interested in studying the interaction of an electron with a metallic surface, which can be considered rough. Considering a bumpy surface one could explore the probability of excitation of surface plasmons by incident (high energy) electrons. This can be attributed as the source of energy loss of outgoing

electrons. Because of the complicated nature of the problem, we actually consider scattering from a sphere. It should be noted that only high energy electrons are considered, so that their trajectories can be approximated by straight paths, uninfluenced by the surface potential.

Finally our study concerning the effects of the presence of a rough surface on a molecule undergoing photochemical reaction is presented in Chapter IV. Based on the fact that local electric fields near a bumpy surface or a small particle are enhanced, one expects enhancement of a photochemical reaction. A study of this process for a molecule near a spherical particle has recently been reported (51), and enhancements predicted. However, the presence of a substrate can introduce qualitative changes in the behavior of the reaction rate and therefore the problem needs additional study.

Chapter V gives a summary and concluding remarks of the results obtained.

References

1. J. R. Schrieffer and Paul Soven, Physics Today, p-24 (April 1975)
2. D. E. Eastman and M. I. Nathan, Physics Today, p-44 (April 1975) and references therein.
   R. L. Park, ibid, p-52 and references therein.
3. R. H. Muller, in "Advances in Electrochemistry and Electrochemical Engineering" (R. H. Muller, ed), Vol. 9, p-1, Wiley-Interscience, New York, 1973.
4. R. P. Van Duyne, in "Chemical and Biochemical Applications of Lasers", Vol.4, Ch.5, C. B. Moore, ed and references therein.
5. M. Fleischman, P. J. Hendra, and A. J. McQillan, Chem. Phys. Lett. 26 , 163 (1974)
   Y. J. Chen, W. P. Chen, and E. Burstein, Phys. Rev. Lett. 36 , 1207 (1976)
   E. Burstein, C. Y. Chen, and S. Lundquist in "Light Scattering in Solids", ed. by J. L. Birman, H. Z. Cummins and K. K. Rebane (Plenum, New York, 1979)
6. "Surface Enhanced Raman Scattering", ed. by R. K. Chang and T. E. Furtak (Plenum, New York, 1981)
   For an excellent review of the field see R. P. VanDuyne in ref. 4.
7. See M. Fleischman et al in ref. 5
   A. J. McQuillan, P. J. Hendra, and M. Fleischman, J. Electroanal. Chem. 65 , 933 (1975)

R. C. Paul, A. J. McQuillan, P. J. Hendra, and M.Fleischman, J. Electroanal. Chem. 66 , 248 (1975)

D. L. Jeanmaire and R. P. VanDuyne, J. Electroanal. Chem. 84 , 1 (1977)

M. G. Albrecht and J. A. Creighton, J. Am. Chem. Soc. 99, 5215 (1977)

8. M. Fleischman et al in ref. 5.

9. See M. G. Albrecht et al and D. L. Jeanmaire et al in ref. 7.

R. P. VanDuyne, J. Phys. (Paris) 38 , C5-239 (1977)

G. Hagen, B. Simic-Glavaski, and E. Yeager, J. Electroanal. Chem. 88 , 269 (1978)

J. Creighton, M. Albretch, R. Hester, and J. Matthew, Chem. Phys. Lett. 55 , 55 (1978)

10. See ref. 4 (p-42).

11. B. Pettinger and U. Wenning, Chem. Phys. Lett. 56 , 253 (1978) and in the Proceedings of the Conference on Vibrations in the Adsorbed Layer, Julich, Germany, 1978

12. T. H. Wood and M. V. Klein, J. Vac. Sci. Tech. 16 , 459 (1979)

13. A. Otto, Surf. Sci. 75 , L392 (1978)

14. J. C. Tsang and J. Kirtley, Solid State Commun. 30 , 617 (1979)

15. F. W. King, R. P. VanDuyne, and G. C. Schatz, J. Chem. Phys. 69 , 4472 (1978)

S. Efrima and H. Metiu, Chem. Phys. Lett. 60, 59 (1978); J. Chem. Phys. 70 , 1602, 1939, and 2297 (1979); Surf. Sci. 92 , 433 (1980)

G. L. Eesley and J. R. Smith, Solid State Commun. 31 , 815 (1979)

N. D. Lang and A. R. Williams,Phys. Rev. B18 , 616 (1978)

W. C. Meixner and P. R. Antoniewicz, Phys. Rev. B13 , 3276 (1976) and references therein.

16. P. R. Hilton and D. W. Oxtoby, J. Chem. Phys. 72 , 6346 (1980)

17. C. A. Murray, D. L. Allara, and M. Rhinwin, Phys. Rev. Lett. 46 , 57 (1981)

18. A. Otto in Proc. Intern. Conf. on Vibrations in Adsorbed Layers, Julich, 1978

19. S. L. McCall and P. M. Platzman, Bull. Am. Phys. Soc. 24 , 340 (1979)

E. Burstein, Y. J. Chen, S. Lundquist, and E. Tossatti, Solid State Commun. 29 , 576 (1979)

J. I. Gersten, R. L. Birke, and J. R. Lombardi, Phys. Rev. Lett. 43 , 147 (1979)

20. M. R. Philpott, J. Chem. Phys. 62 , 1812 (1975)

S. Efrima and H. Metiu in ref. 15.

F. W. King and G. C. Schatz, Chem. Phys. Lett. 38 , 245 (1979)

21. M. R. Philpott in ref. 20

S. S. Jha,J. R. Kirtley, and J. C. Tsang, Phys. Rev. B22, 3973 (1980)

W. H. Weber and G. W. Ford, Phys. Rev. Lett. 44 , 1774 (1980)

M. Kerker, D. S. Wang, and H. Chew, Appl. Opt. 19 , 2256 (1980)

T. K. Lee and J. L. Birman, Phys. Rev. B22 , 5953, 5961 (1980)

See S. Efrima et al in ref. 5

22. M. Moskovits, J. Chem. Phys. 69 , 4159 (1978)
23. J. E. Rowe, C. V. Shank, D. A. Zwemer, and C. A. Murray, Phys. Rev. Lett. 44 , 1770 (1980)

J. F. Evans, M. G. Albrecht, D. E. Ullevig, and R. M. Hexter, J. Electroanal. Chem. 106 , 209 (1980)

24. J. I. Gersten and A. Nitzan, J. Chem. Phys. 73 , 3023 (1980)
25. D. A. Weitz, T. J. Gramila, A. Z. Genack, and J. I. Gersten, Phys. Rev. Lett. 45 , 355 (1980)

J. I. Gersten, D. A. Weitz, T. J. Gramila, and A. Z. Genack, Phys. Rev B22 , 4562 (1980)

26. P. F. Liao, J. G. Bergman, D. S. Chemla, A. Wokaun, J. Mellingailis, A. M. Hawryluk, and N. P. Economou, Chem. Phys. Lett. 82 , 355 (1981)
27. See ref. 17 and references therein.
28. See ref. 24 and references therein
29. C. K. Chen, A. R. B. deCastro, and Y. R. Shen, Phys. Rev. Lett. 46 , 145 (1981)

30. C. K. Chen, T. F. Heinz, D. Ricard, and Y. R. Shen, Phys. Rev. Lett. 46 , 1010 (1981)

31. T. F. Heinz, C. K. Chen, D. Ricard, and Y. R. Shen, Phys. Rev. Lett. 48 , 478 (1982)

32. See ref. 30
A. Wokaun, T. G. Bergman, J. P. Heritage, A. M. Glass, P. F. Liao, and D. H. Olson, Phys. Rev. B24, 849 (1981)

33. G. S. Agarwal and S. S. Jha, Solid State Commun. 1981

34. R. R. Chance, A. Prock, and R. Silbey, Adv. Chem. Phys. 37 , 1 (1978)

35. J. Brambring and H. Raether, Phys. Rev. Lett. 15 , 882 (1965)
H. Morawitz and M. R. Philpott, Phys. Rev. B10 , 4863 (1974)
J. Bohersheim and A. Otto, Surf. Sci. 45 , 441 (1974)
J. I. Gersten and A. Nitzan, J. Chem. Phys. 75 , 1139 (1981)

36. J. Bilman, G. Kovacs, and A. Otto, Surf. Sci.

37. T. H. Wood and M. V. Klein, J. Vac. Sci. Tech. 16 , 459 (1979)

38. J. F. Owen, P. W. Barber, P. B. Dorain, and R. K. Chang, Phys. Rev. Lett. 47 , 1075 (1981)

39. C. Y. Chen and E. Burstein, Phys. Rev. Lett. 45 , 1287 (1980)
S. L. McCall, P. M. Platzman, and P. A. Wolff, Phys. Lett. 6 , 33 (1981)
W. H. Weber and G. W. Ford, Phys. Rev. Lett. 44 , 1774 (1980)

M. Kerker, D. S. Wang, and H. Chew, Appl. Opt. 19 , 4159 (1980)

J. Gersten and A. Nitzan, J. Chem. Phys. 73 , 3023 (1980)

40. D. A. Weitz, S. Garoff, C. D. Hanson, T. J. Gramila, and J. I. Gersten, J. Luminescence. 24/25 , 83 (1981)

41. A. M. Glass, P. F. Liao, J. G. Bergman, and D. H. Olson, Opt. Lett. 5 , 368 (1980)

S. Garoff, D. A, Weitz, T. J. Gramila, and C. D. Hanson, Opt. Lett. 6 , 245 (1981)

42. A. Schmidt-Ott, P. Schurtenberger, and H. C. Siegmann, Phys. Rev. Lett. 45 , 1284 (1980)

43. D. R. Penn and R. W. Rendell, Phys. Rev. Lett. 47 , 1067 (1981)

44. R. Ruppin, Phys. Rev. 11 , 2871 (1975)

45. B. B. Dasgupta and R. Fuchs, Phys. Rev. B24 , 554 (1981)

46. A. J. Glick and E. D. Yorke, Phys. Rev. B18 , 2490 (1978)

47. D. B. Tanner, A. J. Sievers, and R. A. Buhrman, Phys. Rev. B11 , 1330 (1975)

48. L. P. Gorkov and G. M. Eliashberg, Zh. Exsp. Theor. Fiz. 48 , 1407 (1965) (Sov. Phys.-JETP 21 , 940 (1965))

49. A. Hartstein, J. R. Kirtley, and J. C. Tsang, Phys. Rev. Lett. 45 , 201 (1980)

50. See J. I. Gersten et al in ref. 35

51. A. Nitzan and L. E. Brus, J. Chem. Phys. 75 , 2205 (1981)

CHAPTER I

SPONTANEOUS ELECTRIC DIPOLE MOMENTS FOR SMALL PARTICLES

I.1 Introduction

Recently chemists and physicists have been showing an interest in the properties of small particles of solid matter and in their interaction with molecular adsorbates. Aside from such obvious problems as heterogeneous catalysis, in which the solid particles play a fundamental role, small particles and rough surfaces have been shown to possess very interesting and anomalous optical properties [1]. Some examples of these interesting optical properties have been given in the introduction to this thesis. To mention briefly, surface enhanced Raman scattering [2] is one such anomalous optical property. Although a precise concensus as to the origin of this effect does not yet exist, the phenomenon is believed to be closely related to the existence of bumps on a rough surface [3]. Similar enhancement factors have been observed for molecules adsorbed on sol particles and for molecules on metal island films. The typical scale size of the bumps on particles involved in these experiments is in the range 10 to 1000 $\mathring{A}$.

The radiative and nonradiative decay rates of molecules near particles or rough surfaces are found to be strongly

modified from what they would be near smooth surfaces [4] or in gas phase or in solution [5].

The correspondence between small particles and rough surfaces, makes the study of them even more important because of the association of surface roughness with SERS.

The anomalous optical properties studied to date have been in the visible part of the electromagnetic spectrum. It would be of considerable interest to know if electromagnetic anomalies exist in other parts of the spectrum. One would like to know what happens in the far infrared region of the spectrum, a region with a paucity of data and techniques. In that case one would study the infrared optical activity of solid state particles with or without molecular adsorbates.

The study would parallel conventional infrared and microwave molecular spectroscopy experiments. In place of a molecule one would have a small particle. Corresponding to infrared or microwave molecular spectroscopy, if a small particle possesses a spontaneous dipole moment, its fluctuations due to rotation or vibration can couple to an external photon field. The frequencies it will be able to couple to will be determined by the normal mode frequencies of the partcle. The typical vibrational frequencies of these objects lie in the far infrared and microwave regions of the spectrum. This frequency range is obtained by simply dividing the scale size of the particle by the speed of sound in the solid. Acoustic vibrations of such surface

roughness features have been observed by Weitz et al [6], as low frequency Raman side bands. This is attributed to an acoustic vibration of surface features selected by a resonant excitation of a localized plasmon. The localized nature of the excited states implied by the data suggests considering the excitation of individual roughness features. Also from the data, one concludes that the resonant plasmon frequencies of the bump decrease as their characteristic dimensions increase.

As pointed out earlier, there exists some experimental evidence that infrared absorption anomalies exist for particulate smokes [7]. The amount of absorption observed is very large and can not be accounted for in terms of the dielectric properties of the system, even if finite size effects are taken into account. The existence of a finite fluctuating dipole does open up additional absorption modes, however. The additional absorption will be associated with the (collective) normal modes of vibration of the particle. The actual calculation of the absorption cross section is naturally complicated because one needs to know the normal modes. One must solve the associated mechanical problem of finding the normal modes of vibration of the particle. Only then can one proceed to compute the desired cross section. Here we have given some thought to the origin of such spontaneous dipole moments in both homogeneous structures lacking inversion symmetry and inhomogeneous structures.

The following sections are organised under two main headings: Homogeneous Structures and Inhomogeneous Structures. In section I.2 we deal with homogeneous structures, by asking under what condition will a system composed of one type of atom possess an electric dipole moment. In section I.3 our study of inhomogeneous structures concentrates on two problems. The first is to find the dipole moment of an atom near a particle. This problem is of importance in determining the infrared activity of a solid with an adsorbate on it. Secondly we consider the problem of finding the dipole moment of a bimetallic particle (where one part consists of one type and another part consists of the other type). These particles may be fabricated by sputtering a metallic surface which is coated by a different metallic film. Finally a discussion of the results and conclusions are given in section I.4. Atomic units ($e=m=\hbar=1$ and $c=137$) are used throughout.

I.2 Homogeneous Structures

We start by considering a highly idealized model. We variationally compute the dipole moment of an one-electron "atom", where the "nucleus" lacks inversion symmetry. This model may be thought of as a prototype for a solid which is homogeneous, but lacks inversion symmetry. In such a case the ionic background lacks inversion symmetry. We then proceed to a more realistic case of computing the dipole

moment of an extended metal structure which lacks inversion symmetry. Here we use the density functional formalism[8], which has been moderately successful in surface studies. Such a calculation gives us an estimate of the magnitude of the dipole moment. This calculation may be used as a basis for estimating the typical magnitude of the dipole moment of a surface roughness feature.

I.2.1 One-electron Atom

Let us take a fixed positive charge of uniform density in the shape of a hemisphere and put a single electron around it. The system as a whole is electrically neutral. The lack of inversion symmetry implies the existence of an axis along which the dipole moment, if it existed, could point. This problem is a well defined quantum mechanical one and will be solved in this section using the variational method. Our aim is to see if a dipole exists and, if it does, to find its magnitude as a function of the radius of the hemisphere.

We consider the Z-axis to be the symmetry axis and let the positive background charge density be described by the distribution

$$\rho_+(\vec{r}) = \rho_0\, \Theta(a-r)\, \Theta\left(\tfrac{\pi}{2}-\theta\right), \qquad \text{(I.1)}$$

where ρ_0 is the magnitude of the charge density, a is the

radius of the hemisphere, and Θ is a unit step function. Only the domain defined by $z \geq 0$ and $r \leq a$ has positive charge. The magnitude ρ_0 is chosen so that $2\pi\rho_0 a^3/3 = 1$, where we are working in atomic units. We minimize the electronic energy functional

$$\langle\psi|H|\psi\rangle = \int d\vec{r}\left[-\tfrac{1}{2}\psi^*\nabla^2\psi - |\psi(\vec{r})|^2 \int d\vec{r}\,' \frac{\rho_+(\vec{r}\,')}{|\vec{r}-\vec{r}\,'|}\right] \quad , (I.2)$$

where ψ is the electronic wave function. The minimization is carried out by choosing a trial wave function of the form

$$\psi(\vec{r}) = \sum_{n,\lambda} A_{n\lambda} z^{\lambda} \exp(-b_n r) \quad , \qquad (I.3)$$

where $\lambda = 0$ or 1 and n ranges from 1 up to some truncation index N. $A_{n\lambda}$ and b_n are the variational parameters. The b_n exponents are not optimized but rather are chosen to be simply 1/n corresponding to hydrogenic wave functions. We are thus left with 2N coefficients $A_{n\lambda}$ to be determined.

A straightforward substitution of Eq.(I.3) into Eq.(I.2) and subsequent integration gives the expectation values for kinetic and potential energies. The kinetic energy expectation value is

$$\langle T\rangle = -\pi \sum_{m,n}\left[4A_{m0}A_{n0}\left(b_n^2\beta_{mn}^{-3} - b_n\beta_{mn}^{-2}\right) + 16A_{m1}A_{n1}\left(b_n^2\beta_{mn}^{-5} - b_n\beta_{mn}^{-4}\right)\right] \quad . (I.4)$$

The potential energy expectation value is

$$\langle V\rangle = -4\pi\rho_0 \sum_{m,n} \Big\{ 2A_{m0}A_{n0}\big[a^2\beta_{mn}^{-3} - 4\beta_{mn}^{-5} + (a^2\beta_{mn}^{-3} + 4a\beta_{mn}^{-4} + 4\beta_{mn}^{-5})\, e^{-\beta_{mn}a}\big] + \frac{1}{3}(A_{m0}A_{n1} + A_{m1}A_{n0})\big[-90\beta_{mn}^{-6} + 24a\beta_{mn}^{-5} + (21a^2\beta_{mn}^{-4} + 3a^3\beta_{mn}^{-3} + 66a\beta_{mn}^{-5} + 90\beta_{mn}^{-6})\, e^{-\beta_{mn}a}\big] + \frac{2}{3}A_{m1}A_{n1}\big[-120\beta_{mn}^{-7} + 12a^2\beta_{mn}^{-5} + (a^4\beta_{mn}^{-3} + 10a^3\beta_{mn}^{-4} + 48a^2\beta_{mn}^{-5} + 120a\beta_{mn}^{-6} + 120\beta_{mn}^{-7})\, e^{-\beta_{mn}a}\big]\Big\} \quad . (I.5)$$

Here $\beta_{mn} = b_n + b_m$. The overlap expectation value is

$$\langle\psi|\psi\rangle = 8\pi \sum_{m,n} \left(A_{m0}A_{n0}\beta_{mn}^{-3} + 4A_{n1}A_{m1}\beta_{mn}^{-5}\right) \quad , (I.6)$$

and the electronic dipole expectation value is given by

$$\langle\psi|z|\psi\rangle = 32\pi \sum_{m,n} \left(A_{m0}A_{n1} + A_{m1}A_{n0}\right)\beta_{mn}^{-5} \quad . (I.7)$$

This dipole moment has to be added to the dipole of the background charge distribution to obtain the net dipole of the system. The dipole of the background charge distribution is

$$\mu_z^b = \pi\rho_0 a^4/4 \quad . \quad (I.8)$$

Hence the net dipole for the atom is

$$\mu_z = \frac{\pi \rho_0 a^4}{4} - 32\pi \sum_{m,n} \left(A_{m0} A_{n1} + A_{m1} A_{n0}\right) \beta_{mn}^{-5} \quad .(I.9)$$

The coefficients $A_{n\lambda}$ are obtained by solving the problem in the following manner.

One can write in matrix notation

$$\langle \psi | H | \psi \rangle = \sum_{\substack{n',n=1 \\ \lambda',\lambda}}^{N} A_{n'\lambda'} A_{n\lambda} H_{n'\lambda',n\lambda} \quad ,(I.10)$$

where λ', λ = 0 or 1 ,and

$$\langle \psi | \psi \rangle = \sum_{\substack{n',n=1 \\ \lambda',\lambda}}^{N} A_{n'\lambda'} A_{n\lambda} S_{n'\lambda',n\lambda} \quad .(I.11)$$

The variation of $\langle \psi | H | \psi \rangle$ consistent with the normalization condition implies that Eq.(I.11) can be written as

$$\frac{\partial}{\partial A_{n'\lambda'}} \left[\langle \psi | H | \psi \rangle - \epsilon \langle \psi | \psi \rangle \right] = 0 \quad .(I.12)$$

This leads us to seeking the solution of the linear problem

$$\sum_{n,\lambda} A_{n\lambda} \left[H_{n'\lambda',n\lambda} - \epsilon S_{n'\lambda',n\lambda} \right] = 0 \quad .(I.13)$$

We then solve the matrix equation

$$S^{-1}HA - \epsilon A = 0 \quad , \qquad (I.14)$$

for eigenvalues ϵ and eigenvectors $A_{n\lambda}$. The number of orbitals included are increased until convergence in the ground state energy and the expectation value of the dipole moment is achieved. Typically this is achieved by taking N=7 (14 parameters).

I.2.2 Small Particle of Hemispherical Shape

We apply the density functional formalism to find the dipole moment of a hemispherical chunk of metal as a function of its radius and free electron density n . This problem is complicated by the lack of spherical symmetry and the need for considering functions of two variables, r and θ . We, therefore, shall make the following simplifying approximations.

We consider a finite sphere of radius a and compute the dipole moment per unit area on its surface. The net dipole moment for the sphere is zero, as is demanded by rotational invariance. The dipole moment per unit area, however, is nonzero and is directed perpendicular to the surface. Its magnitude depends, as we shall see, on the radius of the sphere. In the limit $a \to \infty$ it becomes just equal to that associated with a plane.

Now, for an arbitrary surface the net dipole is

$$\vec{\mu} = \int \hat{n} \frac{d\mu}{dA} dA \quad . \qquad \text{(I.15)}$$

If $d\mu/dA$ were constant, μ would vanish according to Green's theorem. However, if $d\mu/dA$ is a function of the radius of curvature

$$\frac{d\mu}{dA} = f(a) \quad , \qquad \text{(I.16)}$$

then this integral need not vanish. For the case of the hemispherical particle, we have therefore

$$\mu_z = [f(a) - f(\infty)] \pi a^2 \quad , \qquad \text{(I.17)}$$

assuming the plane is oriented parallel to the XY-plane. We use the density functional formalism to compute $f(a)$ and $f(\infty)$ and Eq.(I.17) then furnishes the net dipole moment of the hemispherical particle.

In the density functional formalism [9] we extremize the energy functional of a sphere with respect to the electron density function n(r). The energy functional is:

$$E = U + G[n] \quad , \qquad \text{(I.18)}$$

where U denotes the coulomb energy of the sphere

$$U = \frac{1}{2}\int d\vec{r}\int d\vec{r}\,' \frac{\rho(\vec{r})\,\rho(\vec{r}\,')}{|\vec{r}-\vec{r}\,'|} \quad , \qquad \text{(I.19)}$$

and G[n] is a universal local density functional

$$G[n] = \int d\vec{r}\left[n(\vec{r})\left(\frac{1.105}{r_s^{\,2}} - \frac{.458}{r_s} - \frac{.44}{r_s+7.8}\right)\right.$$

$$\left. + \left(\frac{1}{72n} + \frac{.00591}{n^{4/3}}\right)|\nabla n(\vec{r})|^2\right] \qquad \text{(I.20)}^{*}$$

Here, $4\pi n r_s^{\,3}/3 = 1$ and $n(r)$ is normalized so that there are N electrons in the sample

$$N = \int d\vec{r}\; n(\vec{r}) \quad . \qquad \text{(I.21)}$$

In Eq.(I.21) $\rho(\vec{r})$ is the charge density, which is the sum of a uniform sphere of positive charge density and a contribution from the negative charge distribution

$$\rho(\vec{r}) = \rho_0\,\Theta(a-r) - n(\vec{r}) \quad . \qquad \text{(I.22)}$$

In Eq.(I.20) the first and the second terms on the right hand side are, respectively, the kinetic and exchange energies of the uniform electron gas treated in the Hartree-Fock approximation. The third term on the right hand side is the correlation energy of the electron gas in the

* see Appendix A

metallic density range due to Wigner and is defined as the total energy of the uniform interacting electron gas with Hartree-Fock term subtracted out. Other terms in Eq.(I.20) are due to Hohenberg-Kohn expansion of G[n] as a series in density gradients for the case in which n(r) varies slowly over distances large compared with $r_s(n)$. Hence the fifth term represents the gradient correction to exchange and correlation contributions. The charge neutrality condition is

$$\int d\vec{r}\, \rho(\vec{r}) = 0 \qquad , \quad \text{(I.23)}$$

and $f(a)$ of Eq.(I.16) is defined as

$$f(a) = \frac{1}{4\pi a^2} \int d\vec{r}\; r\, \rho(\vec{r}) \qquad . \text{(I.24)}$$

The trial density functional used by us is a simple extension of the one used in earlier studies [11]:

$$\rho(\vec{r}) = \begin{cases} A\, e^{-\alpha (r-a)} & , \; r > a \\ B\, e^{\beta (r-a)} & , \; r < a \end{cases} \qquad \text{(I.25)}$$

where α and β are the variational parameters.

From Eqs.(I.22) and (I.25) the negative charge distribution is given by

$$n(\vec{r}) = \begin{cases} -A\, e^{-\alpha (r-a)}, & r > a \\ \rho_0 - B\, e^{\beta (r-a)}, & r < a \end{cases} \qquad \text{(I.26)}$$

Continuity of n(r) demands that

$$B = A + \rho_0 \quad , \qquad \text{(I.27)}$$

and charge neutrality then pins down the value of A,

$$A = \rho_0 I_2(\beta)\left[2\alpha^{-3} + 2a\alpha^{-2} + a^2\alpha^{-1} - I_2(\beta)\right]^{-1} \quad , \text{(I.28)}$$

where

$$I_n(\beta) = -\int_0^a dx\; x^n\, e^{\beta (x-a)} \qquad . \text{(I.29)}$$

The function $f(a)$ is

$$f(a) = \frac{A}{a^2}\left[6\alpha^{-4} + 6a\alpha^{-3} + 3a^2\alpha^{-2} + a^3\alpha^{-1}\right] - Ba^{-2} I_3(\beta) \quad . \text{(I.30)}$$

The parameters α and β are obtained by minimizing the energy functional $E[n]$ of Eq.(I.18).

To evaluate the coulomb energy U, let us write $U = U_- + U_+$, where U_- and U_+ are Coulomb energies,

respectively, for the regions $r < a$ and $r > a$. Hence

$$U_- = 2\pi \int_0^a r^2 \rho(r) \phi(r) dr \qquad ,(I.31)$$

and

$$U_+ = 2\pi \int_a^\infty r^2 \rho(r) \phi(r) dr \qquad ,(I.32)$$

where the potential $\phi(r)$ satisfies Poisson's equation

$$\frac{1}{r^2} \frac{d}{dr} r^2 \frac{d\phi}{dr} = -4\pi \rho(r) \qquad .(I.33)$$

Eqs.(I.31) and (I.32) can be rewritten, using Poisson's equation and partial integration, as

$$U_- = \frac{1}{2} \int_0^a dr\, r^2 [\phi'(r)]^2 - \frac{a^2}{2} \phi(a) \phi'(a) \qquad ,(I.34a)$$

and

$$U_+ = \frac{1}{2} \int_a^\infty dr\, r^2 [\phi'(r)]^2 + \frac{a^2}{2} \phi(a) \phi'(a) \qquad ,(I.34b)$$

where $\phi'(r) = d\phi(r)/dr$. Combining Eqs.(I.34a) and (I.34b) we get

$$U = \frac{1}{2} \int_0^\infty dr\, r^2 [\phi'(r)]^2 \qquad .(I.35)$$

Eq. (I.35) is readily evaluated and found to be

$$U = 8\pi^2 \left[2B^2 S_{12} + 2AB\, J_2(\alpha) I_1(\beta) + 2A^2 T_{12} \right] \quad , (I.36)$$

where

$$J_n(\alpha) = \int_0^\infty dr\, r^n e^{-\alpha(r-a)} \quad , (I.37)$$

$$T_{12} = -\left[-\alpha^{-1} J_3(2\alpha) + 2\alpha^{-2} J_2(2\alpha) + 2\alpha^{-3} J_1(2\alpha) \right] \quad , (I.38)$$

and

$$S_{12} = -\beta^{-1} I_3(2\beta) + 2\beta^{-2} I_2(2\beta) - 2\beta^{-3} I_1(2\beta) + 2\beta^{-3} I_1(\beta) \left[-2\beta^{-3} + 2a\beta^{-2} - a^2\beta^{-1} \right] e^{-\beta a} \quad . (I.39)$$

Analytic expressions for I_n, J_n, T_{12}, and S_{12} are obtained readily. The integral for G[n] in Eq. (I.20), however, was carried out numerically.

The variational calculation is performed by specifying a given number of electrons and a bulk r_s value (denoted by $\bar{r}_s$). The positive charge density is then

$$\rho_0 = \frac{3}{4\pi \bar{r}_s^3} \quad , \quad (I.40)$$

and the radius of the charge distribution is

$$a = \bar{r}_s N^{1/3} \quad . \qquad (I.41)$$

Values for α and β are then proposed and a search is made for the minimum system energy given by Eq. (I.18).

In the limit of a plane ($a \rightarrow \infty$) we write simpler expressions for the relevant quantities. Thus the charge density is

$$\rho(x) = \begin{cases} A\, e^{-\alpha x} & , \; x < a \\ B\, e^{\beta x} & , \; x > a \end{cases} \qquad (I.42)$$

where now $x=r-a$. We again have $B=A+\rho_0$, but now A is simply

$$A = -\rho_0 \left[1 + \frac{\beta}{\alpha}\right]^{-1} \quad . \qquad (I.43)$$

The dipole moment per unit area is

$$f(\infty) = \int \rho(x)\, x\, dx = -\rho_0 (\alpha\beta)^{-1} \quad . \qquad (I.44)$$

The coulomb energy per unit area is

$$\frac{U}{\text{area}} = \pi \left[B^2 \beta^{-3} + A^2 \alpha^{-3} \right] \quad , \qquad \text{(I.45)}$$

and the value of the functional G[n]/area is given by

$$\frac{G[n]}{\text{area}} = \int_{-\infty}^{+\infty} dx \left[n(x) \left(\frac{1.105}{r_s^2} - \frac{.458}{r_s} - \frac{.44}{r_s + 7.8} \right) + \left(\frac{1}{72n} + \frac{.00591}{n^{4/3}} \right) \left(\frac{dn}{dx} \right)^2 \right] \qquad \text{(I.46)}^*$$

Implementation of the variational procedure proceeds as before. Eqs.(I.44) and (I.30) can then be combined to obtain the net dipole moment μ_z as in Eq.(I.17).

I.3 Inhomogeneous Structures

What we have said so far has been limited to homogeneous systems. Inhomogeneous structures are by no means unimportant. We have seen the existence of modified decay rates of molecules adsorbed on a surface, as predicted by Gersten and Nitzan [5]. Heterogeneous catalysis often involves catalysts consisting of dissimilar materials. Here we consider the origin and properties of the electric dipole moment of (i) an atom near a small spheroidal particle and (ii) a bimetallic spheroid.

It is well known that even at the atomic level of description, two dissimilar atoms in close proximity will spontaneously develop an electric dipole moment [12].

* see Appendix A

This dipole falls off asymptotically as R^{-7}, where R is the internuclear separation . Atoms adsorbed on a metal surface have also been shown [13] to acquire an induced dipole moment. The dipole there was found to fall off asymptotically as D^{-4}, where D is the atom-surface separation. This result can be obtained directly by the use of macroscopic electrostatics and quantum mechanics. We generalize this calculation to the case of an atom near a small particle. It will be seen that gross departures from the atom-near-flat-surface results emerge. As a side result we also obtain the van der Waals dispersion energy of an atom near a solid particle. Finally we study the problem of finding the dipole moment of a bimetallic particle.

I.3.1 Atom Near a Spheroidally Shaped Particle

Consider the system consisting of a hydrogen atom near a dielectric spheroid of dielectric constant ϵ . The spheroid surface will be denoted by $\xi = \xi_0$, where (ξ, η, ϕ) are prolate spheroidal coordinates defined as

$$\begin{aligned} x &= f\left[(\xi^2-1)(1-\eta^2)\right]^{\frac{1}{2}} \cos\phi \\ y &= f\left[(\xi^2-1)(1-\eta^2)\right]^{\frac{1}{2}} \sin\phi \\ z &= f\xi\eta \end{aligned} \qquad \text{(I.47)}$$

The position of the proton will be (ξ_1, η_1, ϕ_1) and that of the electron (ξ_2, η_2, ϕ_2), where $\xi_1 > \xi_0$ and $\xi_2 > \xi_0$. The spheroid is asumed oriented along the Z-direction and we

define a scale length $f=(a^2-b^2)^{1/2}$, where a and b are the semimajor and semiminor axes, respectively. The geometry of the system is shown in Fig. I.1.

We limit ourselves to dispersion dipoles and the dispersion interaction. Consequently we are limited to the asymptotic domain, i.e. distances far from the surface. Our goal is to study the effect of the surface shape on the size of these dispersion terms.

The calculation proceeds in two steps. First, we obtain an expression for the interaction energy between the atom and the spheroid. Then we insert this into the Schrödinger equation and compute the dipole moment of the system, using perturbation theory.

Following Smythe [14] the electrostatic potentials, both inside and outside the spheroid, can be written as

$$\Phi_{in}(\vec{r}) = \sum_{l=0}^{\infty}(2l+1)\sum_{m=0}^{l}\left[C_l^m P_l^m(\xi) P_l^m(\eta)\cos\phi + D_l^m P_l^m(\xi) P_l^m(\eta)\sin m\phi\right], \quad \xi < \xi_0 \tag{I.48}$$

and

$$\Phi_{out}(\vec{r}) = \sum_{l=0}^{\infty}(2l+1)\sum_{m=0}^{l}\left[A_l^m Q_l^m(\xi) P_l^m(\eta)\cos m\phi + B_l^m Q_l^m(\xi) P_l^m(\eta)\sin m\phi\right] + \frac{e}{|\vec{r}-\vec{r}_1|} - \frac{e}{|\vec{r}-\vec{r}_2|}, \quad \xi > \xi_0 \tag{I.49}$$

where $P_l^m(\eta)$ and $Q_l^m(\xi)$ are associated Legendre functions of the first and second kind respectively and $\vec{r}_i$ denotes the position of charges $\pm e$. The coefficients A_l^m, B_l^m, C_l^m,

and D_ℓ^m are to be determined from the appropriate boundary conditions. The coulomb terms appearing in Eq.(I.49) can be expanded as [14]

$$\frac{e}{|\vec{r}-\vec{r}_1|} = \frac{e}{f}\sum_{\ell=0}^{\infty}(2\ell+1)\sum_{m=0}^{\ell}\epsilon_m(-)^m\left[\frac{(\ell-m)!}{(\ell+m)!}\right]^2 \cos[m(\phi-\phi_1)]\,P_\ell^m(\eta)P_\ell^m(\eta_1)\,P_\ell^m(\xi_<^{(1)})\,Q_\ell^m(\xi_>^{(1)}), \quad (I.50)$$

and

$$\frac{e}{|\vec{r}-\vec{r}_2|} = \frac{e}{f}\sum_{\ell=0}^{\infty}(2\ell+1)\sum_{m=0}^{\ell}\epsilon_m(-)^m\left[\frac{(\ell-m)!}{(\ell+m)!}\right]^2 \cos[m(\phi-\phi_2)]\,P_\ell^m(\eta)\,P_\ell^m(\eta_2)\,P_\ell^m(\xi_<^{(2)})\,Q_\ell^m(\xi_>^{(2)}), \quad (I.51)$$

where $\epsilon_0=1$, $\epsilon_m=2$ for $m\neq 0$, and $\xi_<^{(i)}=\min(\xi,\xi_i)$ and $\xi_>^{(i)}=\max(\xi,\xi_i)$. The potential outside the spheroid can be written as

$$\Phi_{out}(\vec{r}) = \sum_{\ell=0}^{\infty}(2\ell+1)\sum_{m=0}^{\ell}\left[A_\ell^m\,Q_\ell^m(\xi)P_\ell^m(\eta)\cos m\phi + B_\ell^m\,Q_\ell^m(\xi)\,P_\ell^m(\eta)\sin m\phi\right] + \frac{e}{f}\sum_{\ell=0}^{\infty}(2\ell+1)\sum_{m=0}^{\ell}\epsilon_m(-)^m\left[\frac{(\ell-m)!}{(\ell+m)!}\right]^2 P_\ell^m(\eta)\left\{\cos[m(\phi-\phi_1)]\,P_\ell^m(\eta_1)P_\ell^m(\xi_<^{(1)})Q_\ell^m(\xi_>^{(1)}) - \cos[m(\phi-\phi_2)]\,P_\ell^m(\eta_2)P_\ell^m(\xi_<^{(2)})Q_\ell^m(\xi_>^{(2)})\right\}, \quad \xi>\xi_0. \quad (I.52)$$

Utilizing Eqs.(I.48) and (I.52), the ξ-component of the displacement field, D_ξ, can be written as

$$D_\xi^{in} = -\epsilon\sum_{\ell=0}^{\infty}(2\ell+1)\sum_{m=0}^{\ell}\left[C_\ell^m\,P_\ell'^m(\xi)\,P_\ell^m(\eta)\cos m\phi + D_\ell^m\,P_\ell'^m(\xi)\,P_\ell^m(\eta)\sin m\phi\right], \quad (I.53)$$

and

$$D_{\xi}^{out} = -\sum_{l=0}^{\infty}(2l+1)\sum_{m=0}^{l}\left[A_l^m Q_l'^m(\xi) P_l^m(\eta)\cos m\phi + B_l^m Q_l'^m(\xi) P_l^m(\eta)\sin m\phi\right] - \frac{e}{f}\sum_{l=0}^{\infty}(2l+1)\sum_{m=0}^{l}\epsilon_m(-)^m\left[\frac{(l-m)!}{(l+m)!}\right]^2 P_l^m(\eta)\left\{\cos\left[m(\phi-\phi_1)\right]P_l^m(\eta_1)P_l'^m(\xi_<^{(1)})Q_l'^m(\xi_>^{(1)}) - \cos\left[m(\phi-\phi_2)\right]P_l^m(\eta_2)P_l'^m(\xi_<^{(2)})Q_l'^m(\xi_>^{(2)})\right\}, \qquad (I.54)$$

where the prime symbol indicates first derivative with respect to ξ. It should be noted that in $P_l'^m(\xi_<^{(i)})$ and $Q_l'^m(\xi_>^{(i)})$, derivatives of the appropriate function will be taken eventually.

Imposition of the boundary conditions that $\Phi(\vec{r})$ and $D_\xi(\vec{r})$ be continuous at $\xi = \xi_0$ leads to the following expressions for the coefficients A_l^m, B_l^m, C_l^m, and D_l^m:

$$A_l^m = \left[P_l^m(\xi_0)K_l'^m - \epsilon P_l'^m(\xi_0)K_l^m\right]/\Delta_l^m, \qquad (I.55)$$

$$B_l^m = \left[P_l^m(\xi_0)S_l'^m - \epsilon P_l'^m(\xi_0)S_l^m\right]/\Delta_l^m, \qquad (I.56)$$

$$C_l^m = \left[Q_l^m(\xi_0)K_l'^m - Q_l'^m(\xi_0)K_l^m\right]/\Delta_l^m, \qquad (I.57)$$

$$D_l^m = \left[Q_l^m(\xi_0)S_l'^m - Q_l'^m(\xi_0)S_l^m\right]/\Delta_l^m, \qquad (I.58)$$

where

$$\Delta_\ell^m = \epsilon\, Q_\ell^m(\xi_0)\, P_\ell'^m(\xi_0) - P_\ell^m(\xi_0)\, Q_\ell'^m(\xi_0) \quad , \tag{I.59}$$

and

$$K_\ell^m = \frac{e}{f}\,\epsilon_m (-)^m \left[\frac{(\ell-m)!}{(\ell+m)!}\right]^2 \Big\{ \cos m\phi_1\, P_\ell^m(\eta_1)\, P_\ell^m(\xi_0)\, Q_\ell^m(\xi_1) - \cos m\phi_2\, P_\ell^m(\eta_2)\, P_\ell^m(\xi_0)\, Q_\ell^m(\xi_2) \Big\} \quad , \tag{I.60}$$

$$S_\ell^m = \frac{e}{f}\,\epsilon_m (-)^m \left[\frac{(\ell-m)!}{(\ell+m)!}\right]^2 \Big\{ \sin m\phi_1\, P_\ell^m(\eta_1)\, P_\ell^m(\xi_0)\, Q_\ell^m(\xi_1) - \sin m\phi_2\, P_\ell^m(\eta_2)\, P_\ell^m(\xi_0)\, Q_\ell^m(\xi_2) \Big\} \quad . \tag{I.61}$$

$K_\ell'^m$ and $S_\ell'^m$ denote derivatives with respect to the variable ξ_0 .

The dipole operator of the system (atom plus spheroid) is obtained by examining the asymptotic form of the potential in Eq. (I.52). It is seen that the asymptotic expression for $\Phi_{out}(\vec{r})$ as $r \to \infty$ can be written as

$$\Phi_{out}(\vec{r}) \longrightarrow 3\eta A_1^0 Q_1^0(\xi) + 3 Q_1^1(\xi)\left[A_1^1 \cos\phi + B_1^1 \sin\phi\right] (1-\eta^2)^{1/2} + \frac{3e\eta}{f}\,(\eta_1\xi_1 - \eta_2\xi_2)\, Q_1^0(\xi) - \frac{3e}{2f}\left\{\cos\phi\left[\cos\phi_1 - \cos\phi_2\right] + \sin\phi\left[\sin\phi_1 - \sin\phi_2\right]\right\} . \tag{I.62}$$

It should be remembered that asymptotic expressions for

$Q_l^m(\xi)$ as $\xi \to \infty$ should be used in Eq. (I.62). Asymptotically (as $r \to \infty$)

$$\Phi_{out}(\vec{r}) \longrightarrow \frac{\vec{\mu}\cdot\vec{r}}{r^3} \quad , \tag{I.63}$$

or, in spheroidal coordinates,

$$\Phi_{out}(\vec{r}) \to \frac{1}{(f\xi)^2}\left\{\eta\mu_z + (1-\eta^2)^{1/2}\left(\mu_x \cos\phi + \mu_y \sin\phi\right)\right\} . \tag{I.64}$$

Hence if we define

$$U_l^m = \frac{e}{f}\epsilon_m(-)^m\left[\frac{(l-m)!}{(l+m)!}\right]^2\left[\cos m\phi_1\, P_l^m(\eta_1) P_l^m(\xi_1) - \cos m\phi_2\, P_l^m(\eta_2) P_l^m(\xi_2)\right] , \tag{I.65a}$$

$$V_l^m = \frac{e}{f}\epsilon_m(-)^m\left[\frac{(l-m)!}{(l+m)!}\right]^2\left[\sin m\phi_1\, P_l^m(\eta_1) P_l^m(\xi_1) - \sin m\phi_2\, P_l^m(\eta_2) P_l^m(\xi_2)\right] , \tag{I.65b}$$

and use the asymptotic formula

$$Q_1^m(\xi) \xrightarrow{\xi\to\infty} \frac{(-)^m\sqrt{\pi}\,(m+1)!}{4\xi^2\,\Gamma(5/2)} \quad , \tag{I.66}$$

then inspection of Eqs. (I.62) and (I.64) leads to the following expressions for the components of the dipole moment $\vec{\mu}$:

$$\mu_x = 2f^2 (A_1' + U_1') \quad , \tag{I.67}$$

$$\mu_y = 2f^2 (B_1' + V_1') \quad , \tag{I.68}$$

$$\mu_z = f^2 (A_1^0 + U_1^0) \quad . \tag{I.69}$$

The interaction energy V is calculated from the electron-proton interaction and from the self-energy of the atom

$$U = \frac{e}{2} \left\{ \tilde{\Phi}(\vec{r}_1) - \tilde{\Phi}(\vec{r}_2) \right\} \quad , \tag{I.70}$$

where the tilde denotes the fact that we exclude the infinite part due to the interaction of the electron with itself or of the proton with itself. Hence

$$\begin{aligned} V &= U + e^2/|\vec{r}_1 - \vec{r}_2| \\ &= \frac{e^2}{2f} \sum_{l=0}^{\infty} (2l+1) \sum_{m=0}^{l} \epsilon_m \left[(-)^m/\Delta_l^m\right] \left[\frac{(l-m)!}{(l+m)!} \right]^2 P_l^m(\xi_0) \\ &\quad P_l'^m(\xi_0) (1-\epsilon) \left\{ \left[Q_l^m(\xi_1) P_l^m(\eta_1) \right]^2 + \left[Q_l^m(\xi_2) P_l^m(\eta_2) \right]^2 \right. \\ &\quad \left. -2 P_l^m(\eta_1) Q_l^m(\xi_1) P_l^m(\eta_2) Q_l^m(\xi_2) \cos\left[m(\phi_1 - \phi_2)\right] \right\} \end{aligned} \tag{I.71}$$

The quantity V describes the interaction of the atom with the spheroid. The spheroid is characterized by the quantities: a scale size f, a shape parameter ξ_0 , and a dielectric constant ϵ . V is an operator which may be

introduced into Schrodinger equation and its perturbative effects may be studied.

For the purpose of simplicity, we assume the proton to be located on the Z-axis. Then $\eta_1 = 1$ and V reduces to

$$V = \frac{e^2}{2f} \sum_{l=0}^{\infty} (2l+1) \sum_{m=0}^{l} \frac{\epsilon_m (-)^m}{\Delta_l^m} \left[\frac{(l-m)!}{(l+m)!} \right]^2 P_l^m(\xi_0) P_l'^m(\xi_0)$$
$$(1-\epsilon) \left[Q_l^m(\xi_1) \delta_{m0} - P_l^m(\eta_2) Q_l^m(\xi_2) \right]^2 . \qquad \text{(I.72)}$$

To make the computation procedure easier we make the further assumption that the size of the atom is small compared with the size of the spheroid. Let us define atomic relative coordinates

$$\rho = f \left[(\xi_2^2 - 1)(1 - \eta_2^2) \right]^{1/2} \qquad \text{(I.73a)}$$

and

$$\varphi = f \left[\xi_2 \eta_2 - \xi_1 \right] \qquad \text{(I.73b)}$$

Both ρ and φ are of first order smallness. Then

$$\xi_2 = \xi_1 + \frac{\varphi}{f} + \frac{\rho^2}{2f^3 (\xi_1 - 1)^2} \left[f \xi_1 (\xi_1^2 - 1) - \varphi (\xi_1^2 + 1) \right], \qquad \text{(I.74a)}$$

and

$$\eta_2 = 1 - \frac{\rho^2}{2f^2 (\xi_1^2 - 1)} \left[1 - \frac{2 \varphi \xi_1}{f (\xi_1^2 - 1)} \right] . \qquad \text{(I.74b)}$$

We decompose the interaction potential into contributions from various azimuthal numbers m. For m=0 we have (through cubic order)

$$V_o = V_o^{(2)} + V_o^{(3)} \quad , \tag{I.75}$$

where $V_o^{(2)}$ is quadratic in atomic coordinates

$$V_o^{(2)} = -\frac{e^2}{2f^3}\sum_{l=0}^{\infty}(2l+1)\left[\frac{\epsilon-1}{\Delta_l^o}\right]P_l(\xi_o)P_l'(\xi_o)\varphi^2\left[Q_l'(\xi_1)\right]^2, \tag{I.76}$$

and $V_o^{(3)}$ is cubic in those coordinates

$$V_o^{(3)} = -\frac{e^2}{2f^4}\sum_{l=0}^{\infty}(2l+1)\left[\frac{\epsilon-1}{\Delta_l^o}\right]P_l(\xi_o)P_l'(\xi_o) Q_l''(\xi_1)\varphi\left[\varphi^2-\rho^2/2\right] \quad . \tag{I.77}$$

It is not needed to go to higher order in atomic size than as in the above.

For m=1 we have

$$V_1 = V_1^{(2)} + V_1^{(3)} \quad , \tag{I.78}$$

where

$$V_1^{(2)} = -\frac{1}{4f^3}\sum_{l=1}^{\infty}\frac{(2l+1)}{\Delta_l^1}(1-\epsilon)P_l(\xi_o)P_l'(\xi_o) \rho^2\left[Q_l'(\xi_1)\right]^2 l(l+1)\left\{1-\frac{\xi_o P_l'(\xi_o)}{l(l+1)P_l(\xi_o)}\right\} \quad , \tag{I.79}$$

$$V_1^{(3)} = -\frac{1}{2f^4}\sum_{l=1}^{\infty}(2l+1)\frac{(1-\epsilon)}{\Delta_l^1}P_l(\xi_o)P_l'(\xi_o)\varphi\rho^2 l(l+1) Q_l'(\xi_1)Q_l''(\xi_1)\left[1-\frac{\xi_o P_l'(\xi_o)}{l(l+1)P_l(\xi_o)}\right] \quad . \tag{I.80}$$

Terms in the potential arising from $m \geqslant 2$ are not considered here, since they are of order higher than cubic.

The dipole operator may be expressed (through quadratic order) as

$$\mu_z = \mu^{(1)} + \mu^{(2)} \quad , \tag{I.81}$$

where

$$\mu^{(1)} = -e\varphi \left\{ 1 + \xi_0 Q_1'(\xi_1) \frac{1-\epsilon}{\Delta_1^0} \right\} \quad , \tag{I.82a}$$

$$\mu^{(2)} = -\frac{e}{2f}\left(\varphi^2 - \frac{\rho^2}{2}\right) Q_1''(\xi_1) \frac{\xi_0(1-\epsilon)}{\Delta_1^0} \quad . \tag{I.82b}$$

I.3.1(a) <u>The Dispersion Energy</u>

We obtain the dispersion energy by evaluating the ground state expectation value of the operator V. We make use of the fact that for hydrogen atom,

$$\langle \varphi^2 \rangle = a_0^2 \quad , \tag{I.83a}$$

$$\langle \rho^2 \rangle = 2a_0^2 \quad , \tag{I.83b}$$

where a_0 is the Bohr radius. The total dispersion energy is given by

$$\langle V \rangle = \langle V_0 \rangle + \langle V_1 \rangle \quad , \tag{I.84}$$

where

$$\langle V_0 \rangle = \frac{(ea_0)^2}{2f^3} \sum_{l=0}^{\infty} (2l+1) \frac{1-\epsilon}{\Delta_l^0} P_l(\xi_0) P_l'(\xi_0) \left[Q_l'(\xi_1) \right]^2 , \tag{I.85}$$

and

$$\langle V_1 \rangle = - \frac{(ea_0)^2}{2f^3} \sum_{l=1}^{\infty} \frac{l(l+1)(2l+1)}{\Delta_l^1} (1-\epsilon) P_l(\xi_0) P_l'(\xi_0)$$

$$[Q_l'(\xi_1)]^2 \left\{ 1 - \frac{\xi_0 P_l'(\xi_0)}{l(l+1) P_l(\xi_0)} \right\} \quad . \qquad \text{(I.86)}$$

We now study the case of a metallic sphere by letting ξ_0 and ξ_1, and $|\epsilon|$ become infinite. Thus employing the asymptotic formulas

$$P_n'(\xi_0) \longrightarrow \frac{2^n n \Gamma(n+\frac{1}{2}) \xi_0^{n-1}}{\sqrt{\pi}\, n!} \qquad \text{(I.87)}$$

and

$$Q_n'(\xi_0) \longrightarrow - \frac{(n+1)\sqrt{\pi}\, n!}{2^{n+1} \Gamma(n+\frac{3}{2}) \xi_0^{n+2}} \quad , \qquad \text{(I.88)}$$

we find

$$\langle V_0 \rangle \rightarrow - \frac{(ea_0)^2}{2(f\xi_1)^3} \frac{\xi_0}{\xi_1} \left\{ \frac{1 + (\xi_0/\xi_1)^2}{[1 - (\xi_0/\xi_1)^2]^3} \right\} \quad , \qquad \text{(I.89)}$$

$$\langle V_1 \rangle \longrightarrow - \left(\frac{\xi_0}{f\xi_1^2} \right)^3 \frac{(ea_0)^2}{[1 - (\xi_0/\xi_1)^2]^3} \quad . \qquad \text{(I.90)}$$

Let us now define H to be the distance of the atom from the sphere tip. Then $\xi_0/\xi_1 = a/(a+H)$. Hence for $H \ll a$,

$$\langle V_0 \rangle \longrightarrow - \frac{(ea_0)^2}{8H^3} \quad , \qquad \text{(I.91)}$$

and

$$\langle V_1 \rangle \longrightarrow - \frac{(ea_0)^2}{8H^3} \quad , \qquad \text{(I.92)}$$

so that

$$\langle V \rangle \longrightarrow - \frac{(ea_0)^2}{4H^3} \quad . \tag{I.93}$$

This result is in agreement with that for an atom near a plane [13,15] as may be expected.

From Eqs.(I.84), (I.85), and (I.86) we note that there is a simple scaling relation $\langle V \rangle = -f^{-3} F(\xi_0, \xi_1)$.

I.3.1(b) The Dispersion Dipole

The dispersion dipole is seen to vanish in zeroth order perturbation theory. The leading term stems from first order perturbation theory. Hence we can write

$$\langle \mu_z \rangle = \langle \phi_0 | (\mu^{(1)} + \mu^{(2)}) | \phi_1 \rangle + \langle \phi_1 | (\mu^{(1)} + \mu^{(2)}) | \phi_0 \rangle \, , \tag{I.94}$$

where $|\phi_n\rangle$ denotes the n^{th} state of the atom with energy eigenvalue E_n. In terms of the Green's function

$$G = \sum_{n \neq 0} \frac{|\phi_n\rangle\langle\phi_n|}{E_0 - E_n} \quad , \tag{I.95}$$

Eq.(I.94) can be written as

$$\langle \mu_z \rangle = 2\langle \phi_0 | V_0^{(2)} G \mu^{(2)} | \phi_0 \rangle + 2\langle \phi_0 | V_0^{(3)} G \mu^{(1)} | \phi_0 \rangle$$

$$+ 2\langle \phi_0 | V_1^{(2)} G \mu^{(2)} | \phi_0 \rangle + 2\langle \phi_0 | V_1^{(3)} G \mu^{(1)} | \phi_0 \rangle \, , \tag{I.96}$$

where other terms vanish because of parity considerations.

The following matrix elements are evaluated using the method of Dalgarno and Lewis [16]**:

$$\langle\phi_0|\varphi^2 G\left[\varphi^2-\tfrac{1}{2}\rho^2\right]|\phi_0\rangle = -\frac{5a_0^5}{e^2}\ , \qquad \text{(I.97)}$$

$$\langle\phi_0|\varphi\left[\varphi^2-\tfrac{1}{2}\rho^2\right]G\varphi|\phi_0\rangle = -\frac{33}{4}\ \frac{a_0^5}{e^2}\ , \qquad \text{(I.98)}^{**}$$

$$\langle\phi_0|\rho^2 G\left[\varphi^2-\tfrac{1}{2}\rho^2\right]|\phi_0\rangle = -\frac{5a_0^5}{e^2}\ , \qquad \text{(I.99)}$$

$$\langle\phi_0|\varphi\rho^2 G\varphi|\phi_0\rangle = -\frac{33}{4}\ \frac{a_0^5}{e^2}\ . \qquad \text{(I.100)}$$

Hence,

$$\begin{aligned}\langle\mu_z\rangle = \frac{e a_0^5}{2f^4}\Bigg\{ &\sum_{l=0}^{\infty}(2l+1)\ \frac{\epsilon-1}{\Delta_l^0}\ P_l(\xi_0)P_l'(\xi_0)Q_l'(\xi_1)\\
&\left[-5\xi_0 Q_1''(\xi_1)\ \frac{1-\epsilon}{\Delta_1^0}\ Q_l'(\xi_1)-\frac{33}{2}Q_l''(\xi_1)-\frac{33}{2}\xi_0 Q_1'(\xi_1)\right.\\
&\left.Q_l''(\xi_1)\ \frac{1-\epsilon}{\Delta_1^0}\right]-\frac{5}{2}\xi_0 Q_1''(\xi_1)\ \frac{1-\epsilon}{\Delta_1^0}\ \sum_{l=1}^{\infty} l(l+1)(2l+1)\\
&\frac{\epsilon-1}{\Delta_l^1}P_l(\xi_0)P_l'(\xi_0)\left[Q_l'(\xi_1)\right]^2\left[1-\frac{\xi_0 P_l'(\xi_0)}{l(l+1)\ P_l(\xi_0)}\right]+\\
&\frac{33}{2}\left[1+\xi_0 Q_1'(\xi_1)\ \frac{1-\epsilon}{\Delta_1^0}\ \sum_{l=1}^{\infty} l(l+1)(2l+1)\ \frac{\epsilon-1}{\Delta_l^1}\ P_l(\xi_0)\right.\\
&\left.P_l'(\xi_0)Q_l'(\xi_1)\ Q_l''(\xi_1)\left[1-\frac{\xi_0 P_l'(\xi_0)}{l(l+1)\ P_l(\xi_0)}\right]\right\}\ . \qquad \text{(I.101)}\end{aligned}$$

This final expression for the dipole moment, while analytic, is too general to draw any conclusion. So we study this

** see Appendix B

expression for the case of a perfectly conducting sphere ($\xi_0 \to \infty$, $|\epsilon| \to \infty$).

Then

$$\langle \mu_z \rangle \to \frac{z^5 e a_0^5}{2a^4 (1-z^2)^4} \left\{ 33 + 462 z^2 + 96 z^3 + 804 z^5 + 90 z^7 \right\} , \qquad \text{(I.102)}$$

where $z \equiv \xi_0/\xi_1$. When $H \ll a$, this becomes

$$\langle \mu_z \rangle \to \frac{297\ e a_0^5}{16 H^4} . \qquad \text{(I.103)}$$

This is three times the dipole moment of the atom when it is near a plane.

As in the case of the dispersion energy, the general expression for the dispersion dipole obeys a simple scaling relation $\langle \mu_z \rangle = f^{-4} G(\xi_0, \xi_1)$.

I.3.2 Bimetallic Spheroid

Consider the structure formed by joining two dissimilar metal prolate hemispheroids. The hemispheroids are joined by the plane containing their minor axes. The metals will be treated as perfect conductors at the electrodynamic level.

Dissimilar metals have, in general, different work functions. So, a charge transfer between the two structures will occur as the Fermi levels equilibrate and the spheroid is expected to develop a net dipole. We wish to evaluate this dipole moment.

Let hemispheroid 1 be at potential Φ_1 , and hemispheroid 2 be at potential Φ_2 . Since the electrochemical potential must be constant throughout the system at equilibrium, $\Phi_1 - \Phi_2 = \Delta W$, where ΔW is the work function difference expressed in potential units. In prolate spheroidal coordinates the potential outside the metal is

$$\Phi(\xi,\eta) = \sum_n a_n P_n(\eta) Q_n(\xi) \quad . \qquad \text{(I.104)}$$

Evaluation of Φ on the surface gives

$$\Phi(\xi_o,\eta) = \Phi_1 \Theta(\eta) + \Phi_2 \Theta(-\eta) \quad , \qquad \text{(I.105)}$$

where

$$\Phi_1 = \sum_n a_n P_n(\eta) Q_n(\xi_o) \quad , \; 0<\eta<1 \; , \; \xi = \xi_o \; , \qquad \text{(I.106)}$$

$$\Phi_2 = \sum_n a_n P_n(\eta) Q_n(\xi_o) \; , \; -1<\eta<0 \; , \; \xi = \xi_o \; . \qquad \text{(I.107)}$$

We multiply both Φ_1 and Φ_2 by $P_m(\eta)$ and integrate over the variable η to get

$$\int_0^1 d\eta \, P_m(\eta) \Phi_1 = \sum_n a_n \int_0^1 d\eta \, P_m(\eta) P_n(\eta) Q_n(\xi_o) \; , \qquad \text{(I.108)}$$

and

$$\int_{-1}^0 d\eta \, P_m(\eta) \Phi_2 = \sum_n a_n \int_{-1}^0 d\eta \, P_m(\eta) P_n(\eta) Q_n(\xi_o) \; . \qquad \text{(I.109)}$$

Addition of Eqs.(I.108) and (I.109) gives

$$a_m = \frac{(m+\frac{1}{2})}{Q_m(\xi_0)} \left\{ \Phi_1 \int_0^1 d\eta\, P_m(\eta) + \Phi_2 \int_{-1}^0 d\eta\, P_m(\eta) \right\} . \quad \text{(I.110)}$$

For m=1,

$$a_1 = \frac{3}{4} \frac{\Delta W}{Q_1(\xi_0)} . \quad \text{(I.111)}$$

Hence the dipole moment is given by

$$\mu = \frac{a_1 f^2}{3}$$

$$= f^2 \frac{\Delta W}{4 Q_1(\xi_0)} . \quad \text{(I.112)}$$

In the sphere limit this reduces to

$$\mu \rightarrow \frac{3}{4} a^2 \Delta W . \quad \text{(I.114)}$$

I.4 Results and Discussion

In our study of the one electron atom, where we computed the net dipole moment of the atom lacking inversion symmetry, we note that even at this level of simplicity there exists an electric dipole. This dipole is oriented along the symmetry axis and an expression for it is given in Eq.(I.9). Results for the ground state energy and dipole moment are tabulated in Table 1, for a range of a values, the radius of the hemispherical nuclear charge distribution.

The dipole grows with increasing radius. For small values of a, the dipole is directed from the round surface towards the planar surface. At larger values of a this trend is reversed. For very small values of a the dipole should again get smaller in magnitude and should vanish as $a \rightarrow 0$. At this microscopic level, however, it is hard to make any fruitful comment regarding the orientation of the dipole moment, except to note that the results clearly show the dipole to be of quantum mechanical origin. None the less it encouraged us to study more realistic situations.

We therefore dealt with the problem of finding the dipole moment of a hemispherical small particle in section I.2.2. There we applied the density functional formalism. It is worthwhile to mention at this point that after this calculation was completed and published [17] several recent improvements and corrections in the density functional formalism were brought to our attention by Professor V. Sahni. A discussion of these improvements and their effects on the present results will be given in Appendix A.

The results of our density functional calculation are presented here. In Fig.I.2 the dipole moment per unit area, $f(a)-f(\infty)$, is plotted as a function of the jellium radius a for a range of r_s values typical of metals. It is found that the dipole moment per unit area falls off with increasing a and asymptotically approaches the value

expected for a planar surface as $a \to \infty$. This, of course, is to be expected on the ground that electron localization in the jellium background is difficult for small values of a and the electron penetrates the vacuum giving rise to a large negative dipole moment. Further, for a small sphere, the electron is able to delocalize in all three directions, where as for larger spheres the electron delocalization can take place only in a direction perpendicular to the surface.

The net dipole moment, μ_z , of a hemisphere of radius a is evaluated by the use of Eq.(I.17). Fig.I.3 shows the behavior of μ_z as a function of a for a range of r_s values. It is seen that for small a values the dipole moment is small and increases to large magnitudes for large a values.

It should be noted that, for a given value of a, the largest dipoles occur at $r_s=3$. For larger or smaller values of r_s the magnitude of the dipole falls off. While this result is a consequence of the detailed numerical calculation, we can analyse some underlying trends that would produce this behavior. We note that as r_s is increased, the number density of electrons is decreased and fewer electrons find themselves in the neighbourhood of the surface. Hence the dipole moment would decrease. On the other hand, an opposite trend may be operative, which has to do with the work function of the jellium metal. As r_s is increased the work function decreases [7]. Consequently

electrons can penetrate into the vacuum with greater ease and hence the dipole moment would increase. Finally larger r_s values would allow the electron to better realize that the surface is curved than smaller r_s values. This would tend to favor increased dipoles at larger r_s values. Hence it is the competetion among the various trends that give rise to such results as are presented here.

We would like to emphasize the fact that the above trends in the evaluation of dipole moments for homogeneous structures are only a qualitative means of describing the complex situation. Hence a more detailed numerical calculation would probably be helpful.

Techniques are now becoming available to fabricate particles in the size range of interest. These include supersonic jet cluster formation, ion sputtering methods, and smoke fabrication. It may thus be possible to do a direct measurement of the electric dipole moment of small particles by dc electrostatic techniques. An additional experimental technique that may probe the surface dipole moment is infrared absorption of rough surfaces. By taking the difference between the rough and smooth surface absorbances, one may possibly extract the surface contribution due to the surface dipole.

Another possible experiment is to study collision induced absorption in systems consisting of solid particles and molecules. The transient dipole, that develops during

the collision between a molecule and a solid, will couple to the electromagnetic field and give rise to microwave and far infrared absorption.

In section I.3 we considered inhomogeneous structures, where we calculated expressions for the dipole moment of an atom near a particle and of a bimetallic spheroidal particle. The results of some numerical computation are presented here in Figs.I.4 and I.5. In Fig.I.4 the system dipole is plotted as a function of the atom-spheroid separation H. The dipole is taken in units of the system dipole of an atom near a sphere (i.e. divided by $297/16H^4$). This, in turn, is three times the dipole induced on an atom when it is near a plane. The factor of three arises because the image dipole in a sphere is twice that of an atom if the atom is near the sphere. The aspect ratio of the spheroid is chosen to be large to see what effect the sharpness of the structure has, and the spheroid is taken to be a perfect conductor ($|\epsilon| \rightarrow \infty$). The dipole moment decreases with increasing H, as might be expected. For $H \lesssim 20$ Å the dipole moment is larger than it would be for a sphere.

In Fig.I.5 the behavior of the dispersion energy as a function of H is presented. The dispersion energy is plotted in units of $-1/4H^3$, which is the corresponding dispersion energy for an atom near a plane. It is interesting to note that the dispersion energy is weaker than it would be

if the spheroid were replaced by a plane. This would mean that atoms tend to avoid sharp pointy objects. One can expect this on geometrical grounds since, for a sharp object like a spheroid, there are fewer solid atoms which are "near" neighbors to the external atom. The total dispersion energy is the sum of the van der Waal's contributions to all the solid's atoms, so that the net attraction is thereby softened.

The dipole moment for a bimetallic sphere was obtained in Eq.(I.113). This dipole may be seen to be typically quite large. Taking $\Delta W \sim 1\,V$ and a=100 Å gives μ =1000 ea_0. If such a sphere were allowed to undergo spheroidal vibrations, the resulting fluctuating dipole would couple strongly to electromagnetic radiation.

The basic conclusions concerning homogeneous structures that may be reached is that the dipole moment of the system is small until one gets to rather larger scale sizes. For the inhomogeneous structures, on the other hand, sizable dipoles may be present for even small structures. Hence inhomogeneous structures are potentially better candidates for experimental study than homogeneous structures. It is hoped that our work will provide a stimulus for more experimental work in this field.

References

1. D. W. Bereman, Phys. Rev. 163 , 855 (1967)
2. R. K. Chang and T. E. Furtak, "Surface Enhanced Raman Scattering" (Plenum, New York, 1981)
3. J. I. Gersten and A. Nitzan, J. Chem. Phys. 73 , 3023 (1980)
4. R. R. Chance, A. Prock, and R. Silbey, Adv. Chem. Phys. 37 , 1 (1978)
5. J. I. Gersten and A. Nitzan, J. Chem. Phys. 75 , 1139 (1981)
6. D. A. Weitz, A. Z. Genack, T. J. Gramila, and J. I. Gersten, Phys. Rev. Lett. 45 , 355 (1980)
7. D. B. Tanner, A. J. Seivers, and R. A. Buhrman, Phys. Rev. B11 , 1330 (1975)
8. N. D. Lang in "Solid State Physics", ed. by H. Ehrenreich, F. Seitz, and D. Turnabull (Academic, New York, 1973), Vol. 28, p-225
9. W. Kohn and L. J. Sham, Phys. Rev. 140 , A1133 (1965)
10. P. Hohenberg and W. Kohn, Phys. Rev. 136 , B864 (1964)
11. J. R. Smith, Phys. Rev. 181 , 522 (1969)
12. J. I. Gersten, Phys. Rev. 179 , 1 (1969)
13. P. R. Antoniewicz, Phys. Rev. Lett. 32 , 1424 (1974)
14. W. R. Smythe, "Static and Dynamic Electricity" (McGraw-Hill, New York, 1950), 2nd ed., p-210
15. L. W. Bruch and Th. W. Ruyijgrok, Surf. Sci. 79 , 509 (1979)

16. L. I. Schiff, "Quantum Mechanics" (McGraw-Hill, New York, 1972), 3rd ed.

17. P. C. Das and J. I. Gersten, J. Chem. Phys. 76 , 3177 (1982)

CHAPTER II

ELECTROMAGNETIC SHAPE RESONANCES OF A ROUGH SURFACE

II.1 Introduction

"Surface shape resonances" is a term we have coined to describe the resonances which occur on a convoluted surface. The electromagnetic surface shape resonances owe their existence to the geometrical shape of the surface. The two problems, surface effects in small solid state particles and their consequences, and the characterization of surface shape resonances, have some similarity between them, because roughness features on a surface could be thought of as some homogeneous structures (small particles) sitting on a plane surface. The motivation behind this study concerning the electromagnetic properties of rough surfaces lies in the fact that the electrodynamic properties of surfaces with nontrivial shapes has been of considerable interest lately.

It has been found that the optical properties of molecules in the vicinity of rough surfaces or surfaces deliberately prepared with undulations or "posts" differ markedly from those of isolated molecules or molecules near smooth surfaces. It is now believed that a significant part of the phenomenon of SERS is associated with an enhanced local field [1]. In addition, observation of fluorescence anomalies [2] and even nonlinear phenomena at weak field

strengths [3] lend credence to the importance of the enhancement of the local fields. It is shown here that the origin of the strong local field is due to the excitation of a surface electromagnetic shape resonance and we study its properties.

Gersten and Nitzan [4] have modelled a rough surface as a set of hemispheroidal protrusions sticking out of the base plane. The bumps were endowed with a dielectric function characteristic of the bulk metal. It was found that the plasmon frequency of the bump was a sensitive function of the aspect ratio of the spheroid, and hence of the surface roughness. The substrate was assumed to be a pefect conductor. Therefore, surface plasma oscillations of the substrate were absent. However, if the substrate consists of a general dielectric material, it can support travelling surface plasmon modes. The bump plasmon is a localized state whereas the surface plasmon is a running wave, which is delocalized over the surface of the substrate. In the absence of retardation effects, therefore, the excitation spectrum consists of a continuum of propagating states and a discrete set of localized states. These excitations are uncoupled. The low-lying discrete states are characterized by having large field amplitudes in the neighborhood of a surface protrusion. The higher-lying discrete states have significant field amplitudes over a localized region of the surface around the bump.

The discrete states are the "bump" plasma oscillations, in the case of a metal, and "bump" vibrations of the lattice, in the case of an insulator or semiconductor whose ions are vibrating. In the case of electronic excitations the continuum states of interest are of three types: (i) the surface plasmons, (ii) the photons, and (iii) the resistive loss spectrum consisting of phonons at low momentum transfer and electron-hole pairs at high momentum transfers. Weber and Ford [5] have considered such excitations in the context of SERS. We point out here that our study is restricted to a bare (but rough) surface without any molecular adsorbate. In the case of ionic excitations of an insulator or semiconductor the continuum states of interest are surface phonons, photons, and other bulk phonons which may be excited through anharmonic couplings. Naturally more complicated situations where phonons and plasmons must be jointly considered, can be treated.

Let us focus our attention on the electronic excitation case, and restrict ourselves to the case of surface plasmons. The energy-wave-vector dispersion curve for a surface plasmon is shown in Fig.II.1(a). The dispersion curve is basically flat (except for effects due to nonlocality at very large wave vectors, $\vec{k}_{//}$). At small wave vectors retardation effects set in and the curve falls towards zero. The energies of the discrete states (Fig.II.1(b)) lie below the energy of the surface plasmon in

the large $\vec{k}_{//}$ - region . In the small $\vec{k}_{//}$ domain, they will be degenerate with some plasmon states. Thus we have a situation where a discrete localized state is coupled with a continuum of delocalized states. This occurs when the electric dipole of the bump couples with the electric field of the extended surface plasmons. The discrete state broadens into a resonance. We thus have a situation, in which the localized state develops a finite lifetime and hence we have our surface shape resonance.

Coupling to resistive losses causes a deacy of the localized state, whereby the energy of the localized state goes into Ohmic heating of the dielectric. Such energy deposition is relatively short ranged and is shown not to be severely sensitive to the surface shape. On the other hand decay into surface plasmons and photons are long range energy deposition mechanisms. Thus, although all three decay channels will be studied, it is the latter two that are of primary interest.

In the following sections we derive expressions for the resonance frequency as a function of the shape of the bump, and calculations are given for the decay rates into photons and surface plasmons. Before a final section on results and discussion is added we briefly discuss a general case (InSb), where both electronic and ionic excitations are important.

The basic principles involved in the following calculation are illustrated for the case of an isolated sphere in Appendix C.

II.2 Frequencies of Shapr Resonances

The model to be considered consists of a dielectric half space with a hemisheroidal protrusion. The dielectric constant of the solid is $\epsilon(\omega)$ and is, in genral, complex. The semi axis of the protrusion perpendicular to the plane is denoted by a and semi axis on the surface plane (radius) by b. The case a=b corresponds to a hemispherical bump and has already been treated by Berreman [6], and recently by Ruppin [7], in the context of SERS. We assume a and b to be very small compared to the wave length of light, so that retardation effects are small, and may be taken into account perturbatively.

The frequencies of the shape resonances are determined by solving Laplace's equation subject to the appropriate boundary conditions. The problem is solved in prolate spheroidal coordinates (ξ , η , ϕ). We introduce a scale size parameter $f=(a^2-b^2)^{1/2}$ and a shape parameter $\xi_0 = a/f$. Our attention will be limited to the case of axially symmetric modes of excitation, although azimuthally excited states also exist. For the sake of generality let us assume for now that an external electric field E_0 is applied perpendicular to the surface.

The geometry of the problem is illustrated in Fig.II.2. Three regions are depicted: I, II, and III. The potential in these three regions is expandable in terms of Legendre functions of the first and second kind, P_n and Q_n, respectively:

$$\Phi_I = \sum_n A_n P_n(\xi) P_n(\eta) \quad , \qquad \text{(II.1a)}$$

$$\Phi_{II} = \sum_n B_n Q_n(\xi) P_n(\eta) - E_0 f P_1(\xi) P_1(\eta) , \qquad \text{(II.1b)}$$

$$\Phi_{III} = \sum_n C_n Q_n(\xi) P_n(\eta) - E_1 f P_1(\xi) P_1(\eta) . \qquad \text{(II.1c)}$$

The coefficients A_n, B_n, C_n, and E_1 are determined by matching appropriate boundary conditions at the surfaces. The surfaces of interest are defined by $\xi = \xi_0$ for $0 < \eta < 1$, $\eta = 0$ for $\xi_0 < \xi < \infty$, and $\xi = \xi_0$ for $-1 < \eta < 0$. The last surface corresponds to a fiduciary surface in the dielectric while the former two surfaces correspond to real dielectric-vacuum boundaries. The following equations are obtained by matching Φ and the normal component of the electric displacement vector across the surfaces.

$$\sum_n A_n P_n(\xi_0) P_n(\eta) = \sum_n B_n Q_n(\xi_0) P_n(\eta) - E_0 f \xi_0 P_1(\eta) , \qquad \text{(II.2a)}$$

$$\epsilon \sum_n A_n P_n'(\xi_0) P_n(\eta) = \sum_n B_n Q_n'(\xi_0) P_n(\eta) - E_0 f P_1(\eta) , \qquad \text{(II.2b)}$$

$$\sum_n A_n P_n(\xi_0) P_n(\eta) = \sum_n C_n Q_n(\xi_0) P_n(\eta) - E_1 f P_1(\xi_0) P_1(\eta) , \quad \text{(II.2c)}$$

$$\sum_n A_n P_n'(\xi_0) P_n(\eta) = \sum_n C_n Q_n'(\xi_0) P_n(\eta) - E_1 f P_1(\eta), \quad \text{(II.2d)}$$

$$\sum_n B_n Q_n(\xi) P_n(0) - E_0 f P_1(\xi) P_1(0) = \sum_n C_n Q_n(\xi) P_n(0) - E_1 f P_1(\xi) P_1(0), \quad \text{(II.2e)}$$

$$\sum_n B_n Q_n(\xi) P_n'(0) - E_0 f P_1(\xi) P_1'(0) = \epsilon \sum_n C_n Q_n(\xi) P_n'(0) - \epsilon E_1 f P_1(\xi) P_1'(0) . \quad \text{(II.2f)}$$

Eqs.(II.2a) and (II.2b) hold for $0 < \eta < 1$ while (II.2c) and (II.2d) hold for $-1 < \eta < 0$ .Eqs (II.2e) and (II.2f) are valid for $\xi = \xi_0$. Eqs. (II.2a)-(II.2f) may be thought of as generalizations of the corresponding equations derived by Berreman [6] for the case of a hemispherical bump. The purpose of our calculation here is two fold. Besides obtaining the resonance frequencies of the bump, we are interested in finding out the natural decay rate, Γ_e, of the localized bump-plasmon modes due to local heating; i.e. resistive losses due to scattering of electrons from other electrons, phonons, and may be from impurities.

The system dipole moment, μ , is obtained by examining the asymptotic nature of Φ_{II} as $\xi \to \infty$.

$$\Phi_{II} \xrightarrow{\xi \to \infty} B_1 Q_1(\xi) \eta \longrightarrow \frac{B_1 \eta}{3\xi^2} = \frac{B_1 f^2}{3} \frac{z}{r^3} \equiv \mu \frac{z}{r^3} . \quad \text{(II.3)}$$

Hence we find the dipole to be

$$\mu = \frac{B_1 f^2}{3} \quad , \qquad \text{(II.4)}$$

evidencing the simple relationship between the dipole moment and the coefficient B_1.

Let us proceed to obtain expressions for the various expansion coefficients. Multiplying Eq. (II.2a) by $P_j(n)$ and integrating over η for $0 < \eta < 1$ gives

$$\int_0^1 d\eta\, P_j(\eta) \sum_n \left\{ A_n P_n(\xi_0) - B_n Q_n(\xi_0) + E_0 f\, \xi_0 \delta_{n1} \right\} P_n(\eta) = 0 \quad . \qquad \text{(II.5)}$$

Defining

$$X_{jn} \equiv \int_0^1 d\eta\, P_j(\eta)\, P_n(\eta) \quad , \qquad \text{(II.6)}$$

Eq. (II.5) can be written as

$$\sum_n \left[A_n P_n(\xi_0) - B_n Q_n(\xi_0) + E_0 f\, \xi_0 \delta_{n1} \right] X_{jn} = 0 \quad . \qquad \text{(II.7)}$$

Values of X_{jn} have been tabulated by Berreman [6].
Likewise, from Eq. (II.2b) we find

$$\sum_n \left[A_n P_n(\xi_0) - B_n Q_n(\xi_0) + E_0 f\, \xi_0 \delta_{n1} \right] X_{jn} = 0 \quad . \qquad \text{(II.8)}$$

Introducing

$$Y_{jn} \equiv \int_{-1}^{0} d\eta\, P_j(\eta) P_n(\eta) = (-)^{j+n} X_{jn} \quad , \qquad \text{(II.9)}$$

we may write Eqs.(II.2c) and (II.2d) as

$$\sum_n \left[A_n P_n(\xi_0) - C_n Q_n(\xi_0) + E_1 f\, \xi_0 \delta_{n1} \right] Y_{jn} = 0 \quad , \qquad \text{(II.10)}$$

and

$$\sum_n \left[A_n P_n'(\xi_0) - C_n Q_n'(\xi_0) + E_1 f\, \delta_{n1} \right] Y_{jn} = 0 \quad . \qquad \text{(II.11)}$$

Since Eqs.(II.2e) and (II.2f) must be true for a continuous range of ξ , it follows that

$$B_n P_n(0) = C_n P_n(0) \quad . \qquad \text{(II.12)}$$

Our knowledge that $P_n(0) \neq 0$ for n even gives us

$$B_n = C_n \quad , \quad n=0,\ 2,\ 4,\ldots\ldots \qquad \text{(II.13)}$$

Also

$$B_n P_n'(0) = C_n P_n'(0) \quad . \qquad \text{(II.14)}$$

$P_n'(0)$ is zero for n even and nonzero for n odd. Hence we get

$$B_n = \epsilon\, C_n \,, \quad n=1, 3, 5, \ldots\ldots \qquad \text{(II.15)}$$

Finally the internal electric field, E_1, is given by

$$E_1 = E_0/\epsilon \quad . \qquad \text{(II.16)}$$

Eqs.(II.13) and (II.15) connecting coefficients B_n and C_n can be combined and written as

$$C_n = \frac{B_n}{2}\left\{(1+\epsilon^{-1}) + (-)^n(1-\epsilon^{-1})\right\} \quad . \qquad \text{(II.17)}$$

We also note that

$$X_{jn} + Y_{jn} = \frac{2\delta_{jn}}{2n+1} \quad , \qquad \text{(II.18)}$$

and hence from Eqs.(II.7) and (II.10) one obtains

$$\frac{2}{2j+1} A_j P_j(\xi_0) = \sum_n \left[B_n Q_n(\xi_0) X_{jn} + C_n Q_n(\xi_0) Y_{jn} \right] - f\xi_0 E_0 X_{j1} - E_1 f \xi_0 Y_{j1} \quad . \qquad \text{(II.19)}$$

Similar manipulations of Eqs.(II.8) and (II.11) gives us

$$\frac{2}{2j+1} A_j P_j'(\xi_0) = \sum_n \left[B_n \epsilon^{-1} Q_n'(\xi_0) X_{jn} + C_n Q_n'(\xi_0) Y_{jn} \right] - E_0 f \epsilon^{-1} X_{j1} - E_1 f\, Y_{j1} \quad . \qquad \text{(II.20)}$$

Noting that

$$X_{j1} + Y_{j1} = \frac{2\delta_{j1}}{3} \quad , \tag{II.21}$$

and dividing Eq.(II.20) by (II.19), a few simple algebraic manipulations leads us to the following equation for the coefficients B_n:

$$\begin{aligned} \sum_n B_n X_{jn} \Big\{ & \left[Q_n(\xi_0) P_j'(\xi_0) - \epsilon^{-1} Q_n'(\xi_0) P_j(\xi_0) \right] + \\ & \frac{(-)^{j+n}}{2} \left[Q_n(\xi_0) P_j'(\xi_0) - Q_n'(\xi_0) P_j(\xi_0) \right] \\ & \left[(1+\epsilon^{-1}) + (-)^n (1-\epsilon^{-1}) \right] \Big\} \\ = f \xi_0 E_0 & \left[P_j'(\xi_0) X_{j1} \left(1 - \frac{(-)^j}{\epsilon} \right) - \frac{2\delta_{j1}}{3} \right] . \end{aligned} \tag{II.22}$$

Finally this is written in the form

$$\sum_n T_{jn} B_n = R_j \quad , \tag{II.23}$$

where

$$\begin{aligned} T_{jn} = X_{jn} \Big\{ & \left[Q_n(\xi_0) P_j'(\xi_0) - \epsilon^{-1} Q_n'(\xi_0) P_j(\xi_0) \right] \\ & + \frac{(-)^{j+n}}{2} \left[Q_n(\xi_0) P_j'(\xi_0) - Q_n'(\xi_0) P_j(\xi_0) \right] \\ & \left[(1+\epsilon^{-1}) + (-)^n (1-\epsilon^{-1}) \right] \Big\} , \end{aligned} \tag{II.24}$$

and

$$R_j = E_0 f \xi_0 \left\{ P_j'(\xi_0) X_{j1} \left[1 - (-)^j \epsilon^{-1} \right] - \frac{2}{3} \delta_{j1} \epsilon^{-1} \right\} . \tag{II.25}$$

Eq. (II.23) is to be solved for B_n. A formal solution for B_n is obtained in the form

$$B=T^{-1}R \qquad \text{(II.26)}$$

where T^{-1} denotes the inverse to the T-matrix. The coefficient A_j are then given by

$$A_j = \frac{(j+\frac{1}{2})}{P_j(\xi_0)}\left\{\sum_n\left[B_nQ_n(\xi_0)X_{jn}+C_nQ_n(\xi_0)Y_{jn}\right]\right.$$
$$\left. - f\xi_0E_0X_{j1}+E_0f\epsilon^{-1}\xi_0(-)^jX_{j1}\right\} \quad , \qquad \text{(II.27)}$$

where B_n and C_n are given by Eqs. (II.26) and (II.17). We consider the natural oscillations of the system. Hence the condition that a nonzero amplitude exist even when $E_0=0$ is obeyed. In this case R_j vanishes and the nonvanishing set of B_n are obtained by equating the secular determinant to zero, i.e.

$$\Delta(\omega) = \det T = 0 \quad . \qquad \text{(II.28)}$$

This is the condition for a surface shape resonance. The roots of this equation are denoted by $\omega = \omega_r$.

We now calculate the natural decay rate of the vibrational modes of the bump due to local heating, i.e. excitations disappearing into local (energy deposition) excitations. In the case of electronic excitations these are

from inelastic electron scattering (resistive losses) and in the case of ionic excitations these are low frequency phonons. In either case the theory is developed in such a way that only the dielectric constant will enter the formulas.

In principle the ω_r roots are complex numbers, because ϵ and hence T are generally complex quantities. The real part of ω_r is the resonance frequency and the imaginary part is proportional to the decay rate into "local" excitations. Hence, if the imaginary part of ϵ is small, one may define the resonance frequencies by the condition

$$\text{Re} \quad \Delta (\omega_r) = 0 \quad . \qquad \text{(II.29)}$$

We then expand $\Delta(\omega)$ around the shape resonance:

$$\Delta(\omega) = \Delta(\omega_r) + (\omega-\omega_r)\left[\frac{\partial\Delta(\omega)}{\partial\omega} \right]_{\omega_r} + \cdots\cdots \qquad \text{(II.30)}$$

or

$$\Delta(\omega) \simeq \text{Re}\, \Delta'(\omega_r)\left\{(\omega-\omega_r) + \frac{i\, \text{Im}\, \Delta(\omega_r)}{\text{Re}\, \Delta'(\omega_r)} \right\} \qquad \text{(II.31)}$$

which may be interpreted as

$$\Delta(\omega) \sim (\omega-\omega_r) + \frac{i\,\Gamma_e}{2} \quad , \qquad \text{(II.32)}$$

where Γ_e is the desired decay rate

$$\Gamma_e = \frac{2\ \mathrm{Im}\ \Delta(\omega_r)}{\mathrm{Re}\ \Delta'(\omega_r)} \quad . \qquad \text{(II.33)}$$

In order to determine the absolute magnitude of the dipole moment of the surface shape resonance, we introduce the following normalization condition. Note that the power delivered to "local" excitations is

$$P_e = \hbar\omega_r \Gamma_e \quad , \qquad \text{(II.34)}$$

where $\hbar\omega_r$ is the energy corresponding to one quantum of bump excitation. The power is obtained also from the expression for Joule heating

$$P_e = \int \frac{\sigma}{2} |\vec{E}|^2 d\vec{r} \quad , \qquad \text{(II.35)}$$

where σ is the conductivity of the solid and the integral extends over the entire solid. In terms of the potentials, Eq.(II.35) can be written as

$$P_e = \frac{\sigma}{2}\int_{S_1} dS_1 \frac{\Phi_I^*}{h_{\xi_o}} \frac{\partial \Phi_I}{\partial \xi_o} + \frac{\sigma}{2}\int_{S_2} dS_2 \frac{\Phi_{III}^*}{h_{\eta_o}} \frac{\partial \Phi_{III}}{\partial \eta_o} \quad , \qquad \text{(II.36)}$$

where we have integrated by parts and employed Laplace's equation. Surfaces S_1 and S_2 are specified by

$$S_1 : \quad \xi = \xi_o \ , \quad 0 < \eta < 1 \ , \quad 0 < \phi < 2\pi \ , \qquad \text{(II.37a)}$$

and

$$S_2 : \xi_0 < \xi < \infty, \quad \eta = 0 \quad , \quad 0 < \phi < 2\pi \quad . \qquad \text{(II.37b)}$$

In Eq. (II.36) h_{ξ_0} and h_{η_0} refer to the standard curvilinear metric coefficients. The surface area elements are $ds_1 = h_{\eta_0} h_\phi \, d\eta \, d\phi$ and $ds_2 = h_{\xi_0} h_\phi \, d\xi \, d\phi$. Hence integration of Eq. (II.36) in the variable ϕ yields

$$P_e = \sigma \pi f (\xi_0^2 - 1) \int_0^1 d\eta \, \Phi_I^* \, \frac{\partial \Phi_I}{\partial \xi_0} + \sigma \pi f \int_{\xi_0}^{\infty} d\xi \, \Phi_{III}^* \, \frac{\partial \Phi_{III}}{\partial \eta_0} \quad . \qquad \text{(II.38)}$$

Integrals in the above equation, when expressions for Φ_I and Φ_{III} in the absence of external field are substituted, take the forms

$$\int_0^1 d\eta \, \Phi_I^* \, \frac{\partial \Phi_I}{\partial \xi_0} = \sum_{n,\nu} A_n^* A_\nu P_n(\xi_0) P_\nu'(\xi_0) \chi_{n\nu} \qquad \text{(II.39)}$$

and

$$\int_{\xi_0}^{\infty} d\xi \, \Phi_{III}^* \, \frac{\partial \Phi_{III}}{\partial \eta_0} = \int_{\xi_0}^{\infty} d\xi \sum_{n,\nu} \left[C_n^* C_\nu Q_n(\xi) Q_\nu(\xi) P_n(0) P_\nu'(0) \right]. \qquad \text{(II.40)}$$

Finally defining

$$I_{n\nu} \equiv \int_{\xi_0}^{\infty} d\xi \, Q_n(\xi) Q_\nu(\xi) \quad , \qquad \text{(II.41)}$$

we obtain

$$P_e = \sigma \pi f (\xi_0^2 - 1) \sum_{n,\nu} A_n^* A_\nu P_n(\xi_0) P_\nu'(\xi_0) X_{n\nu}$$

$$+ \sigma \pi f \sum_{n,\nu} C_n^* C_\nu P_n(0) P_\nu'(0) I_{n\nu} \quad . \quad \text{(II.42)}$$

Eq.(II.42), along with Eqs.(II.34) and (II.33), will be used as a normalization condition to determine the magnitudes of A_n, B_n, C_n, and the dipole moment, μ .

II.3 Decay to Surface Plasmons

As mentioned earlier, the degeneracy of the frequency ω_r with some surface plasmon frequency allows a decay channel to open up which damps out the local bump excitation. Our goal in this section is two fold. First we wish to study the coupling of a charge to a surface plasmon including the effects of retardation. Calculation of the coupling constant in the electrostatic limit have been given in the literature [8]. A calculation including the effects of retardation has been given for the special case of an electron gas [9]. In the following we give a general derivation of the coupling constant. It expresses the coupling to surface plasmons solely in terms of the dielectric function. In the limit where the dielectric constant is that of an electron gas, the expression reduces to that obtained earlier [9]. Since it involves only the dielectric function, it may be applied to more general situations involving ionic excitations or many body effects.

The second goal of this section is to derive a formula for the decay rate of the surface shape resonance to surface plasmon modes.

First the calculation of the power delivered by the surface shape resonance to a classical surface plasma wave is carried out. On comparing this result with the quantum mechanical calculation, the desired coupling constant is obtained. The rate of decay to surface plasmons is then calculated.

Let us place a test charge on a perfectly flat surface and ignore, for now, the presence of the bump. The test charge is taken to be a sheet of charge of density

$$\rho = \sigma_0 \, \delta(z) \, e^{i(kx - \omega t)} + \text{c.c.} \quad . \quad \text{(II.43)}$$

The continuity equation $\vec{\nabla}.\vec{J} + \partial\rho/\partial t = 0$ is used to obtain the corresponding current

$$\vec{J} = \frac{\sigma_0 \omega}{k} \hat{i} \, \delta(z) \, e^{i(kx - \omega t)} + \text{c.c.} \quad . \quad \text{(II.44)}$$

From Gauss's law

$$\int \vec{D}.\hat{n} \, ds = 4\pi \sigma_0 A \, e^{i(kx - \omega t)} + \text{c.c.} \quad \text{(II.45)}$$

where A is the area of the Gaussian surface chosen, it follows that

$$E_z(0^+) - \epsilon E_z(0^-) = 4\pi \sigma_0 \, e^{i(kx - \omega t)} + \text{c.c.} \quad \text{(II.46)}$$

Eq. (II.46) specifies the discontinuity in D_z due to the sheet of charge. From Ampere's law

$$\oint \vec{\nabla} \times \vec{B} \cdot \hat{n}\, ds = \frac{4\pi}{c} \int \vec{J} \cdot \hat{n}\, ds \quad , \tag{II.47}$$

we get the discontinuity in B_y due to the sheet of current,

$$B_y(0^+) - B_y(0^-) = -\frac{4\pi \sigma_0 \omega}{kc} e^{i(kx-\omega t)} + c.c. \tag{II.48}$$

Maxwell's equations for the system can be written as

$$\vec{\nabla} \cdot \epsilon(z) \vec{E} = 4\pi\rho \quad , \tag{II.49a}$$

$$\vec{\nabla} \cdot \vec{B} = 0 \quad , \tag{II.49b}$$

$$\vec{\nabla} \times \vec{E} = -\frac{1}{c} \frac{\partial \vec{B}}{\partial t} = -\frac{i\omega}{c} \vec{B} \quad , \tag{II.49c}$$

$$\vec{\nabla} \times \vec{B} = \frac{4\pi}{c} \vec{J} - \frac{i\omega}{c} \epsilon(z) \vec{E} \quad , \tag{II.49d}$$

where the dependence of the fields on frequency is $\vec{E} \sim e^{-i\omega t}$ and $\vec{B} \sim e^{-i\omega t}$. We look for driven wave solutions to these equations:

$$\vec{E} = \vec{E}(z)\, e^{i(kx-\omega t)} + c.c. \tag{II.50}$$

and

$$\vec{B} = B(z)\, e^{i(kx - \omega t)} + c.c. \qquad \text{(II.51)}$$

Substitution of $\vec{E}$ and $\vec{B}$ into Eqs.(II.49a)-(II.49d) then yields

$$B_x = \frac{ic}{\omega} E_y' \quad , \qquad \text{(II.52a)}$$

$$B_y = -\frac{\omega \epsilon(z)}{kc} E_z \quad , \qquad \text{(II.52b)}$$

$$B_z = \frac{kc}{\omega} E_y \quad , \qquad \text{(II.52c)}$$

$$E_x' + ik\left[\left(\frac{\omega}{kc}\right)^2 \epsilon(z) - 1\right] E_z = 0 \quad , \qquad \text{(II.52d)}$$

$$E_y'' + \left[\left(\frac{\omega}{c}\right)^2 \epsilon(z) - k\right] E_y = 0 \quad , \qquad \text{(II.52e)}$$

and

$$E_z' + ikE_x = 0 \quad . \qquad \text{(II.52f)}$$

Surface wave solutions are sought with

$$E_y \sim \begin{cases} e^{-q_+ z} & , \quad z > 0 \\ e^{q_- z} & , \quad z < 0 \end{cases} \qquad \text{(II.53)}$$

where we find

$$q_+ = \left[k^2 - (\omega/c)^2 \right]^{1/2} , \qquad \text{(II.54a)}$$

$$q_- = \left[k^2 - (\omega^2 \epsilon / c) \right]^{1/2} , \qquad \text{(II.54b)}$$

and

$$E_{x+} = -\frac{i}{k} q_+ E_{z+} , \qquad \text{(II.55a)}$$

$$E_{x-} = \frac{i q_-}{k} E_{z-} . \qquad \text{(II.55b)}$$

In these equations the subscripts +, - indicate whether the region concerned is in vacuum or in the solid respectively. The following continuity relations must hold at the interface:

$$B_{z+}(0) = B_{z-}(0) , \qquad \text{(II.56a)}$$

$$B_{x+}(0) = B_{x-}(0) , \qquad \text{(II.56b)}$$

$$E_{x+}(0) = E_{x-}(0) , \qquad \text{(II.56c)}$$

$$E_{y+}(0) = E_{y-}(0) , \qquad \text{(II.56d)}$$

$$E_{z+}(0) - \epsilon E_{z-}(0) = 4\pi \sigma_0 \qquad \text{(II.56e)}$$

$$B_{y+}(0) - B_{y-}(0) = -\frac{4\pi\omega\sigma_0}{Rc} \quad . \tag{II.56f}$$

Conditions (II.56c) and (II.56e) give

$$q_+ E_{z+}(0) + q_- E_{z-}(0) = 0 \quad , \tag{II.57a}$$

$$E_{z+}(0) - \epsilon E_{z-}(0) = 4\pi\sigma_0 \quad . \tag{II.57b}$$

From Eqs.(II.57) and (II.55) we then obtain

$$E_{z\pm}(0) = \pm \frac{4\pi\sigma_0 q_-}{\epsilon q_+ + q_-} \quad , \tag{II.58a}$$

and

$$E_{x\pm}(0) = -\frac{4\pi i\sigma_0 q_+ q_-}{R[\epsilon q_+ + q_-]} \quad . \tag{II.58b}$$

We have taken $E_{y\pm} = 0$ without loss of generality.

The total rate of doing work is given by

$$P = \frac{1}{2}\int \vec{E}^* \cdot \vec{J}\, d\vec{r} \tag{II.59}$$

$$= \frac{8\pi A|\sigma_0|^2\omega}{R^2} \mathrm{Im}\left[\frac{q_+ q_-}{\epsilon q_+ + q_-}\right] \quad , \tag{II.60}$$

where A is the surface area. Let

$$\Lambda(\omega) = \epsilon q_+ + q_- \quad , \tag{II.61}$$

and expand it around the pole defined by

$$\mathrm{Re}\ \Lambda(\omega_s) = 0 \quad , \tag{II.62}$$

so

$$\Lambda(\omega) \simeq \Lambda'(\omega_s)\left[(\omega-\omega_s) + \frac{i\,\mathrm{Im}\,\Lambda(\omega_s)}{\Lambda'(\omega_s)}\right] \quad , \tag{II.63}$$

where ω_s is the resonance frequency. Then if the imaginary part is small,

$$P \simeq \frac{8\pi A\omega|\sigma_0|^2}{k^2}\,\mathrm{Im}\left\{\frac{q_+^s q_-^s}{\Lambda'(\omega_s)\left[\omega-\omega_s + i\,\mathrm{Im}\,\Lambda(\omega_s)/\Lambda'(\omega_s)\right]}\right\}$$

$$\simeq \frac{8\pi A\omega|\sigma_0|^2}{k^2}\,\mathrm{Im}\left\{\frac{q_+^s q_-^s(-i\pi)\,\delta(\omega-\omega_s)}{\Lambda'(\omega_s)}\right\} \quad , \tag{II.64}$$

where

$$\Lambda'(\omega_s) = \left[\frac{\partial\Lambda(\omega)}{\partial\omega_s}\right]_{\omega_s} \quad . \tag{II.65}$$

The quantity ϵ_s is determined from Eq.(II.62) to be

$$\epsilon_s = \frac{k^2}{(\omega/c)^2 - k^2} \quad . \tag{II.66}$$

Since $q_+^s q_-^s = k^2$, we obtain

$$P \simeq 8\pi A|\sigma_0|^2\omega\ \mathrm{Im}\left[-\frac{i\pi\,\delta(\omega-\omega_s)}{\Lambda'(\omega_s)}\right]$$

$$= -8\pi^2 A|\sigma_0|^2\omega\ \mathrm{Re}\frac{1}{\Lambda'(\omega_s)}\,\delta(\omega-\omega_s) \quad . \tag{II.67}$$

This is the work done per unit time by the system on the charge. Hence the power delivered by the charge is

$$P_d^c = 8\pi^2 A |\sigma_0|^2 \delta(\omega-\omega_s) \, Re \, \frac{\omega}{\Lambda'(\omega_s)} \quad . \tag{II.68}$$

After a little algebra we finally obtain

$$P_d^c = \frac{8\pi^2 A \omega_s |\sigma_0|^2 \delta(\omega-\omega_s)}{k \epsilon_s' f_s (-\epsilon_s)^{-1/2} + c^{-1}(1-\epsilon_s)(-1-\epsilon_s)^{1/2}} \quad , \tag{II.69}$$

where

$$f_s = \frac{\epsilon_s - 1}{2\epsilon_s} \tag{II.70}$$

Let us now proceed with a quantum mechanical calculation of the power dissipated into surface plasmons. The plasmon field is written as

$$E_x = \sum_k \gamma_k a_k e^{ikx} + c.c. \quad , \tag{II.71}$$

where a_k is an annihilation operator and γ_k is the appropriate normalization constant. The vector potential A_x is

$$A_x = -i \sum_k \frac{c\gamma_k}{\omega_k} a_k e^{ikx} + c.c. \tag{II.72}$$

The interaction Hamiltonian is

$$H_{int} = -\frac{1}{c}\int \vec{J}\cdot\vec{A}\, d\vec{r} \quad , \tag{II.73}$$

where $\vec{J}$ is given by Eq.(II.44). Thus

$$H_{int} = \frac{i\gamma_k A \sigma_0}{k} a_k + h.c. \quad , \tag{II.74}$$

where we limit our attention to a plasmon with a specific wave vector. Employing Fermi's "golden rule" the dissipated power is

$$P_d^q = \frac{2\pi\omega}{\hbar}\,\frac{|\gamma_k|^2 A^2 |\sigma_0|^2}{k^2}\,\delta(\omega-\omega_s) \quad . \tag{II.75}$$

Comparison of this formula with Eq.(II.69) yields

$$|\gamma_k|^2 = \frac{4\pi\hbar k}{A}\left[f_s \epsilon_s' (-\epsilon_s)^{-1/2} + (1-\epsilon_s)(-1-\epsilon_s)^{1/2}(kc)^{-1}\right]^{-1} \tag{II.76}$$

This formula reduces to that of Elson and Ritchie [9] when the dielectric constant of the free electron gas is employed. The vector potential for a surface plasmon, according to ref. 9 is given by

$$\vec{A}_s = \sum_{\vec{k}}\left(\frac{4\pi\hbar c}{L^2 P_k}\right)^{1/2}\left\{\left(i\hat{k} - \hat{z}\frac{k}{\nu}\right)e^{-\nu z}\Theta(z) + \left(i\hat{k} + \hat{z}\frac{k}{\nu_0}\right)e^{\nu_0 z}\Theta(-z)\right\} e^{i\vec{k}\cdot\vec{\rho}}\left(b_{\vec{k}} + b_{-\vec{k}}\right) \quad , \tag{II.77}$$

where L^2 is the area of the surface, $\vec{k}$ is the propagation vector and $\vec{\rho}$ is a vector in the xy-plane. The magnitude of the propagation vector, $\vec{k}$, is given by

$$K^2 = \left(\frac{\omega}{c}\right)^2 \epsilon \left[1+\epsilon\right]^{-1} \quad , \tag{II.78}$$

where

$$\epsilon = 1 - \left(\omega_p / \omega_k\right)^2 \quad , \tag{II.79}$$

and

$$\omega_k^2 = \frac{\omega_p^2}{2} + c^2K^2 - \left[\left(\frac{\omega_p^2}{2}\right)^2 + \left(cK\right)^4\right]^{1/2} \quad , \tag{II.80}$$

ω_p being the plasmon frequency. ν and ν_o are related to k by

$$\nu^2 = K^2 - \left(\omega_k^2 - \omega_p^2\right)/c^2 \quad , \tag{II.81}$$

$$\nu_o^2 = K^2 - \omega_k^2/c^2 \quad . \tag{II.82}$$

In Eq. (II.77) the quantity P_k is given by

$$P_k = \frac{\epsilon^4 - 1}{\epsilon^2\left[-(\epsilon+1)\right]^{1/2}} \quad , \tag{II.83}$$

and b_k is a surface plasmon annihilation operator. Aside

from a phase factor the vector potential in Eq. (II.72) is given by

$$A_x = \frac{c\gamma_k}{i\omega} \qquad \text{(II.84)}$$

$$\equiv \frac{1}{i}\left[\frac{4\pi\hbar c}{A P_k}\right]^{1/2} . \qquad \text{(II.85)}$$

Eq. (II.85) is obtained by a direct comparison of Eq. (II.84) with Eq. (II.77). Here A is the surface area. Eqs. (II.84) and (II.85) are solved for γ_k, and comparing the result with Eq. (II.76) yields

$$P_k = \frac{\omega}{kc}\left[-\frac{(\epsilon-1)^2}{\epsilon\sqrt{-\epsilon}} + \frac{\omega}{kc}(1-\epsilon)\sqrt{-1-\epsilon}\right] , \qquad \text{(II.86)}$$

where we have used the electronic dielectric function $\epsilon = 1 - \omega_p^2/\omega^2$, whose first derivative with respect to ω gives $\epsilon' = \frac{2}{3}(1-\epsilon)$. From Eq. (II.66) we get

$$\omega = kc\left(\frac{\epsilon+1}{\epsilon}\right)^{1/2} . \qquad \text{(II.87)}$$

Substitution of Eq. (II.87) into Eq. (II.86) then gives

$$P_k = \frac{\epsilon^4-1}{\epsilon^2(-\epsilon-1)^{1/2}} , \qquad \text{(II.88)}$$

which is same as in Eq. (II.83). Hence is the agreement between Eq. (II.76) and the result of Elson and Ritchie [9]

Having accomplished the task of writing the surface plasmon field in quantized form (Eq.(II.71)) we now proceed to calculate the decay rate of the oscillations of a single spheroidal bump on the plane. The bump is characterized by its dipole moment μ which is perpendicular to the surface. This dipole is responsible for "radiation" of surface plasmons along the surface. An expression for this radiation will be obtained shortly. The dipole is also responsible for radiation of photons into all solid angles. This will be dealt with in the next section.

The interaction of the dipole with the plasmon field is given by

$$H' = -\mu E_{z+} \quad , \qquad \text{(II.89)}$$

where we assume the dipole of the bump to be above the plane. The fields may be obtained from Eqs.(II.55) and (II.71). Thus

$$H' = -i\mu(-\epsilon_s)^{1/2} E_x(0) \quad . \qquad \text{(II.90)}$$

Taking matrix elements of this and employing the Fermi "golden rule" again gives us an expression for the decay rate into surface plasmons:

$$\Gamma_{sp} = \frac{4\pi|\mu|^2}{\hbar}\left(\frac{\omega_0}{c}\right)^3 \frac{(-\epsilon_s)^3}{(-\epsilon_s^{-1})^{5/2}(1-\epsilon_s)} \quad , \qquad \text{(II.91)}$$

where we have set ω_0 equal to the frequency of the surface shape resonance and used $k^2 = \omega_0^2 \epsilon_s/[c^2(\epsilon_s+1)]$.

Equation (II.91) represents the desired result - an expression for the decay rate of the localized excitation into delocalized surface plasmons. In absolute terms it may be calculated since an expression for μ has already been obtained (see Eq.(II.4)).

II.4 Decay to Photons

We have treated the spheroidal bump on a plane surface as a dipole oscillating due to natural electronic charge fluctuations in the system. The coupling of the electric dipole above the surface to the delocalized surface plasmon modes determined part of the decay rate of the localized plasmon mode. Other channels of decay obviously exist, however. One such channel, that of resistive losses, was taken into account in section II.2. In this section we study the decay into photons. This problem has a long history going back to Sommerfeld's study of a radiating dipole antenna on the earth's surface. More recently Chance, Prock, and Silbey [10] have studied the radiation properties of a molecule near a surface. We shall apply their formalism to the problem of a bump on a surface without a nearby molecule.

For a dipole oriented perpendicular to the interface the decay rate is given, in the dipole approximation, by

$$\hat{\Gamma}_{rad} = q - \frac{3}{2} q \, Im \int_0^1 R^{\parallel} e^{-2\ell_1 \hat{d}} \frac{u^3}{\ell_1} du \quad , \quad \text{(II.92)}$$

where

$$R^{\parallel} = \frac{\epsilon_1 \ell_2 - \epsilon_2 \ell_1}{\epsilon_1 \ell_2 + \epsilon_2 \ell_1} \quad , \tag{II.93}$$

$$\ell_j = -i\left[\frac{\epsilon_j}{\epsilon_1} - u^2\right] \quad , \quad j = 1, 2 \quad , \tag{II.94}$$

$$\hat{d} = k_1 d \quad , \quad k_1 = \frac{\omega}{c} n_1 \quad , \quad n_1 = \sqrt{\epsilon_1} \quad , \tag{II.95}$$

and

$$q = \frac{\Gamma_{rad}}{\Gamma_o} \tag{II.96}$$

Here d is the distance of the dipole from the surface, $\vec{k}_1$ is the propagation vector in the medium 1, and ϵ_1 and ϵ_2 are the dielectric functions of medium 1 and 2 respectively. The radiative quantum yield of the system, q, is the ratio of the radiative decay rate to the total decay rate of the bump. The hat on Γ_{rad} in Eq. (II.92) indicates that the decay rate is normalized to that in the absence of the surface. In our case $\epsilon_1 = 1$ and $\epsilon_2 = \epsilon(\omega)$. Hence $k_1 = \omega/c$ and carrying out the integration yields

$$\Gamma_{rad} = \Gamma_{rad}^{free}\left[1 + \frac{3}{2}\int_0^{\frac{\pi}{2}} d\theta \, \frac{\sin^3\theta}{(\epsilon-1)\left[(\epsilon+1)\cos^2\theta - 1\right]}\right.$$
$$\left\{\left[(\epsilon^2+1)\cos^2\theta + (\epsilon-1)\right]\cos(2k_1 d\cos\theta) + \right.$$
$$\left.\left. 2\epsilon\cos\theta\left(\sin^2\theta - \epsilon\right)^{1/2}\sin(2k_1 d\cos\theta)\right\}\right] . \tag{II.97}$$

From the classical theory of radiation, the free radiative decay rate is

$$\Gamma_{rad}^{free} = \frac{|\mu|^2 \omega^3}{3c^3} \tag{II.98}$$

Combining Eqs.(II.97) and (II.98) and employing atomic units we find

$$\Gamma_{rad} = \frac{|\mu|^2 \omega^3}{3c^3}\left[1 + \frac{3}{2}\int_0^{\frac{\pi}{2}} d\theta \, \frac{\sin^3\theta}{(\epsilon-1)\left[(\epsilon+1)\cos^2\theta - 1\right]}\right.$$
$$\left\{\left[(\epsilon^2+1)\cos^2\theta + (\epsilon-1)\right]\cos\left(2\frac{\omega}{c}d\cos\theta\right) + \right.$$
$$\left.\left. 2\epsilon\cos\theta\left(\sin^2\theta - \epsilon\right)^{1/2}\sin\left(2\frac{\omega}{c}d\cos\theta\right)\right\}\right] . \tag{II.99}$$

At small distances, i.e. $k_1 d \ll 1$, we write Eq.(II.99) approximately as

$$\Gamma_{rad} = \frac{|\mu|^2 \omega^3}{3c^3}\left[1 + \frac{3}{2}\int_0^{\frac{\pi}{2}} d\theta \, \frac{\sin^3\theta}{(\epsilon-1)\left[(\epsilon+1)\cos^2\theta - 1\right]}\right.$$
$$\left.\left\{(\epsilon^2+1)\cos^2\theta + (\epsilon-1)\right\}\right] \tag{II.100}$$

The integral is evaluated by numerical quadrature.

II.5 Surface Shape Resonances in InSb

Here we present numerical results of the shape resonance characteristics of a rough surface of InSb, which is modelled to be a spheroidal bump protruding from the plane of the substrate. We determine the decay rates, Γ , of the bump vibrations into various decay channels, as has been discussed earlier.

The elctromagnetic surface shape resonances are brought about by the coupling of the discrete bump states to the delocalized excitations propagating on the surface of the smooth substrate. The delocalized excitations considered so far were those of surface plasmons, photons, and resistive loss mechanisms in the case of electronic excitations. However, in ionic solids and insulators, lattice excitations are important and then the delocalized modes are surface phonons, photons, and acoustic phonons. Acoustic phonon excitations, like resistive losses in the case of electronic solids, is an energy deposition mechanism.

In a semiconductor, such as InSb, one would expect both electronic and ionic excitations to be present. So both surface plasmons and surface phonons are taken into account while considering shape resonances. Obviously more complicated processes involving the couplings between electronic and ionic excitations, may contribute. We limit ourselves, however, to the uncoupled situation and work in the no retardation limit as before.

Our goal here is to determine the widths of the appropriate resonances, whose frequencies are a sensitive function of the shape of the bump, for the case of InSb and consequently examine if it can be chosen as an experimental sample for testing these effects.

The general analytic procedure remains the same as that described in earlier sections for the case of Ag. We work

under the same assumption that $\epsilon_2 \ll \epsilon_1$, where ϵ_1 and ϵ_2 are the real and imaginary parts of the dielectric function, ϵ, of the medium. In our study of shape resonances of Ag, ϵ was chosen to be electronic and was fitted to the experimental data of Johnson and Christy [11]. In this case the system is characterized by a model dielectric function [12]

$$\epsilon(\omega) = \epsilon_\infty \left\{ 1 - \frac{\omega_p^2}{\omega^2 + i\omega\tau_e^{-1}} + \frac{\omega_L^2 - \omega^2 - i\omega\tau_n^{-1}}{\omega_T^2 - \omega^2 - i\omega\tau_n^{-1}} \right\} \quad \text{(II.101)}$$

This $\epsilon(\omega)$ has contributions from both electronic and ionic excitations. Here ϵ_∞ is the high frequency optical dielectric constant, ω_p is the electronic plasma frequency, ω_T and ω_L are the transverse and longitudinal phonon frequencies respectively, and τ_e^{-1} and τ_n^{-1} are the respective electronic and ionic damping parameters.

The results of this numerical study will be presented in the following section.

II.6 Results and Discussion

In the previous sections we have derived formulas for the frequency of a surface shape resonance and its decay rate into various excitations of interest. Before stating the results and discussing them, let us consider the calculational procedure.

In our calculation we restricted our attention to the case where Im ϵ was sufficiently small to allow it to be treated as a perturbation parameter. This assumption is somewhat restrictive but is valid for some metals, e.g. Ag, at optical frequencies. The restriction may be lifted in a straightforward manner, however.

The eigenfrequencies are determined as roots of the determinant of the T matrix defined by Eq.(II.24). In principle the T matrix is of infinite dimension. In practice one truncates the size of the matrix and checks for convergence of the roots as the size is increased. The low lying frequencies converge rapidly while the higher frequencies converge more slowly. A ten by ten matrix was used in this numerical work. In determining the T matrix only the real part of ϵ was used.

The eigenvectors of the T matrix (see Eq.(II.23) with $R_j=0$) were obtained by solving the appropriate set of linear equations and imposing the normalization condition defined by Eqs(II.33), (II.34), and (II.42). Use was made of the following expansion for the determinant of the T matrix for small Im ϵ :

$$\det T \approx (\det T_1)\left[1 - i\epsilon_2 \epsilon_1^{-1} Tr\left(T_1^{-1} G\right)\right] \quad , \text{(II.102)}$$

where T_1 is the T matrix defined with real ϵ and

$$G_{jn} = X_{jn}\left\{ - Q_n'(\xi_0) P_j(\xi_0) + \frac{(-)^{j+n}}{2}\left[Q_n(\xi_0) P_j'(\xi_0) - Q_n'(\xi_0) P_j(\xi_0)\right]\left[1 - (-)^n\right]\right\} \quad . \text{(II.103)}$$

The calculations done here are for silver protrusions sticking out of a silver metal half-space. We will not be concerned with how the surface shape resonance is excited, although a number of methods can be designed. One is through the use of optical radiation impinging on the surface. Another is through the use of an incident electron or ion beam. The excitation of the resonance may readily be monitored through the secondary radiation that is produced. In the case of charged projectiles it may also be seen in the electron energy loss spectrum.

One way of characterizing the shape resonance is through the value of the real part of the dielectric constant at the resonance frequency. In table II.2 the low lying azimuthally symmetric shape resonances are studied as a function of the aspect ratio of the bump, a/b. The lowest lying resonance occurs at a dielectric constant given by ϵ_r^0. The first excited state occurs at ϵ_r^1 and the second excited state (which is azimuthally symmetric) occurs at ϵ_r^2. The excited states correspond to excitations with nodes of potential on the solid's surface while the ground state is nodeless. The general trend is for ϵ to get more negative as the aspect ratio is increased. This is in qualitative agreement with previous studies of isolated spheroids. The magnitude of ϵ, however, is less than that of the corresponding isolated spheroid with the same aspect ratio. It should be emphasized that the numbers presented in table II.2 are universal numbers, valid for any metal or dielectric.

The numbers in table II.2 are translated into frequencies by using the optical data of the material of interest. For Ag the optical constants of Johnson and Christy [11] were used to obtain the resonance frequencies.

In Fig. II.3 a plot is made of the resonant frequency as a function of the aspect ratio for fixed a ($a=200\ a_0$). Two curves are shown: one for the ground state and one for the first excited state. The data is for Ag. As the aspect ratio is increased in magnitude the frequencies of the excitations fall off. Again this is similar to the behavior of isolated spheroids.

Fig. II.4 shows the magnitude of the dipole moment of the system as a function of the aspect ratio a/b for fixed a ($a=200\ a_0$). The upper curve is for the ground state and the lower curve is for the first excited state. It should be noted that the size of the electric dipole moment is very large. This follows from a comparison of the classical and quantum expressions for dipole moments and dipole transition moments. In classical electrodynamics the polarizability of an object is proportional to its volume. Thus, for example, for a sphere $\alpha \sim a^3$, where a is the radius. In the quantum mechanical expression for α one has a sum of terms of the form $\alpha \sim \mu^2/\Delta\omega$, where $\Delta\omega$ is a frequency difference. Simply equating these expressions and letting $a=200\ a_0$, $\hbar\Delta\omega = 3$ eV gives $\mu \approx 10^3\ ea_0$, in agreement with the calculated magnitude.

Fig. II.5 shows the strength of the dipole moment growing as function of axis size for fixed aspect ratio. The three curves correspond to the three most low lying states. As the size of the bump increases, one expects an increase in μ according to the argument just given. The ground state, being nodeless, would be expected to have the largest dipole. The presence of nodes in the excited states causes some degree of cancellation with a subsequent reduction in dipole strength.

In Fig. II.6 we consider the various damping rates, expressed in units of the resonance frequency, for the ground state surface shape resonance, as a function of aspect ratio for fixed $a=200\ a_0$. As the aspect ratio increases the decay rate to frequency ratio for inelastic electron scattering channels remains fairly constant while that for surface plasmons or photons falls off.

Fig. II.7 gives the same ratios as in Fig. II.6, but plotted as a function of the axis a, for fixed aspect ratio ($a/b=2$). It is seen that the radiation into surface plasmons and photons grows substantially with size, whereas the resistive loss rate remains constant. For large sizes ($a \geq 200\ a_0$) the long range energy deposition mechanisms dominate over the resistive loss mechanism and are the main source of the limited Q of the resonance.

Fig. II.8 shows a plot of the radiative yield of the ground and first excited shape resonances as a function of

size for fixed aspect ratio. As one might expect, the radiative yield grows with increasing size. Fig. II.9 shows the same yield as a function of aspect ratio for fixed $a=200\ a_0$. The falloff with increasing a/b is probably due to the reduction in the volume of the bump, and hence of the dipole moment.

It is therefore concluded that a surface with a protrusion possesses a set of shape resonances whose frequencies and damping rates are determined solely by the geometric and dielectric properties of the system.

We now proceed to discuss the results obtained for the case of InSb. The calculational as well as numerical procedures resemble exactly to that for Ag, since similar assumptions have been made. ϵ_1 and ϵ_2 are obtained from Eq.(II.101) with the use of the following parametric values for InSb [12]: $\tau_e^{-1}=30\ cm^{-1}$, $\tau_n^{-1}=2.7\ cm^{-1}$, $\omega_T=179\ cm^{-1}$, $\omega_p=1028\ cm^{-1}$, $\epsilon_0=17.9$ and $\epsilon_\infty=15.7$. ϵ_0 is the static dielectric constant. ω_L is determined using the relation $\omega_L/\omega_T=[\epsilon_o/\epsilon_\infty]^{1/2}$. Carrying out the numerical calculations we determine the desired decay rates.

In Fig. II.10 we show the resonance frequency ω_r (in eV) as a function of the aspect ratio (a/b), for both the ground and first excited states. Although behavior similar to that of Ag system is exhibited, a comparison between them shows that in the case of InSb, the resonance frequencies are lowered by roughly a factor of 30.

Behavior of the magnitude of the system dipole moment is similar to that of the Ag-system when examined as a function of the shape and size of the bump.

In Fig. II.11 the various decay rates expressed in units of the resonance frequency, for the ground state surface shape resonance, are shown as a function of the aspect ratio, for fixed a=10,000 a_0. With increasing a/b the decay rate to resonance frequency ratio, for local energy deposition mechanisms, remains more or less constant while that for surface plasmons and phonons falls off with the sharpening of the bump. It should be noted that the decay of the bump vibrations going into local heating and acoustic phonons is the dominant mechanism.

Fig. II.12 gives the same ratios as in Fig. II.11, but plotted as a function of a, for fixed aspect ratio (a/b=2). The bump size has to get very large ($>$ 10,000 a_0) before the decay rate to surface plasmons and phonons becomes appreciable.

In conclusion it can be said that rough InSb samples can be used in experiments to test the shape resonance effects, provided the roughness features are of large sizes. Techniques for the preparation of such surfaces are known to exist.

References

1. "Surface Enhanced Raman Scattering", ed. by R. K. Chang and T. E. Furtak (Plenum, New York, 1981)
2. D. A. Weitz, S. Garoff, C. D. Hanson, T. J. Gramila, and J. I. Gersten, Opt. Lett. 7 , 89 (1982)
3. C. K. Chen, A. R. B. deCastro, and Y. R. Shen, Phys. Rev. Lett. 46 , 145 (1981)
   C. K. Chen, T. F. Heinz, D. Ricard, and Y. R. Shen, Phys. Rev. Lett. 46 , 1010 (1981)
4. J. I. Gersten and A. Nitzan, J. Chem. Phys. 73 , 3023 (1980)
5. W. H. Weber and G. W. Ford, Phys. Rev. Lett. 44 , 1774 (1980)
6. D. W. Berreman, Phys. Rev. 163 , 855 (1967)
7. R. Ruppin, Solid State Commun. 39 , 908 (1981)
8. J. I. Gersten, Phys. Rev. 188 , 774 (1969)
9. J. M. Elson and R. H. Ritchie, Phys. Rev. B4 , 4129 (1971)
10. R. R. Chance, A. Prock, and R. Silbey, Adv. Chem. Phys. 37 , 1 (1978)
11. P. B. Johnson and R. W. Christy, Phys. Rev. B6 , 4370 (1972)
12. A. Nitzan and L. E. Brus, J. Chem. Phys. 75 , 2205 (1981)

CHAPTER III

INELASTIC ELECTRON SCATTERING FROM SMALL METAL SPHERES

III.1 Introduction

Until now we have seen that the role of small scale structures is crucial to surface physics. In recent years considerable amount of attention has been given to the study of the interaction of light with small metallic or dielectric particles [1]. A number of anomalous phenomena occur near the surface of a particle interacting with light. Most of these phenomena, namely SERS [2], surface enhanced second harmonic generation [3], and radical fluorescence lifetime alterations [4], have been discussed in the introduction to this thesis. The strong fields of plasma oscillations, of the particle, excited by incident light, cause a modification of the apparent optical properties of nearby molecules.

Another area of growing interest in surface physics is that of electron loss spectroscopy [5]. In principle there should be a connection between electron loss spectroscopy and optical spectroscopy. In the former case it is the coulomb field of the projectile electron that causes the excitation whereas in the latter case it is the optical electromagnetic field itself. It is our goal here, to explore further aspects of this connection.

Some experimentation on small particles, either isolated in vacuum, or levitated by an inhomogeneous magnetic field or by a diverging laser field, or falling freely in the gravitational field, are done at present to investigate the interaction of light with such particles. It is also possible to carry out experiments of a similar sort to investigate the interaction of an electron beam with small particles. We consider below the interaction of an electron beam with a small metallic or dielectric sphere.

The electron beam may scatter off the sphere and excite a localized plasma oscillation on the sphere. The excitation energy would then manifest itself as a discrete energy loss in the electron beam. Our goal here will be to calculate the cross section for inelastic electron scattering from the sphere. Sometimes the small particle under investigation may be attached to an "inert" substrate. By "inert" here we mean that the substrate will not couple strongly to the electron. The case where the small particle is attached to a substrate which couples strongly to the electron beam is of immense interest. This would enable us to devise techniques for analysis of rough surfaces using electron loss spectroscopy. The microscopic mechanisms involved in the interaction of electrons with such general systems, as a rough surface, is obviously complicated. We therefore restrict ourselves to the case of an isolated sphere.

Having assumed that the interaction of an electron with the sphere excites a plasma oscillation, we then ask what happens to the energy that went to exciting them. The oscillation will ultimately decay to various channels depending upon the geometrical configuration of the system. One decay channel is to emit a photon with energy equal to the plasma oscillation energy. It is therefore worthwhile calculating the radiative cross section for the sphere upon excitation by electron impact.

III.2 Excitation of Plasmon by Electron

Consider a sphere of radius a and characterized by a complex dielectric constant, $\epsilon(\omega)$. We consider the scattering of an electron beam from such a sphere. The incident electron provides the energy for the excitation of plasma oscillations on the sphere. We work in the no retardation limit by assuming that the size of the sphere (diameter = 2a) is small compared with the wave length of light corresponding to the plasma oscillation frequency of the sphere. For Ag, the plasma oscillation energy of the sphere is 3.50 eV, so the radius must be such that $a \ll 3500$ Å. On the other hand the sphere is considered macroscopic with well defined dielectric properties.

Since $ka \gg 1$, where k is the wave vector of the incident electron (typically the energy E of the electron, E=100 eV and a=50 Å yields ka=256) wave effects are not important. We therefore assume classical trajectories for such electron

motion. Also we consider electron energies high enough so that the interaction potential with the sphere or the plasma oscillation energy may be neglected relative to it. Hence, to a first approximation the electron is assumed to be travelling on a straight line path with constant speed. A schematic drawing of the scattering geometry appears in Fig. III.1. The trajectory is taken to lie in the z=0 plane. Two situations can occur. One is that the impact parameter of the electron, b, is larger than a, and the other in which b is less than a. In the former case the electron suffers no deflection and follows its linear trajectory. But in the latter case, $b < a$, the electron is assumed to undergo specular reflection with some reflection probability R. If the electron enters the sphere, it will be assumed to vanish from the incident beam, since the mean free path of an electron is likely to be smaller than a.

We now proceed to calculate the probability for the electron to excite a plasmon mode. The plasma oscillation is characterized by the orbital quantum number, l, and the azimuthal projection, m. The second quantized Hamiltonian governing the plasma oscillations and their coupling to electrons is

$$H = \sum_{\ell,m} \hbar\omega_\ell \left[A^\dagger_{\ell m} A_{\ell m} + \tfrac{1}{2} \right] - e\Phi(\vec{r}') \quad , \qquad \text{(III.1)}$$

where A_{lm} is a plasma oscillation annihilation operator

and $\Phi(\vec{r}')$ is the scalar potential field operator at the position of the electron $\vec{r}'(t)$. The trajectory is a given function of time. The plasma oscillation frequency is denoted by ω_l, and is independent of m due to rotational symmetry. The scalar potential may be expanded as

$$\Phi(\vec{r}) = \sum_{l,m} g_{lm} A_{lm} \frac{Y_{lm}(\hat{r})}{r^{l+1}} + h.c. \quad , r > a \qquad \text{(III.2)}$$

where g_{lm} is the generalized Frohlich coupling constant. This g_{lm} is obtained by comparing the classical and quantum mechanical self energies of the system.

Consider the interaction of a charged particle of charge q with the sphere. In the presence of the charge outside the sphere at a distance $\vec{r}'$ from its center, taken as the origin of coordinates, the potentials at any point $\vec{r}$ inside and outside the sphere are given by

$$\Phi_1 = \sum_{l,m} b_{lm} r^l Y_{lm}(\hat{r}) \quad , \quad r < a \qquad \text{(III.3)}$$

$$\Phi_2 = \sum_{l,m} c_{lm} \frac{Y_{lm}(\hat{r})}{r^{l+1}} + \frac{q}{|\vec{r}-\vec{r}'|} \quad , \quad r > a \qquad \text{(III.4)}$$

where b_{lm} and c_{lm} are coefficients of expansion to be determined and $Y_{lm}(r)$ are spherical harmonics. Expanding $1/|\vec{r}-\vec{r}'|$ in terms of spherical harmonics we write Φ_2 as

$$\Phi_2 = \sum_{l,m} c_{lm} \frac{Y_{lm}(\hat{r})}{r^{l+1}} + 4\pi q \sum_{l,m} \frac{r^l}{(2l+1)} \frac{Y^*_{lm}(\hat{r}') Y_{lm}(\hat{r})}{r'^{l+1}} \cdot \qquad \text{(III.5)}$$

Matching potentials and the normal components of the displacement field, D_r, at r=a we can obtain the expansion coefficients:

$$b_{\ell m} = \frac{c_{\ell m}}{a^{2\ell+1}} + \frac{4\pi q}{2\ell+1} \frac{Y^*_{\ell m}(\hat{r}')}{r'^{\ell+1}} \quad , \qquad \text{(III.6)}$$

$$c_{\ell m} = \frac{4\pi q}{2\ell+1} \frac{\ell a^{2\ell+1}(1-\epsilon)}{(\ell\epsilon+\ell+1)} \frac{Y^*_{\ell m}(\hat{r}')}{r'^{\ell+1}} \quad . \qquad \text{(III.7)}$$

The classical self energy of the system, U_c, is given by

$$U_c = \frac{q}{2} \mathrm{Re}\, \tilde{\Phi}(\vec{r}') \quad , \qquad \text{(III.8)}$$

where the tilde indicates that the singular term in the potential Φ_2 is excluded. Substitution of $\tilde{\Phi}(\vec{r}')$ yields

$$U_c = \frac{q}{2} \mathrm{Re}\left\{ \sum_{\ell,m} \frac{4\pi q}{2\ell+1} \frac{\ell a^{2\ell+1}(1-\epsilon)}{(\ell\epsilon+\ell+1)} \left| \frac{Y_{\ell m}(\hat{r}')}{r'^{\ell+1}} \right|^2 \right\} \quad . \qquad \text{(III.9)}$$

To second order in perturbation theory the quantum mechanical self energy of the system is given by

$$\begin{aligned} U_q &= \sum_{\ell,m} \left\{ \left[\langle 0 | q\, g_{\ell m} A_{\ell m} \frac{Y_{\ell m}(\hat{r}')}{r'^{\ell+1}} | \ell m \rangle \langle \ell m | q\, g^*_{\ell m} A^\dagger_{\ell m} \frac{Y_{\ell m}(\hat{r}')}{r'^{\ell+1}} | 0 \rangle \right] / \right. \\ &\qquad \left. [\hbar(\omega - \omega_\ell)] \right\} \\ &= \sum_{\ell,m} |g_{\ell m}|^2 q^2 \left| Y_{\ell m}(\hat{r}')\, r'^{-\ell-1} \right|^2 / [\hbar(\omega-\omega_\ell)] \quad . \end{aligned} \qquad \text{(III.10)}$$

Here $|0\rangle$ and $|1m\rangle$ correspond to the ground and one plasmon (l,m) states respectively. Comparing Eqs.(III.9) and

(III.10) we get

$$g_{\ell m} = \left[\hbar(\omega - \omega_\ell) \, Re \left\{ \frac{2\pi}{2\ell+1} \, \frac{(1-\epsilon) a^{2\ell+1}}{\left(\epsilon + \frac{\ell+1}{\ell}\right)} \right\} \right]^{\frac{1}{2}} . \quad \text{(III.11)}$$

The plasmon resonance frequencies ω_ℓ for a sphere characterized by the dielectric function $\epsilon(\omega)$ are given by

$$\epsilon(\omega) + \frac{\ell+1}{\ell} = 0 \quad . \quad \text{(III.12)}$$

So the denominator in Eq.(III.11) can be written, in the vicinity of the resonance ($\omega \approx \omega_\ell$), as

$$\epsilon(\omega) + \frac{\ell+1}{\ell} \approx 0 + \left(\frac{\partial \epsilon}{\partial \omega} \right)_{\omega_\ell} (\omega - \omega_\ell) \quad . \quad \text{(III.13)}$$

Hence in the near resonance situation the coupling coefficient is given by

$$g_{\ell m} = \left[\frac{2\pi\hbar}{\ell} \, a^{2\ell+1} \, Re \, \frac{1}{\left(\frac{\partial \epsilon}{\partial \omega} \right)_{\omega_\ell}} \right]^{1/2} . \quad \text{(III.14)}$$

The corresponding expression for the potential outside the sphere is

$$\Phi(\vec{r}) = \sum_{\ell,m} \left[\frac{2\pi\hbar}{\ell} \, a^{2\ell+1} \, Re \, \frac{1}{\left(\frac{\partial \epsilon}{\partial \omega} \right)_{\omega_\ell}} \right]^{1/2} A_{\ell m} \, \frac{Y_{\ell m}(\hat{r})}{r^{\ell+1}} + h.c. \quad \text{(III.15)}$$

It should be noted that for a moving electron, r is a function of time t. Thus application of time dependent

perturbation theory with $H_{int} = -e\Phi(r)$, yields the probability of excitation of the (l,m) plasmon, P(l,m):

$$P(l,m) = |S_{lm}|^2 \quad , \tag{III.16}$$

where S_{lm} is the transition amplitude and is given by

$$S_{lm} = ie\left[\frac{2\pi}{l\hbar} a^{2l+1} Re \frac{1}{\left(\frac{\partial \epsilon}{\partial \omega}\right)_{\omega_l}}\right]^{1/2} \int_{-\infty}^{+\infty} \frac{Y^*_{lm}(\hat{r})\, e^{i\omega_l t}}{r^{l+1}(t)}\, dt \quad . \tag{III.17}$$

Case (a)

We consider first the case where b > a. Then

$$\vec{r} = b\hat{i} + vt\hat{j} \quad , \tag{III.18}$$

where v is the speed of the electron. The integral in Eq. (III.17) is readily evaluated in terms of Whittaker functions:

$$\int_{-\infty}^{+\infty} dt\, \frac{Y^*_{lm}(\hat{r})\, e^{i\omega_l t}}{r^{l+1}(t)} = \frac{2\pi}{v} Y_{lm}\left(\frac{\pi}{2}, 0\right) \frac{(2b)^{-\frac{l+1}{2}} \left(\frac{\omega_l}{v}\right)^{\frac{l-1}{2}}}{\Gamma\left(\frac{l+m+1}{2}\right)} W_{\frac{m}{2},-\frac{l}{2}}\left(\frac{2b\omega_l}{v}\right) . \tag{III.19}$$

Thus the excitation probability is

$$P(l,m) = \frac{2\pi e^2 a^{2l+1}}{l\hbar} Re \frac{1}{\left(\frac{\partial \epsilon}{\partial \omega}\right)_{\omega_l}} \left(\frac{2\pi}{v}\right)^2 (2b)^{-l-1} \left(\frac{\omega_l}{v}\right)^{l-1} \left[\frac{Y_{lm}\left(\frac{\pi}{2}, 0\right)}{\Gamma\left(\frac{l+m+1}{2}\right)} W_{\frac{m}{2},-\frac{l}{2}}\left(\frac{2b\omega_l}{v}\right)\right]^2 . \tag{III.20}$$

Case (b)

Now let us look at the case of b < a. Note the symmetry properties

$$r(t_o+\tau) = r(t_o-\tau) \quad , \qquad \text{(III.21a)}$$

$$\phi(t_o+\tau) - \phi_o = \phi_o - \phi(t_o-\tau) \, , \qquad \text{(III.21b)}$$

where t_0 is the instant at which the electron strikes the sphere and $\phi_o = \phi(t_0) = -\cos^{-1}(b/a)$. Use of these relations simplifies the evaluation of the integral in Eq. (III.17) and we get

$$\int_{-\infty}^{+\infty} dt \, \frac{Y^*_{lm}(\hat{r}) e^{i\omega_l t}}{r^{l+1}(t)} = \frac{2}{b^l v} Y_{lm}\left(\frac{\pi}{2},0\right) e^{i(\omega_l t_o - m\phi_o)}$$
$$\int_{-\frac{\pi}{2}}^{\phi_o} d\phi \cos^{l-1}\phi \cos\left[\frac{\omega_l b}{v}(\tan\phi - \tan\phi_o) - m(\phi-\phi_o)\right] . \qquad \text{(III.22)}$$

Hence the excitation probability in this case is

$$P(l,m) = \frac{8\pi e^2}{l\hbar v^2} a^{2l+1} b^{-2l} \mathrm{Re}\, \frac{1}{\left(\frac{\partial \epsilon}{\partial \omega}\right)_{\omega_l}} \left| Y_{lm}\left(\frac{\pi}{2},0\right)\right|^2$$
$$\left\{ \int_{-\frac{\pi}{2}}^{\phi_o} d\phi \cos^{l-1}\phi \cos\left[\frac{\omega_l b}{v}(\tan\phi - \tan\phi_o) - m(\phi-\phi_o)\right] \right\}^2 \qquad \text{(III.23)}$$

Dipolar Plsmon

In the special case of dipolar plasmon (l=1) P(1,0) vanishes since $Y_{1,o}(\pi/2,0)=0$. This, however, is expected. We have chosen the Z-axis perpendicular to the scattering

plane. Since the l=1, m=0 mode has a node in this plane, we expect P(1,0) to vanish.

Defining $P_{\pm 1}=P(1,\pm 1)$ we define in place of Eq. (III.20) for b > a

$$P_m = \frac{3\pi}{2}\left(\frac{e}{bv}\right)^2 \frac{2^m a^3}{\hbar} Re \frac{1}{\left(\frac{\partial \epsilon}{\partial \omega}\right)_{\omega_1}} \left[W_{\frac{m}{2},-\frac{1}{2}}\left(\frac{2b\omega_1}{v}\right)\right]^2 \qquad \text{(III.24)}$$

and in place of Eq. (III.23) for b < a

$$P_m = 3\left(\frac{e}{bv}\right)^2 \frac{a^3}{\hbar} Re \frac{1}{\left(\frac{\partial \epsilon}{\partial \omega}\right)_{\omega_1}} \left\{ \int_{-\frac{\pi}{2}}^{\phi_0} d\phi \cos\left[\frac{\omega_1 b}{v}(\tan\phi - \tan\phi_0) - m(\phi - \phi_0)\right]\right\}^2 . \qquad \text{(III.25)}$$

For the case b = a Eqs. (III.24) and (III.25) may readily be shown to be equivalent.

Total Probability

The total probability for plasma oscillation excitation is

$$P = P_{+1} + P_{-1} \quad . \qquad \text{(III.26)}$$

We define two scaled variables, x and y, for b and a:

$$x = \omega b/v \quad , \qquad \text{(III.27)}$$

$$y = \omega a/v \quad . \qquad \text{(III.28)}$$

Then the total probability, P, in Eq. (III.26) may be expressed as

$$P = \frac{3a^3}{\hbar}\left(\frac{e}{bv}\right)^2 \mathrm{Re}\,\frac{1}{\left(\frac{\partial\epsilon}{\partial\omega}\right)_{\omega_1}} S(x,y) \quad , \qquad \text{(III.29)}$$

where, for $b < a$

$$S(x,y) = \sum_{m=1,-1} \left\{ \int_{-\frac{\pi}{2}}^{\phi_0} d\phi \cos\left[x\left(\tan\phi - \tan\phi_0\right) - m\left(\phi - \phi_0\right)\right] \right\}^2 , \qquad \text{(III.30)}$$

and for $b > a$ Eq. (III.30) may be used with $\phi_0 = 0$. In that case $S(x,y)$ is independent of the variable y.

III.3 Cross Sections for Plasma Excitation

We denote the cross section for exciting plasma oscillations corresponding to the case where the electron misses the sphere by σ_+ and by σ_- where the electon bounces off the sphere. These cross sections are obtained from

$$\sigma = 2\pi \int b\, P(b)\, db \quad . \qquad \text{(III.31)}$$

Using Eqs. (III.29) and (III.30) we arrive at the following expressions for σ_+ and σ_-:

$$\sigma_+ = \frac{6\pi e^2 v}{\hbar\omega^3} \mathrm{Re}\,\frac{1}{\left(\frac{\partial\epsilon}{\partial\omega}\right)_{\omega}} F_+(y) \quad , \qquad \text{(III.32)}$$

$$\sigma_- = \frac{6\pi e^2 v}{\hbar\omega^3} \mathrm{Re}\,\frac{1}{\left(\frac{\partial\epsilon}{\partial\omega}\right)_{\omega}} F_-(y) \quad . \qquad \text{(III.33)}$$

Here we have defined two functions $F_{\pm}(y)$ as

$$F_{+}(y) = y^3 \int_{y}^{\infty} \frac{dx}{x} S(x,y) \quad , \quad \text{(III.34)}$$

$$F_{-}(y) = y^3 \int_{0}^{y} \frac{dx}{x} S(x,y) \quad . \quad \text{(III.35)}$$

An analysis of these expressions is given in the following section.

III.4 Results and Discussion

The cross sections for inelastic electron scattering accompanied by plasma excitation of the sphere is given by Eqs. (III.32) and (III.33). Eq. (III.32) gives the contribution due to collisions in which the electron strikes the sphere and bounces off. Before one is able to write an expression for the total cross section one must ascertain what fraction of the electrons that strike the sphere indeed bounce off. This estimation is difficult. One could adopt an empirical approach and use the reflection coefficient measured from electron loss spectroscopy measurements on flat surfaces. This is typically a small number on the order of a percent. On the other hand an isolated particle is likely to become electrically charged when exposed to the electron beam and this would modify the reflection coefficient. Thus the only firm statement that could be made at this time is that the total cross section lies between $\sigma = \sigma_{+}$ and $\sigma = \sigma_{+} + \sigma_{-}$, with $\sigma = \sigma_{+}$ as the more accurate

estimate, given the small reflection coefficients. It should, perhaps, also be noted that all of our theoretical development applies equally well to ion beam scattering. For ions the reflection coefficients are likely to be quite different, although additional inelastic channels are likely to be present which would cloud the issue.

The functions $F_{\pm}(y)$ appearing in Eq. (III.32) and (III.33) are integrals of a universal integrand $S(x,y)$ defined in Eq. (III.30). A plot of this integrand as a function of $x = \omega b/v$ appears in Fig. III.2. Several curves are drawn corresponding to different values of $y = \omega a/v$. For $b < a$ these curves describe $S(x,y)$ while for $b > a$ the envelope curve describes $S(x,y)$. Thus $S(x,y)$ is seen to be small for either small x or large x and to achieve a maximum at $x = y$.

Perhaps of more physical interest is the probability of exciting a plasma oscillation, given by Eq. (III.29). In Fig. III.3 we plot this probability as a function of impact parameter for a sphere of radius $a = 50\ a_0$. A qualitative understanding of the peak as a function of energy may be had by comparing the transit time to the plasma oscillation frequency (which was taken to be that corresponding to a silver sphere, $\hbar\omega = 3.6$ eV for the dipolar plasmon). Thus from the condition $\omega b/v = 1$ we get a peak at an energy equal to $E = m(\omega b)^2/2$. For $b = 100\ a_0$ this corresponds to $E = 2420$ eV and for $b = 120\ a_0$ this corresponds to

E = 3485 eV. These are in crude agreement (factor of 2) with the peak locations in Fig. (III.4) and the trend of increasing peak with increasing b is in the right direction.

In Fig. III.5 a plot of the universal functions $F_+(y)$ and $F_-(y)$ as a function of $y = \omega a/v$ is made. In terms of these functions the cross section plots may be drawn. Fig. III.6 shows the cross sections as a function of energy for fixed sphere radius ($a = 50\ a_0$). Fig. III.7 shows the cross sections plotted as a function of sphere size for fixed energy (E=1000 eV). In Fig. III.8 the total cross section defined as $\sigma_+ + \sigma_-$ is plotted as a function of E for fixed a.

The radiative cross section may be defined as the cross section for plasma excitation multiplied by the radiative yield of the excited particle. An expression for the yield of a sphere has been given in the literature [4]

$$Y = \left[1 + \left(\frac{c}{a\omega}\right)^3 \mathrm{Im}\ \epsilon\right]^{-1}, \qquad \text{(III.36)}$$

so the radiative cross section is

$$\sigma_Y = Y\sigma \qquad \text{(III.37)}$$

Again there is some ambiguity as to which cross section to use on the right hand side of Eq. (III.36). Now those electrons which are not reflected from the surface may still

contribute to the excitation of a plasma oscillation and hence to the radiative signal. As an estimate we employ $\sigma = \sigma_+ + \sigma_-$ in evaluating the right hand side of Eq. (III.37). A plot of the radiative cross section is seen to be three orders of magnitude below the inelastic electron cross section. However, this is for a case where a is only 50 a_0. From Eq. (III.36) we see that the yield will grow as a increases in size, ultimately saturating at a value Y=1. The saturation regime, however, is outside the realm of the validity of neglecting retardation effects. The basic conclusion to be drawn, however, is that the radiative cross section will grow in magnitude as the size of the sphere is increased. This trend is illustrated in Fig. III.9 where the inelastic and radiative cross sections are plotted as a function sphere size for fixed energy (1000 eV).

In our analysis we have restricted our attention to the case of the dipolar plasmon ($l = 1$). Higher multipoles may be treated along similar lines to those drawn in this paper.

In conclusion we see that the excitation of plasma oscillations of small spheres by electrons is a feasible experiment and it is hoped that this work would provide the stimulus for such a study.

References

1. M. Kerker, "The Scattering of Light and Other Electromagnetic Radiation", (Academic Press, New York, 1969)

2. "Surface Enhanced Raman Scattering", ed. by R. K. Chang and T. E. Furtak (Plenum, New York, 1982)

3. C. K. Chen, A. R. B. deCastro, and Y. R. Shen, Phys. Rev. Lett. 46 , 145 (1981)

4. J. I. Gersten and A. Nitzan, J. Chem. Phys. 75, 1139 (1981)

   D. A. Weitz, S. Garoff, C. D. Hanson, T. J. Gramila, and J. I. Gersten, Opt. Lett. 7 , 89 (1982)

5. See review article by H. Froitzheim in Current Topics in Physics, Vol. IV, "Electron Spectroscopy for Surface Analysis", Ed. H. Ibach, (Springer, Berlin, 1977), p. 205.

   A. Many, J. I. Gersten, I. Wagner, A. Rosenthal, and Y. Goldstein, Surf. Sci. 113 , 355 (1982)

CHAPTER IV

EFFECT OF SUBSTRATE ON PHOTOCHEMICAL REACTION (FORMALISM)

IV.1 Introduction

It is believed that the presence of roughness adds significantly to enhancement of the local electromagnetic field. In the light of these observations, a theoretical explanation in terms of resonances, involving macroscopic structures on a rough surface, had been proposed [1]. The enhancement is found to be due to the excitation of plasmon resonances in the substrate particles. One would therefore expect that phenomena, other than SERS, which involve the interaction between molecules and electromagnetic fields, should be enhanced. Since the presence of a molecule near a surface roughness feature is somewhat similar to its presence on or near a small solid state particle, there has indeed been a tremendous surge in the study of rough surfaces and small metallic particles.

Unlike SERS, photochemistry is a resonant phenomenon and involves a finite accumulation of energy in the molecule before the desired process can happen. In the case of a molecule undergoing photochemical reaction, while sitting near a small structure, it would require accumulation and flow of energy within it, for processes like multiphoton dissociation. On the other hand direct photodissociation often proceeds very fast. Since enhanced local field implies

enhanced absorption by the molecule, we can predict enhanced photochemical reaction, provided damping mechanisms are negligible.

Nitzan and Brus [2] have recently studied enhanced photochemistry for molecules near spherical particles. It should be noted that the resonant nature of the phenomenon limits, to a great extent, the substrate composition. A molecule adsorbed to a small sphere of a suitably chosen material, undergoes enhanced photochemical reaction due to resonant excitation of dipolar plasmons in the sphere. The sphere is characterized by a complex dielectric constant $\epsilon(\omega) = \epsilon_1(\omega) + i\,\epsilon_2(\omega)$. As required, the damping is small. The only damping mechanism considered is due to resistive effects leading to local heating. The width of this plasmon resonance is given by

$$\gamma = \left[\frac{2\,\epsilon_2(\omega)}{\epsilon_1'(\omega)} \right]_{\omega = \omega_s} , \qquad \text{(IV.1)}$$

where ω_s is the sphere resonance frequency.

We have studied the decay machanisms for a macroscopic roughness feature (modelled as a spheroidal bump on a flat surface) in Chapter II. The presence of an extended dielectric substrate, the composition of which was considered to be same as that of the spheroidal bump, opened up a new channel of energy dissipation, namely the decay of the bump plasmon states into delocalized substrate plasmon

states. For less sharp and large size ($\gg 200\ a_0$) bumps, it was found that the surface plasmon decay channel dominates over the radiative and resistive loss channels. Hence one can not guarantee enhancement of photochemical reaction in a more realistic situation where a rough surface is present.

One therefore would like to study phtochemistry on a rough surface taking into account this new surface plasmon decay channel. We consider the molecular energy dissipation due to its decay into both radiative and nonradiative channels. The problem is solved self-consistently by considering the decay of the excited molecule-bump-plane suface system and we calculate the enhancement ratio for photochemistry.This is the ratio of the cross section of photochemical reaction of the molecule adsorbed to a bump-plane surface system to that of a free molecule.

IV.2 Dipole Moment of the Molecule-Spheroid System

We wish to compute the effective dipole moment of the molecule-bump-plane system. Our aim is to consider the dynamics of the molecule in the presence of the local enhanced field. This local field consists of the incident field $\vec{E}_0$ and the induced image field $\vec{E}_{im}$ due to the presence of the rough surface, via resonant interaction of the molecule with the bump-plane system.

The subsequent resonant dissipative coupling between the molecule-bump discrete modes and extended surface

plasmon modes associated with the substrate surface, as well as coupling to radiative modes, give rise to reaction fields which aught to be taken into account. Hence the local field experienced by the molecule is composed of the incident field, the image field and the radiation and surface plasmon reaction fields. In order to do a consistent calculation we include the electric dipole moment of the molecule-bump-plane system in the reaction fields as will be seen in the following sections. The model considered is shown in Fig.IV.1. Spheroidal coordinates are used. A molecule characterized by a dipole moment $\vec{\mu} = \hat{z}\mu$ is located along the z-axis at a distance d above the spheroid, as indicated, in vacuum. The incident field E_0 is taken to be along the z-axis. A more general situation, where the spheroidal bump is characterized by a dielectric function $\epsilon(\omega)$, different from that of the substrate, $\epsilon'(\omega)$, is considered. The special case of the bump being of the same material as that of the substrate, can be achieved by setting $\epsilon'(\omega) = \epsilon(\omega)$. The electrostatic potentials, in the three regions indicated, are given by

$$\Phi_I = \sum_n A_n P_n(\xi) P_n(\eta) \quad , \qquad \text{(IV.2)}$$

$$\Phi_{II} = \sum_n B_n Q_n(\xi) P_n(\eta) - E_0 f \xi \eta + \frac{\vec{\mu}\cdot(\vec{r}-\vec{r}_1)}{|\vec{r}-\vec{r}_1|^3} \quad , \qquad \text{(IV.3)}$$

$$\Phi_{III} = \sum_n C_n Q_n(\xi) P_n(\eta) - E_1 f \xi \eta \quad , \qquad \text{(IV.4)}$$

where

$$f = (a^2 - b^2)^{1/2} \quad , \tag{IV.5}$$

$$\vec{r}_1 = (a+d)\hat{k} \quad , \tag{IV.6}$$

$$\xi_0 = \frac{a}{f} \quad , \quad \xi_1 = \frac{a+d}{f} \quad . \tag{IV.7}$$

The last term on the right hand side of Eq. (IV.3) can be reduced into a convenient form by noting that,

$$\frac{1}{|\vec{r} - \vec{r}_1|} = \sum_n \frac{(2n+1)}{f} P_n(\xi_<) Q_n(\xi_>) P_n(\eta) \quad , \tag{IV.8}$$

where $\xi_> = \max(\xi, \xi_1)$, $\xi_< = \min(\xi, \xi_1)$. Hence

$$\Phi_{II} = \sum_n \left\{ B_n Q_n(\xi) - E_0 f \xi \delta_{1n} \right\} P_n(\eta) + \frac{\mu}{f^2} \sum_n (2n+1) P_n(\eta) \begin{cases} P_n(\xi) Q_n'(\xi_1) , & \xi < \xi_1 \\ P_n'(\xi) Q_n(\xi) , & \xi > \xi_1 \end{cases} \tag{IV.3a}$$

$$\Phi_{III} = \sum_n \left\{ C_n Q_n(\xi) - E_1 f \xi \delta_{1n} \right\} P_n(\eta) \quad . \tag{IV.4a}$$

As shown, the boundary separating region II from region III, has essentially two effective surfaces. One is $\xi < \xi_1$, $\eta = 0$ (II-III) and the other is $\xi > \xi_1$, $\eta = 0$ (II-III)'. Coefficients A_n, B_n, and C_n are determined by matching potentials and normal components of the displacement field $\vec{D}$ at the boundaries (I-II), (II-III), (II-III)', and (I-III).

Such matching of boundary conditions leads to the following equations:

$$\sum_n A_n P_n(\xi_0) P_n(\eta) = \sum_n \left[B_n Q_n(\xi_0) - E_0 f \xi_0 \delta_{n1} \right] P_n(\eta) + \frac{\mu}{f^2} \sum_n (2n+1) P_n(\xi_0) Q_n'(\xi_1) P_n(\eta) \,, \quad \xi = \xi_0 \,, \quad 0 < \eta < 1 \tag{IV.9a}$$

$$\sum_n \epsilon A_n P_n'(\xi_0) P_n(\eta) = \sum_n \left[B_n Q_n'(\xi_0) - E_0 f \delta_{n1} \right] P_n(\eta) + \frac{\mu}{f^2} \sum_n (2n+1) P_n'(\xi_0) Q_n'(\xi_1) P_n(\eta) \,, \quad \xi = \xi_0 \,, \quad 0 < \eta < 1 \tag{IV.9b}$$

$$\sum_n A_n P_n(\xi_0) P_n(\eta) = \sum_n \left[C_n Q_n(\xi_0) - E_1 f \xi_0 \delta_{n1} \right] P_n(\eta) \,, \quad \xi = \xi_0 \,, \quad -1 < \eta < 0 \tag{IV.10a}$$

$$\epsilon \sum_n A_n P_n'(\xi_0) P_n(\eta) = \sum_n \epsilon' \left[C_n Q_n'(\xi_0) - E_1 f \delta_{n1} \right] P_n(\eta) \,, \quad \xi = \xi_0 \,, \quad -1 < \eta < 0 \tag{IV.10b}$$

$$\sum_n \left[B_n Q_n(\xi) - E_0 f \xi \delta_{n1} \right] P_n(0) + \frac{\mu}{f^2} \sum_n (2n+1) P_n(\xi) Q_n'(\xi_1) P_n(0) = \sum_n \left[C_n Q_n(\xi) - E_1 f \xi \delta_{n1} \right] P_n(0) \,, \quad \xi < \xi_1 \,, \quad \eta = 0 \tag{IV.11a}$$

$$\sum_n \left[B_n Q_n(\xi) - E_0 f \xi \delta_{n1} \right] P_n'(0) + \frac{\mu}{f^2} \sum_n (2n+1) P_n'(0) P_n(\xi) Q_n'(\xi_1) = \sum_n \left[\epsilon' C_n Q_n(\xi) - E_1 f \epsilon' \xi \delta_{n1} \right] P_n'(0) \,, \quad \xi < \xi_1 \,, \quad \eta = 0 \tag{IV.11b}$$

$$\sum_n \left[B_n Q_n(\xi) - E_0 f \xi \delta_{n1} \right] P_n(0) + \frac{\mu}{f^2} \sum_n (2n+1) P_n(0)$$
$$P_n'(\xi_1) Q_n(\xi) = \sum_n \left[C_n Q_n(\xi) - E_1 f \xi \delta_{n1} \right] P_n(0) ,$$
$$\xi > \xi_1 \ , \ \eta = 0 \qquad \text{(IV.12a)}$$
$$\sum_n \left[B_n Q_n(\xi) - E_0 f \xi \delta_{n1} \right] P_n'(0) + \frac{\mu}{f^2} \sum_n (2n+1) P_n'(0)$$
$$P_n'(\xi_1) Q_n(\xi) = \sum_n \left[\epsilon' C_n Q_n(\xi) - E_0 f \xi \delta_{n1} \right] P_n'(0) ,$$
$$\xi > \xi_1 \ , \ \eta = 0 \qquad \text{(IV.12b)}$$

Continuity of the normal component of $\vec{D}$ between media II and III requires that $E_1 = E_0/\epsilon'$, and the validity of Eqs. (IV.12a-b) suggests that B_n and C_n be related by

$$B_n = -\frac{\mu}{f^2}(2n+1) P_n'(\xi_1) + C_n \left[\frac{1+\epsilon'}{2} + (-)^n \frac{1-\epsilon'}{2} \right] . \qquad \text{(IV.13)}$$

Inspection of Eqs. (11a-b) implies that the following relation be satisfied for $\xi < \xi_1$:

$$\sum_n (2n+1) P_n(0) \left[P_n(\xi) Q_n'(\xi_1) - P_n'(\xi_1) Q_n(\xi) \right] = 0 \qquad \text{(IV.14a)}$$

$$\sum_n (2n+1) P_n'(0) \left[P_n(\xi) Q_n'(\xi_1) - P_n'(\xi_1) Q_n(\xi) \right] = 0 . \qquad \text{(IV.14b)}$$

Simple manipulations of Eqs. (IV.9a-b) give the following relations between A_n and B_n:

$$\frac{2}{2j+1} A_j P_j(\xi_0) = \sum_n B_n \left[1 + (-)^{j+n} \Delta_n \right] Q_n(\xi_0) X_{jn}$$
$$+ \frac{\mu}{f^2} \sum_n (2n+1) \left[P_n(\xi_0) Q_n'(\xi_1) + (-)^{j+n} \Delta_n P_n'(\xi_1) Q_n(\xi_0) \right] X_{jn}$$
$$- E_0 f \xi_0 X_{j1} \left[1 - \frac{(-)^j}{\epsilon'} \right] \ , \qquad \text{(IV.15)}$$

and

$$\frac{2}{2j+1} A_j P_j'(\xi_0) = \sum_n \left[\epsilon^{-1} + (-)^{j+n} \Delta_n \epsilon^{-1} \epsilon' \right] B_n Q_n'(\xi_0) X_{jn}$$
$$+ \frac{\mu \epsilon^{-1}}{f^2} \sum_n (2n+1) \left[P_n'(\xi_0) Q_n'(\xi_1) + (-)^{j+n} \Delta_n \epsilon' P_n'(\xi_1) Q_n'(\xi_0) \right] X_{jn}$$
$$- E_0 f \epsilon^{-1} X_{j1} \left[1 - (-)^j \right] \quad , \tag{IV.16}$$

where

$$\Delta_n = \left[\frac{1+\epsilon'}{2} + (-)^n \frac{1-\epsilon'}{2} \right] \quad , \tag{IV.17}$$

and

$$X_{jn} = \int_0^1 d\eta \; P_j(\eta) P_n(\eta) \quad . \tag{IV.18}$$

Dividing Eq. (IV.15) by Eq. (IV.16) we get the following matrix equation:

$$\sum_n T_{jn} B_n = \mu \sum_n S_{jn} b_n - R_j E_0 \quad , \tag{IV.19}$$

where

$$T_{jn} = X_{jn} \Big\{ \left[\epsilon^{-1} Q_n'(\xi_0) P_j(\xi_0) - Q_n(\xi_0) P_j'(\xi_0) \right]$$
$$+ (-)^{j+n} \left[\frac{1+\epsilon'^{-1}}{2} + \frac{(-)^n}{2} \frac{1-\epsilon'^{-1}}{2} \right]$$
$$\left[\epsilon' \epsilon^{-1} Q_n'(\xi_0) P_j(\xi_0) - Q_n(\xi_0) P_j'(\xi_0) \right] \Big\} \quad , \tag{IV.20}$$

$$S_{jn} = X_{jn}\left\{ Q_n'(\xi_1)\left[P_n(\xi_0) P_j'(\xi_0) - \epsilon^{-1} P_n'(\xi_0) P_j(\xi_0)\right] \right.$$
$$+ (-)^{j+n}\left[\tfrac{1}{2}(1+\epsilon'^{-1}) + (-)^n \tfrac{1}{2}(1-\epsilon'^{-1})\right] P_n'(\xi_1)$$
$$\left.\left[Q_n(\xi_0) P_j'(\xi_0) - \epsilon' \epsilon^{-1} Q_n'(\xi_0) P_j(\xi_0)\right]\right\} \quad , \tag{IV.21}$$

$$b_n = \frac{2n+1}{f^2} \quad , \tag{IV.22}$$

and

$$R_j = f\xi_0\left\{ X_{j1} P_j'(\xi_0)\left[1 - \frac{(-)^j}{\epsilon'}\right] - \frac{2}{3}\epsilon^{-1}\delta_{j1}\right\} \quad . \tag{IV.23}$$

The eigen vectors of the Matrix equation (IV.19) constitute the B_n coefficients, and coefficients A_n and C_n can be obtained by using Eqs. (IV.15) or (IV.16) and (IV.13).

In the asymptotic limit the potential Φ_{II} takes the form:

$$\Phi_{II} \xrightarrow{\xi \to \infty} \frac{B_1 f^2}{3}\frac{z}{r^3} + \mu \frac{z}{r^3} - E_0 z \quad . \tag{IV.24}$$

Hence the electric dipole moment of the system is given by

$$D = \mu + \frac{B_1 f^2}{3} \quad . \tag{IV.25}$$

IV.3 Cross Section for Photochemistry

Now consider the molecule undergoing mechanical oscillations leading to photochemical reaction. In this mechanical oscillator model, equation for the vibrating dipole can be written as

$$\ddot{\mu} + \gamma\dot{\mu} + \omega_o^2\mu = \alpha_o \omega_o^2 E_{loc} \quad , \qquad \text{(IV.26)}$$

where α_o is the static molecular polarizability, ω_o is the molecular resonance frequency, and γ is the molecular decay rate. In the case of direct photodissociation, for example, γ would be the rate associated with the dissociation process. Unlike the model of Nitzan and Brus, the effect of the substrate on the molecular processes is taken into account via E_{loc}, which is the local electric field in which the molecule finds itself.

The local electric field, E_{loc}, would have several components including the incident field E_0. As studied earlier, the decay of the oscillating system dipole, D, into both radiative and nonradiative (surface plasmon) modes give rise to radiation and surface plasmon reaction fields, denoted by E_{rad} and E_{sp} respectively. Image effects, again, give rise to an image field, E_{image}, which can be easily extracted from Φ_{II} . Hence the local field at the location of the molecule can be written as

$$E_{loc} = E_o' - \frac{1}{f}\sum_n B_n Q_n'(\xi_1) \quad , \qquad \text{(IV.27)}$$

where

$$E_o' = E_o + E_{sp} + E_{rad} \quad . \tag{IV.28}$$

The reaction fields are given by the following relations:

$$\vec{E}_{rad} = i\,\frac{2}{3}\left(\frac{\omega}{c}\right)^3 \vec{D}\left\{1+\frac{3}{2}\int_0^{\pi/2} d\theta\, \frac{\sin^3\theta}{(\epsilon'-1)\left[(\epsilon'+1)\cos^2\theta - 1\right]}\right.$$

$$\left.\left[(\epsilon'^2+1)\cos^2\theta + (\epsilon'-1)\right]\right\} \quad , \tag{IV.29}$$

$$\vec{E}_{sp} = 8\pi i\left(\frac{\omega}{c}\right)^3 \vec{D}\;\; \frac{(-\epsilon')^3}{(1-\epsilon')\,(-\epsilon'-1)^{5/2}} \quad , \tag{IV.30}$$

where ω is the frequency of the incident light. Substitution of E_{loc} in Eq. (IV.26) and assuming a harmonic oscillator model, leads to the following relation for μ :

$$\left[\left(\omega_o^2 - \omega^2 - i\omega\gamma\right) - \alpha_o\omega_o^2\,\tilde{C}\right]\mu$$

$$= \alpha_o\omega_o^2\left[E_o - \frac{1}{f}\sum_n B_n Q_n'(\xi_1) + \tilde{C}\;\frac{B_1 f^2}{3}\right] \quad , \tag{IV.31}$$

where

$$\tilde{C} = C_1 + C_2 \quad , \tag{Iv.32}$$

$$C_1 = 8\pi i\left(\frac{\omega}{c}\right)^3 \;\frac{(-\epsilon')^3}{(-\epsilon'-1)^{5/2}\,(1-\epsilon')} \quad , \tag{IV.33}$$

$$C_2 = \frac{2i}{3}\left(\frac{\omega}{c}\right)^3\left\{1+\frac{3}{2}\int_0^{\pi/2} d\theta\,\frac{\sin^3\theta\left[(\epsilon'^2+1)\cos^2\theta + \epsilon' - 1\right]}{(\epsilon'-1)\left[(\epsilon'+1)\cos^2\theta - 1\right]}\right\} . \tag{IV.34}$$

An inspection of Eqs. (IV.19)-(IV.23) tells us that, to maintain consistency, E_0 in those equations should be replaced by E_0'. Hence substituting for B_n, we get from Eq. (IV.31)

$$\left[(\omega_o^2-\omega^2) - i\omega\gamma - \alpha_o\omega_o^2\tilde{C} + \alpha_o\omega_o^2\,\underline{W}\cdot\underline{q}\right]\mu$$

$$= \alpha_o\omega_o^2\left[E_o + E_o'\,\underline{V}\cdot\underline{q} + \tilde{C}\,\frac{B_1 f^2}{3}\right] \quad , \qquad \text{(IV.35)}$$

where

$$\underline{V} = \underline{\underline{T}}^{-1}\cdot\underline{R} \quad , \qquad \text{(IV.36)}$$

$$\underline{W} = (\underline{\underline{T}}^{-1}\cdot\underline{\underline{S}})\cdot\underline{b} \quad , \qquad \text{(IV.37)}$$

and

$$q_n = \frac{Q_n'(\xi_1)}{f} \quad . \qquad \text{(IV.38)}$$

In this new notation, however, B_n's are given by

$$B_n = \mu W_n - E_o' V_n \quad . \qquad \text{(IV.39)}$$

Finally, after some manipulations, μ is given by

$$\mu = \frac{\alpha_o\omega_o^2 E_o\left[1+u\left\{1+\tilde{C}(f^{2/3})V_1\right\}^{-1}\right]}{\omega_o^2-\omega^2-i\omega\gamma-\alpha_o\omega_o^2 F} \quad ,$$

$$F = \tilde{C}\left(1+\frac{f^2}{3}W_1\right)\left(1+\frac{u}{1+\frac{f^2}{3}\tilde{C}V_1}\right) - \underline{W}\cdot\underline{q} \quad , \qquad \text{(IV.40)}$$

where

$$u = \left(\underline{V} \cdot \underline{q} - \tilde{C} \frac{f^2}{3} V_1 \right) . \qquad \text{(IV.41)}$$

We can write Eq. (IV.41) in a more convenient form as:

$$\mu = \rho E_0 , \qquad \text{(IV.42)}$$

where

$$\rho = \alpha_0 \omega_0^2 \frac{(1 + \underline{V} \cdot \underline{q})}{(1 + \tilde{C} \frac{f^2}{3} V_1)}$$

$$\left[\omega_0^2 - \omega^2 - i\omega\gamma - \alpha_0 \omega_0^2 \left\{ \frac{\tilde{C}(1 + \frac{f^2}{3} W_1)(1 + \underline{V} \cdot \underline{q})}{(1 + \tilde{C} \frac{f^2}{3} V_1)} - \underline{W} \cdot \underline{q} \right\} \right]^{-1} . \qquad \text{(IV.43)}$$

The rate of energy transfer into the molecule is given by

$$P = -\frac{\omega}{2} \mathrm{Im}\, \mu^* E_{loc}$$

$$= \Lambda |E_0|^2 , \qquad \text{(IV.44)}$$

where

$$\Lambda = -\frac{\omega}{2} \mathrm{Im} \left[\frac{\omega_0^2 - \omega^2 - i\omega\gamma}{\alpha_0 \omega_0^2} \right] |\rho|^2 \qquad \text{(IV.45)}$$

$$= \frac{\omega^2 \gamma}{2 \alpha_0 \omega_0^2} |\rho|^2 . \qquad \text{(IV.46)}$$

Since the incident energy flux is $c|E_0|^2/8\pi$, the corss section for energy transfer to the molecule is found to be

$$\sigma = \frac{8\pi}{c}\Lambda \quad . \tag{IV.47}$$

The cross section for photochemical reaction is written as

$$\sigma_{Pc} = \eta \frac{8\pi}{c}\Lambda \quad , \tag{IV.48}$$

where η is the quantum efficiency for photochemistry.

IV.4 Enhancement of Photochemical Reaction

The enhancement ratio for photochemistry is defined as the ratio of the cross section for photochemistry when the molecule is adsorbed on a bump-plane system, to that when the molecule is free. Hence the enhancement ratio for photochemistry is given by

$$R_{Pc} = \frac{\Lambda}{\Lambda_0} \quad , \tag{IV.49}$$

where Λ_0 replaces Λ in Eq. (IV.48) for the cross section for photochemistry, σ_{Pc}^{o} , when the molecule is free, and is given by

$$\Lambda_0 = \frac{\omega^2}{2} \quad \frac{\omega_0^2 \alpha_0 \gamma}{(\omega_0^2 - \omega^2)^2 + \omega^2\gamma^2} \quad . \tag{IV.50}$$

Substituting Eq. (IV.46) and (IV.50) into Eq. (IV.49) we get

$$R_{pc} = \frac{\left[(\omega_o^2 - \omega^2)^2 + \omega^2\gamma^2\right]}{(\alpha_o \omega_o^2)^2} |\rho|^2 \quad . \qquad \text{(IV.51)}$$

It is easy to see that R_{pc} simply represents the intensity enhancement factor, since we can write

$$R_{pc} = \left| \frac{E_{loc}}{E_o} \right|^2 \quad . \qquad \text{(IV.52)}$$

Written out explicitly, we get

$$R_{pc} = \left[(\omega_o^2 - \omega^2)^2 + \omega^2\gamma^2\right] \left| \frac{1 + \underline{V}\cdot\underline{q}}{(1 + \tilde{C}\frac{f^2}{3}V_1)\left[(\omega_o^2 - \omega^2 - i\omega\gamma) - \alpha_o\omega_o^2\left\{\frac{\tilde{C}\left(\frac{f^2}{3}W_1 + 1\right)(1+\underline{V}\cdot\underline{q})}{(1+\tilde{C}\frac{f^2}{3}V_1)} - \underline{W}\cdot\underline{q}\right\}\right]} \right|^2 \qquad \text{(IV.53)}$$

This is the expression for the enhancement ratio for photochemical reaction of a molecule on a rough surface modelled as a smooth surface with hemispheroidal protrusions.

References:

1. J. I. Gersten and A. Nitzan, J. Chem. Phys. 73 , 3023 (1980)

P. C. Das and J. I. Gersten, Phys. Rev. B25 , 6281 (1982)

2. A. Nitzan and L. E. Brus, J. Chem. Phys. 75 , 2205 (1981)

CHAPTER V

CONCLUDING REMARKS

We have dealt with several interesting and anomalous optical properties associated with rough srfaces and micro-structures (small particles). It, therefore, poses a challenge of unravelling the truth behind each of these phenomena. No doubt, these are complicated problems which have microscopic origin. Here, in our study of small particles and rough surfaces, we have tried to understand a few of their microscopic as well as macroscopic properties and their origins from a semiclassical point of view.

We have undertaken our study under two main divisions, namely 'small particles' and 'rough surfaces'. They are clearly related to each other. But we have considered them separately with the hope that a connection between the two systems can be rigorously established facilitating a general approach toward both.

In our study of small particles, we have evaluated the spontaneous electric dipole moments possessed by small homogeneous, asymmetric structures and inhomogeneous structures whose symmetry is broken by the presence of a molecule or an atom near it. The basic conclusion here is that homogeneous structures have very small dipole moments except for very large sizes, while inhomogeneous structures (inhomogeneity being due to the presence of a nearby

molecule or atom of a material different from that of the spheroid or due to bimetallic structures) give rise to large dipole moments. Hence inhomogeneous structures are potentially better for experimental study, because of their ability to efficiently couple to external electromagnetic radiation. It should be noted from Fig. I.4 that the electric dipole moment of an inhomogeneous system is dependent on the geometry of the particle considered. With the atom-spheroid separation less than 20 Å one sees that the dipole moment is larger than it would be for a sphere. This fact may be helpful in understanding some observations in SERS-related experiments. For sub-monolayer or monolayer coverages of adsorbates the signals recieved in a SERS experiment would probably come from species located at the tip of a roughness feature. The behavior of the dispersion energy from Fig. I.5 shows that atoms avoid sharp objects. This might be helpful in studying the geometry and structural dependence of adsorption. One, however, has to incorporate the plane substrate and make more detailed calculations to generalize for the case of a rough surface.

We have thrown some light on this issue in our study of surface shape resonances in Chapter II. Figures II.4 and II.5 show the magnitude of the dipole moment of a roughness feature, modelled as a hemi-spheroidal protrusion out of a plane surface, both consisting of the same dielectric material. The dipole moment is shown to grow with the size and shape of the spheroid. Since we had considered here only

a rough surface without the nearby molecule, a comparison of the results for the dipole moment with the case of an atom near a spheroid is impossible. However, there are some noticeable and qualitative agreements.

The presence of a set of shape resonances whose frequencies and damping rates are determined solely by the geometric and dielectric properties of the system, may very well become a mechanism for enhanced local electric field near a rough surface. This may also be helpful in studying infra-red properties associated with rough surfaces. It should be kept in mind that a rough surface does not consist of a single bump, as has been considered. This has been a preliminary study and we hope to extend it statistically to a more realistic surface.

Our finding that a set of shape resonances exist for a rough surface, has been extended to formulate (Chapter IV) the effect of the substrate on photochemical reaction of a molecule situated near it. As in the case of SERS, enhancement of photochemical reaction is based on the fact that there exists an enhanced local electric field in which the molecule finds itself. Moreover the energy transfer to the molecule should not decay quickly enough so as to hinder the process. In the case of a molecule undergoing photochemical reaction near a rough silver surface, we have formulated the problem of finding the reaction cross section and enhancement ratio of photochemistry by taking into account the existence of the shape resonances. Our goal here

was to see if photochemical reaction is enhanced near a rough surface due to enhanced local field. No definite conclusions have been drawn from this study due to the lengthy nature of the computational procedures involved. However, we hope to arrive at some meaningful results in the future.

Further we have utilized our knowledge that a small metal particle, e.g. a silver sphere, possesses a set of localized plasma oscillation modes which can couple to external probes, to understand and estimate the cross section of electron scattering off such a particle. Electrons lose energy by coupling to the plasmon modes of the spherical silver particle and hence the scattering is inelastic. A classical trajectory approximation had been used. The electron beam which strikes the sphere and bounces off or just passes by in a straight line path serves to excite the discrete modes of the sphere. This study, as described in Chapter III is hoped to be useful in understanding electron energy loss spectroscopy.

APPENDIX A

DENSITY FUNCTIONAL THEORY

A.1 Theory of Hohenberg and Kohn

The density functional formalism, a general theory of the inhomogeneous electron gas in its ground state, was introduced by Hohenberg, Kohn, and Sham [1]. The central quantity in this theory is the electron number density $n(\vec{r})$. The properties of the system in its ground state are functionals of the electron density. With the density taken to be trial function, a variational principle is established for the energy. Here we give the basic equations involved in the theory.

Consider a system of electrons in its ground state (assumed nondegenerate) moving in a static external potential $v(\vec{r})$. The second quantized Hamiltonian operator is written as

$$H = T + V + U \quad , \tag{a.1}$$

where

$$T = \frac{1}{2} \int \nabla \psi^*(\vec{r}) \cdot \nabla \psi(\vec{r}) \, d\vec{r} \quad , \tag{a.2}$$

$$V = \int v(\vec{r}) \, \psi^*(\vec{r}) \, \psi(\vec{r}) \, d\vec{r} \quad , \tag{a.3}$$

and

$$U = \frac{1}{2}\int \psi^*(\vec{r})\psi^*(\vec{r}')\frac{1}{|\vec{r}-\vec{r}'|}\psi(\vec{r}')\psi(\vec{r})\,d\vec{r}\,d\vec{r}' \quad . \tag{a.4}$$

T, U, and V correspond, respectively, to the electron kinetic energy, the electron-electron coulomb interaction, and the interaction between an electron and the external potential. Here atomic units are used. It can be shown that $v(\vec{r})$ is a unique functional of the electron density. Hence the Schrodinger wave function is a functional of $n(\vec{r})$.

$$\Psi(\vec{r}) = \Psi[n(\vec{r})] \quad . \tag{a.5}$$

The energy functional is written as

$$E_v[n] = \int v(\vec{r})n(\vec{r})d\vec{r} + \frac{1}{2}\int \frac{n(\vec{r})n(\vec{r}')}{|\vec{r}-\vec{r}'|}d\vec{r}\,d\vec{r}' + G[n] \quad , \tag{a.6}$$

where G[n] is a universal functional,

$$G[n] = \langle \Psi | T + U | \Psi \rangle - \frac{1}{2}\int \frac{n(\vec{r})n(\vec{r}')}{|\vec{r}-\vec{r}'|}d\vec{r}\,d\vec{r}' \quad . \tag{a.7}$$

If we denote the electrostatic potential of the system by then

$$\phi(\vec{r}) = v(\vec{r}) + \int \frac{n(\vec{r}')}{|\vec{r}-\vec{r}'|}d\vec{r}' \quad . \tag{a.8}$$

If the external potential, $v(\vec{r})$, is due to a positive charge distribution of number density $n_+(\vec{r})$, then

$$\phi(\vec{r}) = \int \frac{n(\vec{r}') - n_+(\vec{r}')}{|\vec{r} - \vec{r}'|} d\vec{r}' \quad , \qquad \text{(a.9)}$$

and

$$\nabla^2 \phi(\vec{r}) = -4\pi \left[n(\vec{r}) - n_+(\vec{r}) \right] \quad . \qquad \text{(a.10)}$$

The vanishing of the first variation of $E_v[n]$ about the correct density, subject to the condition that all densities considered satisfy

$$\int n(\vec{r}) d\vec{r} = N \quad , \qquad \text{(a.11)}$$

leads to the variational equation

$$\delta \left\{ E_v[n] - \mu \int n(\vec{r}) d\vec{r} \right\} = 0 \quad , \qquad \text{(a.12)}$$

where μ is a Lagrange multiplier and is determined by Eq. (a.11), and for correct density

$$\mu = \frac{\delta E_v[n]}{\delta n} \quad . \qquad \text{(a.13)}$$

$$= \phi(\vec{r}) + \frac{\delta G[n]}{\delta n} \quad . \qquad \text{(a.14)}$$

Eq. (a.14) is solved for the density distribution, $n(\vec{r})$, in the ground state. The only complication is the explicit form of $G[n]$. One therefore makes approximations.

Case I:

For a gas of nearly constant density $n(\vec{r}) = \bar{n} + \tilde{n}(\vec{r})$, where $\tilde{n}(\vec{r}) \ll \bar{n}$, $G[n]$ is expanded as

$$G[n] = G[\bar{n}] + \int K(|\vec{r}-\vec{r}'|)\tilde{n}(\vec{r})\tilde{n}(\vec{r}')d\vec{r}\,d\vec{r}' + O(\tilde{n}^3) \quad \text{(a.15)}$$

The linear term is absent because

$$\int \tilde{n}(\vec{r})\,d\vec{r} = 0 \quad . \quad \text{(a.16)}$$

The coefficient $K(r)$ has been shown by Hohenberg and Kohn to have an oscillatory behavior, which in turn leads to Friedel type oscillations.

Case II:

For a gas of slowly varying density, when $n(\vec{r})$ varies slowly over distances large compared with $r_s(n)$ $\left[\frac{4\pi}{3} r_s^3(n) = n^{-1}\right]$, $G[n]$ is expanded in density gradients:

$$G[n] = \int d\vec{r}\left[g_0(n(\vec{r})) + g_2(n(\vec{r}))\left|\nabla n(\vec{r})\right|^2 + \cdots\right] . \quad \text{(a.17)}$$

Even in cases when such a series does not converge, it is expected to be useful in an asymptotic sense. The coefficient $g_0[n]$ is the energy density, exclusive of

electrostatic terms, of a uniform gas of density $n(\vec{r})$

$$g_0[n] = [t(n) + \epsilon_x(n) + \epsilon_c(n)]\, n \quad . \qquad \text{(a.18)}$$

Here $t(n)$ and $\epsilon_x(n)$ are, respectively, the average kinetic and exchange energies per particle of the uniform gas treated in the Hartree-Fock approximation, and $\epsilon_c(n)$ is the average correlation energy per particle. They are given by

$$t(n) = \frac{3}{10}(3\pi^2 n)^{\frac{2}{3}} = 1.105/r_s^2(n) \quad , \qquad \text{(a.19)}$$

$$\epsilon_x(n) = -\frac{3}{4}\left(\frac{3n}{\pi}\right)^{\frac{1}{3}} = -\frac{.458}{r_s(n)} \quad , \qquad \text{(a.20)}$$

and in the metallic density range

$$\epsilon_c(n) = -\frac{0.44}{r_s(n) + 7.8} \quad . \qquad \text{(a.21)}$$

The other coefficient $g_2(n)$, with the inclusion of the exchange term is written as

$$g_2(n) \approx \frac{1}{72n} + \frac{0.00167}{n^{4/3}} \quad . \qquad \text{(a.22)}$$

Further, inclusion of the correlation contribution for $r_s \ll 1$, (very high electron density) $g_2(n)$ becomes

$$g_2(n) \approx \frac{1}{72n} + \frac{0.00167}{n^{4/3}} + \frac{0.00424}{n^{4/3}} \quad . \qquad \text{(a.23)}$$

Using the general theory described above Kohn and Sham have derived a set of single particle Schrodinger equations whose self-consistent solution gives the exact ground state density distribution, and hence the energy for the interacting inhomogeneous electron gas. For a system of N electrons moving in an external potential $U_s(\vec{r})$, but non-interacting, the Schrodinger equation is written as

$$\left[-\frac{\nabla^2}{2} + U_s(\vec{r})\right]\psi_i(\vec{r}) = \epsilon_i \psi_i(\vec{r}) \ . \qquad \text{(a.24)}$$

The electron density is given by

$$n(\vec{r}) = \sum_{i=1}^{N} |\psi_i(\vec{r})|^2 \ . \qquad \text{(a.25)}$$

Analogous to Eq. (a.14) one then obtains

$$U_s(\vec{r}) + \frac{\delta T_s[n]}{\delta n} = \mu_s \ , \qquad \text{(a.26)}$$

where $T_s[n]$ is the kinetic energy of the non-interacting system.

For an interacting system of electron gas, the exchange-correlation energy is given by

$$E_{xc}[n] = G[n] - T_s[n] \ . \qquad \text{(a.27)}$$

Hence Eq.(a.14), for the interacting case, can be written as

$$\phi(\vec{r}) + \frac{\delta E_{xc}[n]}{\delta n} + \frac{\delta T_s[n]}{\delta n} = \mu \quad . \qquad \text{(a.28)}$$

This has the form of Eq.(a.26) if we take the function

$$V_{eff}[n, \vec{r}] \equiv \phi(\vec{r}) + \frac{\delta E_{xc}[n]}{\delta n} \qquad \text{(a.29)}$$

to play te role of the single particle potential $V_s(\vec{r})$. Hence $n(\vec{r})$ can be obtained from the following Kohn-Sham equation

$$\left[-\tfrac{1}{2}\nabla^2 + V_{eff}[n,r]\right]\psi_i(\vec{r}) = \epsilon_i \psi_i(\vec{r}) \ , \qquad \text{(a.30)}$$

by the use of Eq.(a.25).

We see that the complexity of the problem lies in our knowledge of $E_{xc}[n]$, which Kohn and Sham expand for a slowly varying density as

$$E_{xc}[n] = \int d\vec{r}\left[\epsilon_{xc}(n(\vec{r}))n(\vec{r}) + \epsilon_{xc}^{(1)}(n(\vec{r}))|\nabla n(\vec{r})|^2 + \cdots\right] \qquad \text{(a.31)}$$

where $\epsilon_{xc} = \epsilon_x + \epsilon_c$, and $\epsilon_{xc}^{(2)}$ is extracted from Eq.(a.23).

The density functional theory has been very successful in determining the work-function and surface energies of metallic surfaces.

A.2 Recent Improvements:

Although the density functional theory looks simple to apply to physical situations it has certain approximational difficulties. Kohn and Sham [1] have shown that it is possible to obtain the exact ground state energy of the system by solving self-consistently a set of single particle Schrodinger-like equations (Eq.(a.30)), provided the exact exchange and correlation energy functional of the density is known. Essentially the kinetic energy is treated as a functional of the density of a non-interacting electron gas. So, besides the difficulty of knowing the exact expression for $E_{xc}[n]$, one of the difficulties of the formalism is the construction of an appropriate functional representing the kinetic energy.

A.2.1 Density Gradient Expansion of Kinetic and Exchange Energies:

Within the Kohn-Sham formalism, the kinetic energy is dependent on a knowledge of the single-particle wave-functions $\psi_i(\vec{r})$. In the variational formalism, however, one obtains directly the density, rather than single-particle wave functions from which the density is obtained. Here the results for the density are correct to second order as is the case for the energy on application of the variational principle. The kinetic energy, therefore, is determined by the density gradient expansion, by using parametrized analytic forms for the density $n(\vec{r})$. This

procedure has been used in the determination of metal surface energies in the jellium approximation. But the results are found to lie considerably below the self-consistent values [2]. Ma and Sahni [2] have studied the convergence properties of the kinetic energy density gradient expansion.

The density gradient expansion for the kinetic energy contribution to the surface energy of an inhomogeneous electron gas may be written as

$$E_K^{GE}(n(\vec{r})) = E_K^{(1)}(n(\vec{r})) + E_K^{(2)}(n(\vec{r})) + E_K^{(3)}(n(\vec{r})), \quad \text{(a.32)}$$

where

$$E_K^{(1)}(n(\vec{r})) = \frac{3}{10}(3\pi^2)^{\frac{2}{3}} \int n(\vec{r})\left[n^{\frac{2}{3}}(\vec{r}) - \bar{n}^{\frac{2}{3}}\right] d\vec{r}, \quad \text{(a.33)}$$

$$E_K^{(2)}(n(\vec{r})) = \frac{1}{72} \int \frac{|\nabla n(\vec{r})|^2}{n(\vec{r})} d\vec{r}, \quad \text{(a.34)}$$

$$E_K^{(3)}(n(\vec{r})) = \frac{\gamma}{(3\pi^2)^{2/3} 540} \int n^{\frac{1}{3}}(\vec{r})\left[\left(\frac{\nabla^2 n(\vec{r})}{n(\vec{r})}\right)^2 - \frac{9}{8}\left(\frac{\nabla^2 n(\vec{r})}{n(\vec{r})}\right)\left(\frac{\nabla n(\vec{r})}{n(\vec{r})}\right)^2 + \frac{1}{3}\left(\frac{\nabla n(\vec{r})}{n(\vec{r})}\right)^4\right] d\vec{r}. \quad \text{(a.35)}$$

Here $E_K^{(1)}$ is density, where $k_F = \left(\frac{9\pi}{4}\right)^3 r_s^{-1} = k_F^3/3\pi^2$ being the bulk den correction. $E_K^{(3)}$ is the second $E_K^{(2)}$ is the first gradient correction. $E_K^{(3)}$ is the second density gradient correction valid for slowly varying densities. The paramater γ has the value 1. For a study of these

corrections, a linear potential model was employed.

$$V(x) = F \times \Theta(x) \quad , \tag{a.36}$$

where F is the field strength and $\Theta(x)$ is the step function. It was demonstrated [2] that the convergence of the gradient expansion E_K^{GE} is excellent for very slowly varying density. Hence the inclusion of the second density gradient term in the series removes practically all error for very slowly varying density. Thus, unlike Smith [3], whose surface energy values lie considerably below the self-consistent results of Lang and Kohn [2] due to the inclusion of only the first gradient correction, we must also include the second density gradient correction as given by Eq. (a.35) in all surface energy calculations of metal surfaces.

It is known that when $n(\vec{r})$ varies slowly over space, i.e. when

$$\frac{|\nabla n(\vec{r})|}{2 k_F n(\vec{r})} \leq 1 \quad , \tag{a.37}$$

and

$$\frac{|\nabla^2 n(\vec{r})|}{2 k_F |\nabla n(\vec{r})|} \ll 1 \quad , \tag{a.38}$$

(where $k_F = (3\pi^2 n)^{1/3}$ is the local Fermi momentum) the

kinetic and the exchange components of the total energy can be approximated by an asymptotic expansion in the density gradients [1]. We have seen that the gradient expansion for the kinetic energy converges as the density becomes more slowly varying. The same has been demonstrated to be true for the exchange energy also [3].

Unlike the Hartree-Fock theory, where the exchange contribution contains terms of order e^2, e^4 etc, e being the electron charge, the Kohn-Sham orbitals depend only on the electron density (and not on e) and hence the gradient expansion of the density functional exchange energy is purely of order e^2. The form of the gradient expansion is

$$E_x[n] = -\left(\frac{3}{4\pi}\right)(3\pi^2)^{\frac{1}{3}} \int d\vec{r}\; n^{\frac{4}{3}}(\vec{r}) - .00167 \int d\vec{r}\; \frac{|\nabla n(\vec{r})|^2}{n^{4/3}(\vec{r})} + \cdots \qquad \text{(a.39)}$$

The first term is the local density approximation for exchange (LDA). The gradient expansion approximation (GEA) retains the first two terms. The gradient term seems to correct all the error of LDA.

A.2.2 Correlation Energy:

Although the first density gradient correction to the exchange contribution gives reasonable results, it had been shown by Perdew et al [4] that the first gradient correction to LDA for exchange and correlation energy is inappropriate near metallic surfaces, in that it fails to

improve the energy. It should be noted that although the gradient expansion provides a systematic method for calculating corrections to LDA, even the lowest order coefficient in it had not been known except in the high density limit.

In the density functional theory, which is exact in principle, correlation is explicitly included in the total energy and one-body potential. In practice exchange and correlation are treated together in the local spin density (LSD) formalism [1,5]. This LSD exchange-correlation energy cancels most of the spurious self-interacting Coulomb energy.

In a study of self interaction correction to the density functional theory, Perdew and Zunger [6] have described SIC-LSD(self interaction correction-local spin density) formalism for an inhomogeneous many electron system. The parametrized electron-gas correlation energy, $\epsilon_c(n_\uparrow, n_\downarrow)$, they have used are based on Ceperley's [7] accurate calculations for low and metallic densities. Ceperley's expression had been matched smoothly to the correct high density limit. They have shown that other parametrized correlation energies commonly used in density functional calculations are in error at the high densities which are important in atoms. Ceperley's parametrized expression for correlation energy, for $r_s \gg 1$ is

$$\epsilon_c^i = \frac{\gamma_i}{\left[1 + \beta_1^i \sqrt{r_s} + \beta_2^i r_s\right]}, \qquad \text{(a.40)}$$

where $i = u$ (unpolarized, $\zeta = 0$) or p(polarized, $\zeta = 1$).

ζ is defined as

$$\zeta = \frac{n_\uparrow - n_\downarrow}{n} \quad , \tag{a.41}$$

where $n = [4\pi r_s^3(n)/3]^{-1}$. For $r_s \gg 1$ and unpolarized electron-gas the Ceperley parameters have the following values:

$$\begin{aligned} \gamma &= -0.1471 \\ \beta_1 &= 1.1581 \\ \beta_2 &= 0.3446 \end{aligned} \tag{a.42}$$

These parameters are obtained by fitting the r_s dependence of the correlation energy and they are in atomic units.

More recently Langreth and Mehl [8] have developed an expression for the exchange and correlation term, E_{xc}, that is based on the RPA.

$$E_{xc} = E_{xc}^{LDA} + (4.28 \times 10^{-3}) \int d\vec{r}\, \frac{|\nabla n|^2}{n^{\frac{4}{3}}} \left[2e^{-F} - \frac{7}{9} \right] , \tag{a.43}$$

where $F = 0.262\, |\nabla n| / n^{\frac{7}{6}}$. The units are such that energy is in Rydbergs and lengths in Bohrs.

The effect of incorporating these improvements in our calculation of spontaneous dipole moments of small metallic particles in Chapter I, has not been conclusively determined

due to computational difficulties. However, we expect to see some changes in the nature of our results and hope to carry the problem to completion in the near future.

References:

1. P. Hohenberg and W. Kohn, Phys. Rev. 136 , B864 (1964)
   W. Kohn and L. J. Sham, Phys. Rev. 140 , A1133 (1965)
   For a review see N. D. Lang in Solid State Physics,
   Vol. 28, p-225, ed. F. Seitz and D. Turnbull.
2. C. Q. Ma and V. Sahni, Phys. Rev. B16 , 4249 (1977)
   N. D. Lang and W. Kohn, Phys. Rev. B1 , 4555 (1970)
3. V. Sahni, J. Gruenebaum, and J. P. Perdew, preprint.
4. J. P. Perdew, D. C. Langreth, and V. Sahni,
   Phys. Rev. Lett. 38 , 1030 (1977)
5. A. K. Rajgopal and J. Callaway, Phys. Rev. B7 , 1912
   (1973)
6. J. P. Perdew and Alex Zunger, Phys. Rev. B23 , 5048
   (1981)
7. D. M. Ceperley, Phys. Rev. B18 , 3126 (1978)
8. D. C. Langreth and M. J. Mehl, Phys. Rev. Lett. 47 ,
   446 (1981)

APPENDIX B

METHOD OF DALGARNO AND LEWIS

Often in the evaluation of the correction to energy of a system, to second order in perturbation theory, we come across summations of the form

$$W_2 = \sum_{n \neq o} \frac{\langle o|H'|n\rangle\langle n|H'|o\rangle}{E_o - E_n} \quad , \qquad (b.1)$$

where H' is the perturbation Hamiltonian and E_n is the energy eigenvalue of the unperturbed state $|n\rangle$. An actual evaluation of W_2 in Eq. (b.1) is difficult if one sets out to determine the value of the infinite summation involved. However, a much simpler method owes its existence to Dalgarno and Lewis [B.1], and can be used to replace the evaluation of the infinite summation by the solution of an inhomogeneous differential equation.

Suppose there exists an operator F such that

$$\frac{\langle n|H'|o\rangle}{E_o - E_n} = \langle n|F|o\rangle \quad , \qquad (b.2)$$

for all states $|n\rangle$ other than the ground state. Substitution of this relation into Eq. (b.1) then gives

$$W_2 = \langle o|H'F|o\rangle - \langle o|H'|o\rangle\langle o|F|o\rangle \quad . \qquad (b.3)$$

Thus, if F can be found, the evaluation of of W_2 is greatly simplified. Usually F is obtained from the solution of an inhomogeneous differential equation.

To illustrate the application of this method we evaluate the expectation value of Eq. (I.98). The left hand side of Eq. (I.98) is

$$I = \langle \phi_0 | \varphi \left[\varphi^2 - \frac{\rho^2}{2} \right] G \varphi | \phi_0 \rangle \quad , \qquad \text{(b.4)}$$

where

$$G = \sum_{n \neq 0} \frac{|\phi_n\rangle\langle\phi_n|}{E_0 - E_n} \quad . \qquad \text{(b.5)}$$

Let us write

$$G \varphi | \phi_0 \rangle = | u \rangle \quad . \qquad \text{(b.6)}$$

Then Eq. (b.4) becomes

$$I = \langle \phi_0 | \varphi \left[\varphi^2 - \frac{\rho^2}{2} \right] | u \rangle \quad . \qquad \text{(b.7)}$$

The state $|u\rangle$ satisfies the equation

$$\sum_{n \neq 0} \frac{|\phi_n\rangle\langle\phi_n|}{E_0 - E_n} \varphi | \phi_0 \rangle = | u \rangle \quad , \qquad \text{(b.8)}$$

which can be written as

$$[E_0 - H]|u\rangle = \varphi|\phi_0\rangle \quad . \qquad (b.9)$$

For hydrogen atom, the Hamiltonian is

$$H = -\frac{1}{2}\nabla^2 - \frac{1}{r} \quad , \qquad (b.10)$$

and E_0=-1/2. Hence $|u\rangle$ satisfies the differential equation

$$\left[-\frac{1}{2} + \frac{1}{2}\nabla^2 + \frac{1}{r}\right]|u\rangle = \varphi|\phi_0\rangle \quad . \qquad (b.11)$$

Our knowledge of the hydrogen ground state $|\phi_0\rangle = e^{-r/a_0}/\sqrt{\pi}$ and φ , provides us with a solution of $|u\rangle$:

$$|u\rangle = -\frac{e^{-\frac{r}{a_0}}}{\sqrt{\pi}}\left(r + \frac{r^2}{2}\right)\cos\theta \quad , \qquad (b.12)$$

where we have used the transformation

$$u = \frac{v}{r}\cos\theta \quad , \qquad (b.13)$$

and have expanded v as follows

$$v = \sum_n a_n r^n e^{-r/a_0} \quad . \qquad (b.14)$$

Then substitution of $|u\rangle$ into Eq. (b.7) and subsequent integration yields

$$I = -\frac{33}{4}\frac{a_o^5}{e^2} \quad . \qquad \text{(b.15)}$$

References

B.1 A. Dalgarno and J. T. Lewis, Proc. Roy. Soc. (London) A233 , 70 (1955)

APPENDIX C

FREE OSCILLATIONS OF A SPHERE

Free oscillations of a sphere have been studied extensively by Mie [C.1] and others in subsequent years. Mie had treated transverse modes of a sphere classically and considered absorption of electromagnetic radiation by such a sphere. Calculations including plasma excitations for a plane surface has been carried out by Ruppin [C.2]. Recently Penn and Rendell [C.3] have obtained the absorption by small metallic spheres, including electron-hole pair excitations.

We have studied the electromagnetics of a spheroidal bump on plane and calculated various quantities including the decay rates of the bump to surface plasmons and phonons and photons etc. (see Chapter II). Our goal here is to bring out the transparency of the procedure by considering a simple system, namely a sphere of radius a and composed of a material of dielectric constant $\epsilon(\omega)$.

C.1 Frequency of Oscillation

The electrostatic potentials inside and outside a sphere are given by

$$\phi_{in} = \sum_{l=0}^{\infty} A_l r^l P_l(\cos\theta) \quad , \qquad (c.1)$$

and

$$\phi_{out} = \sum_{l=0}^{\infty} \left[B_l r^l + C_l r^{-l-1} \right] P_l(\cos\theta) \quad , \qquad (c.2)$$

where $P_l(x)$ are Legendre functions of first kind. Here A_l, B_l, and C_l are expansion coefficients, determined by matching appropriate boundary conditions. Limiting ourselves to dipolar case (l=1) we get

$$\phi(\vec{r}) = \begin{cases} \phi_o r \cos\theta & , \quad r < a \\ \phi_o a^3 \dfrac{\cos\theta}{r^2} & , \quad r > a \end{cases} \qquad (c.3)$$

where ϕ_o is a constant coefficient. Continuity of the normal component of the displacement vector, D_r, gives

$$Re\ \epsilon(\omega) + 2 = 0 \quad . \qquad (c.4)$$

This gives the frequencies of the free oscillations of the sphere. Hence Eq. (c.4) is the condition for a dipolar surface plasmon of the sphere. If we don't restrict ourselves to the dipolar case, the condition for a plasmon of the sphere is

$$Re\ \epsilon(\omega) + \frac{l+1}{l} = 0 \quad . \qquad (c.5)$$

The spherical surface plasmon energy is ~ 3.5 eV and this is below the value for a flat surface where it is 3.68 eV (i.e. Re $\epsilon + 1 = 0$). Both values are below the bulk plasmon frequency $\hbar\omega_B = 3.81$ eV (where $\epsilon = 0$). The above values of surface and bulk plasmon energies are quoted for Ag.

The sphere polarizability, β, is obtained by considering the forced oscillations of the sphere, and is given by

$$\beta = \left(\frac{\epsilon - 1}{\epsilon + 2}\right) a^3 \quad . \qquad \text{(c.6)}$$

C.2 Decay Rate of an Oscillation

The frequencies of oscillation of a sphere are obtained from Eq. (c.4). $\epsilon(\omega)$ is, in general, complex and so also the frequency ω. The real part of ω, denoted by ω_r, is the surface plasmon resonance frequency, so that

$$\text{Re } \epsilon(\omega_r) + 2 = 0 \quad , \qquad \text{(c.7)}$$

and the imaginary part of ω, ω_i, determines the decay rate of an oscillation. So expanding the left hand side of Eq. (c.4) around ω_r, and assuming $\text{Im}\,\epsilon \ll \text{Re}\,\epsilon$, we get

$$\epsilon(\omega) + 2 \simeq \frac{\partial \text{Re}\,\epsilon(\omega_r)}{\partial \omega_r}\left[\omega - \omega_r + \frac{i\,\text{Im}\,\epsilon(\omega_r)}{\frac{\partial}{\partial\omega_r}\text{Re}\,\epsilon(\omega_r)}\right] \qquad \text{(c.8)}$$

$$\sim (\omega - \omega_r) + i\Gamma/2 \quad , \qquad \text{(c.9)}$$

where Γ is the rate at which the oscillation decays. Hence

$$\Gamma = \frac{2\,\mathrm{Im}\,\epsilon(\omega_r)}{\frac{\partial}{\partial\omega_r}\mathrm{Re}\,\epsilon(\omega_r)} \quad . \qquad \text{(c.10)}$$

C.3 Power Delivered by an Oscillation

Power delivered to the system via the conversion of electromagnetic energy to mechanical energy of the sphere is given by the relation

$$P = \int_{r<a} \frac{\sigma}{2} |\vec{E}|^2 d\vec{r} \quad , \qquad \text{(c.11)}$$

where σ is the conductivity of the material of the sphere and E is the electric field inside the sphere. Substituting for the electric field $\vec{E}$ we get

$$P = \frac{2\pi}{3} a^3 \sigma |\phi_0|^2 \quad . \qquad \text{(c.12)}$$

In terms of the dielectric function, $\epsilon(\omega)$,

$$\sigma = \frac{\omega}{4\pi}\,\mathrm{Im}\,\epsilon(\omega) \quad . \qquad \text{(c.13)}$$

Hence Eq. (c.12) becomes

$$P = \frac{\omega a^3}{6}\,\mathrm{Im}\,\epsilon(\omega)\,|\phi_0|^2 \quad . \qquad \text{(c.14)}$$

The constant ϕ_o is obtained by noting that the energy stored in the system is

$$U = \frac{P}{\Gamma} = \frac{\omega a^3}{6} \frac{|\phi_o|^2}{2} \frac{\partial}{\partial \omega_r} Re\, \epsilon(\omega_r) \qquad \text{(c.15)}$$

$$\equiv \hbar \omega_r \quad . \qquad \text{(c.16)}$$

Hence

$$\phi_o = \left[\frac{12\hbar}{a^3 \frac{\partial}{\partial \omega} Re\, \epsilon(\omega)} \right]^{\frac{1}{2}} \quad . \qquad \text{(c.17)}$$

Eqs. (c.14) and (c.17) can be used to calculate the power, P.

C.4 Dipole Moment of the Sphere

A deformable sphere is expected to possess a dipole moment due to charge rearrangement. Hence an oscillating sphere possesses a dipole moment, which is obtained by examining the asymptotic ($r \to \infty$) behavior of the potential ϕ. The dipole moment, μ, is therefore given by

$$\mu = \phi_o a^3 = \left[\frac{12\hbar a^3}{\frac{\partial}{\partial \omega} Re\, \epsilon(\omega)} \right]^{\frac{1}{2}} \quad . \qquad \text{(c.18)}$$

C.5 Decay to Photons

The radiative decay rate, Γ_r , of the oscillations of the sphere is obtained by observing that

$$\Gamma_r = \frac{P_r}{\hbar\omega} \quad , \qquad \text{(c.19)}$$

where P_r is the power radiated and ω is the frequency of radiation. From classical electrodynamics we know that an oscillating dipole radiates and the radiated power is given by

$$P_r = \frac{|M|^2 \omega^4}{3c^3} \quad . \qquad \text{(c.20)}$$

Hence

$$\Gamma_r = \left(\frac{4\omega^3 a^3}{c^3}\right)\left[\frac{\partial}{\partial\omega} Re\, \epsilon(\omega)\right]^{-1} \quad . \qquad \text{(c.21)}$$

This is decay rate of the oscillating sphere dipole to photons. For systems more general, the total decay rate, Γ_{tot} , would include the decay rates to other channels available. The Q of the resonance is then defined according to

$$Q = \frac{\hbar\omega}{\Gamma_{tot}} \quad . \qquad \text{(c.22)}$$

References

C.1 G. Mie, Ann. Phys. (Leipzig) 25 , 377 (1908)

C.2 R. Ruppin, Phys. Rev. 11 , 2871 (1975)

C.3 D. R. Penn and R. W. Rendell, Phys. Rev. Lett. 47 , 1067 (1981)

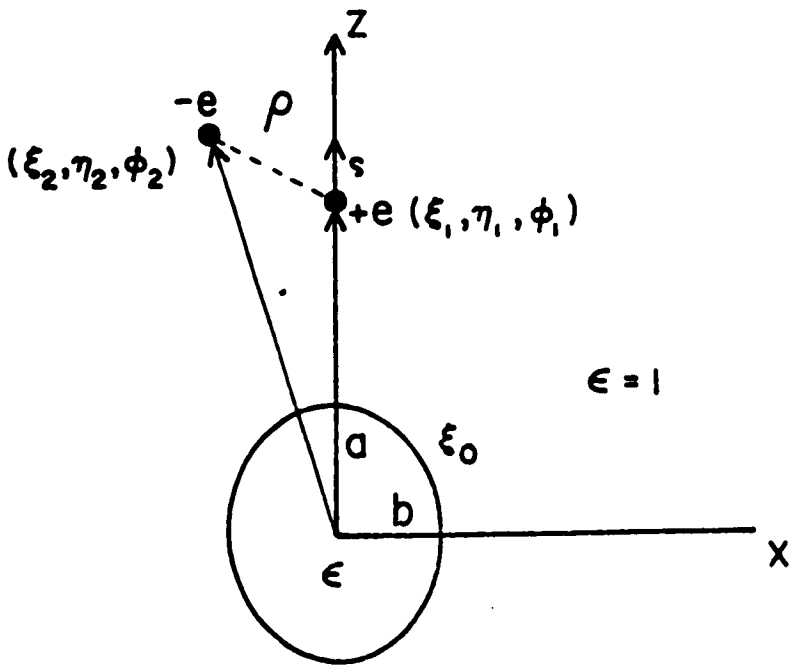

Fig. I.1

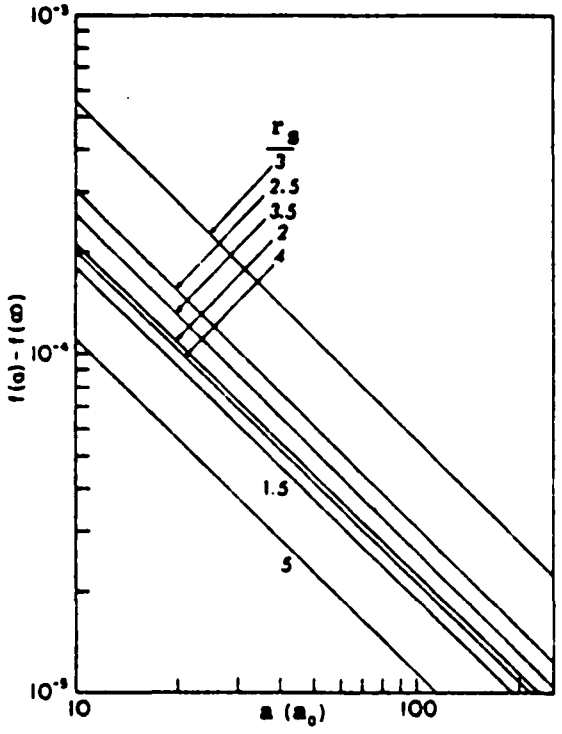

Fig. I.2

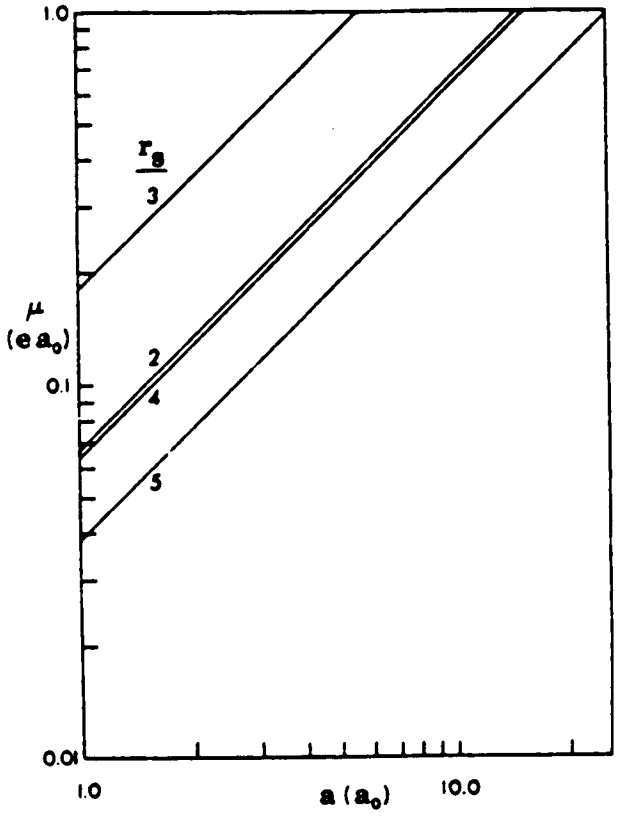

Fig. I.3

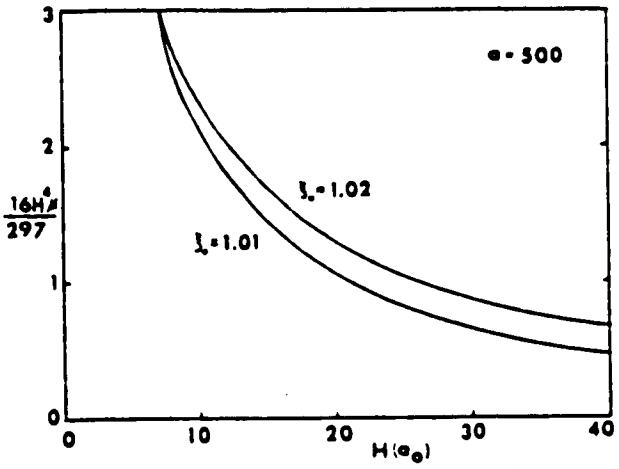

Fig. I.4

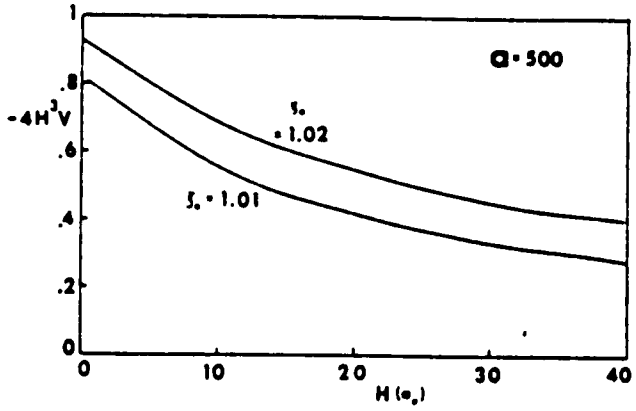

Fig. I.5

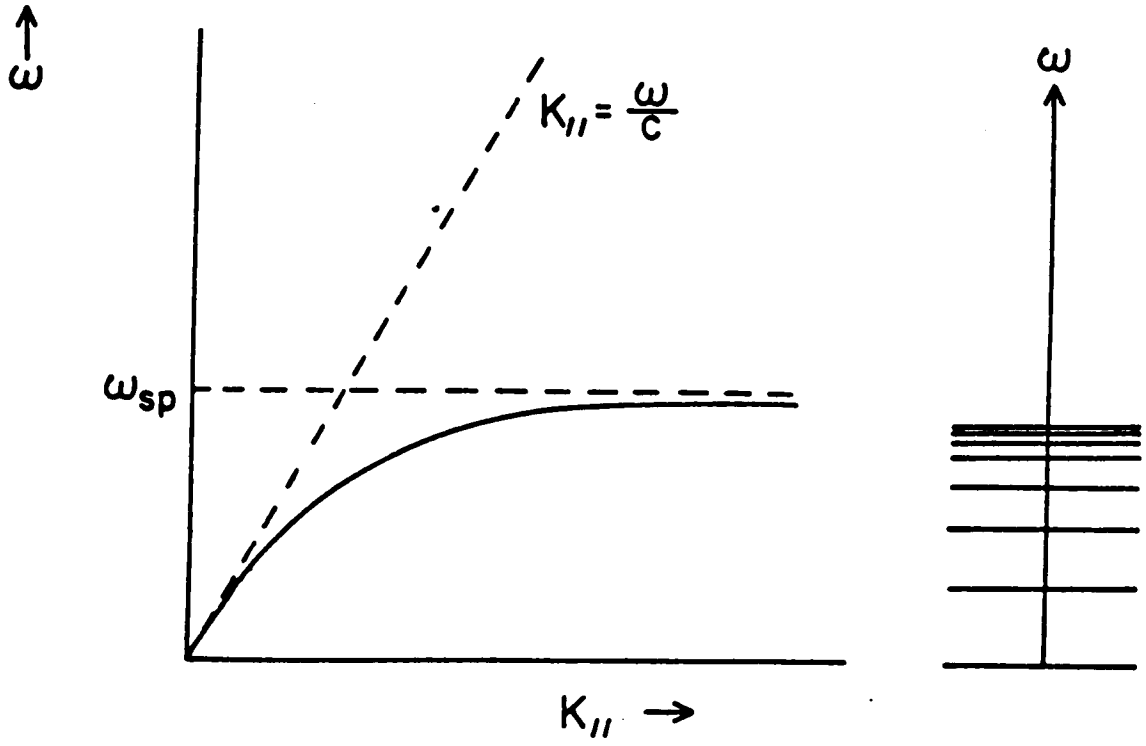

Fig. II.1

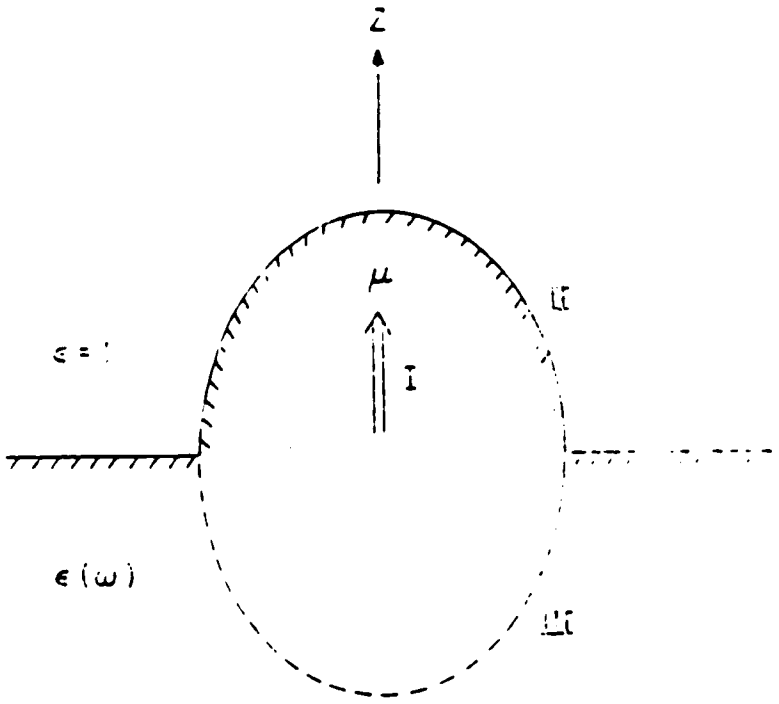

Fig.II.2

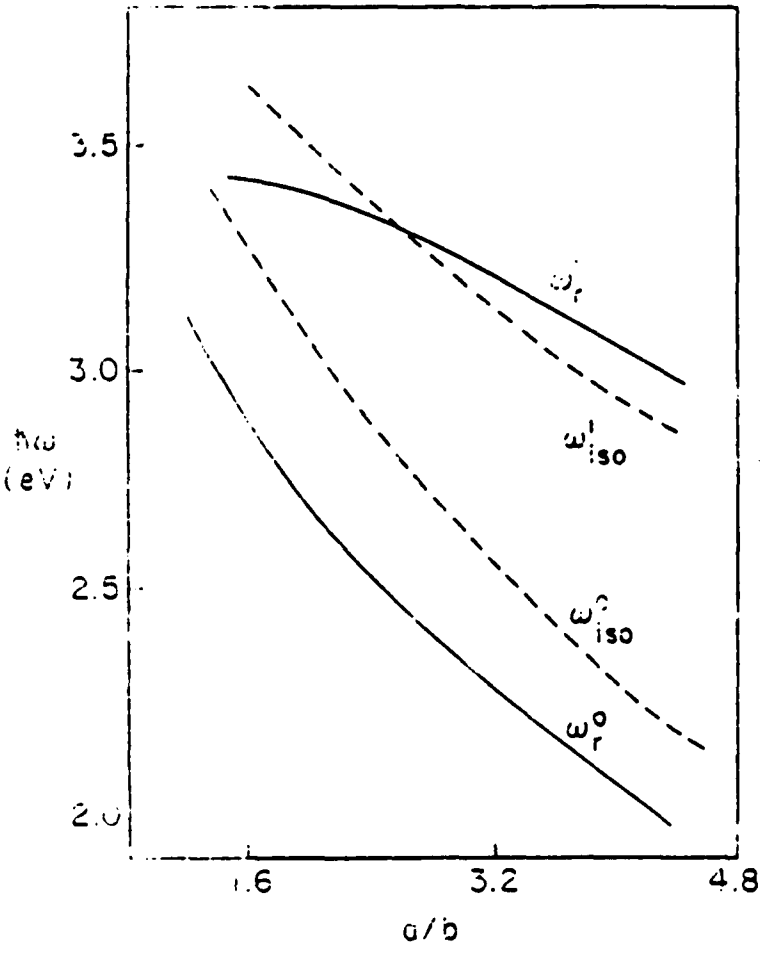
3.5
3.0
2.5
2.0
ħω
(eV)
1.6
3.2
4.8
a/b
ω_r^1
ω_{iso}^1
ω_{iso}^0
ω_r^0

Fig. II.3

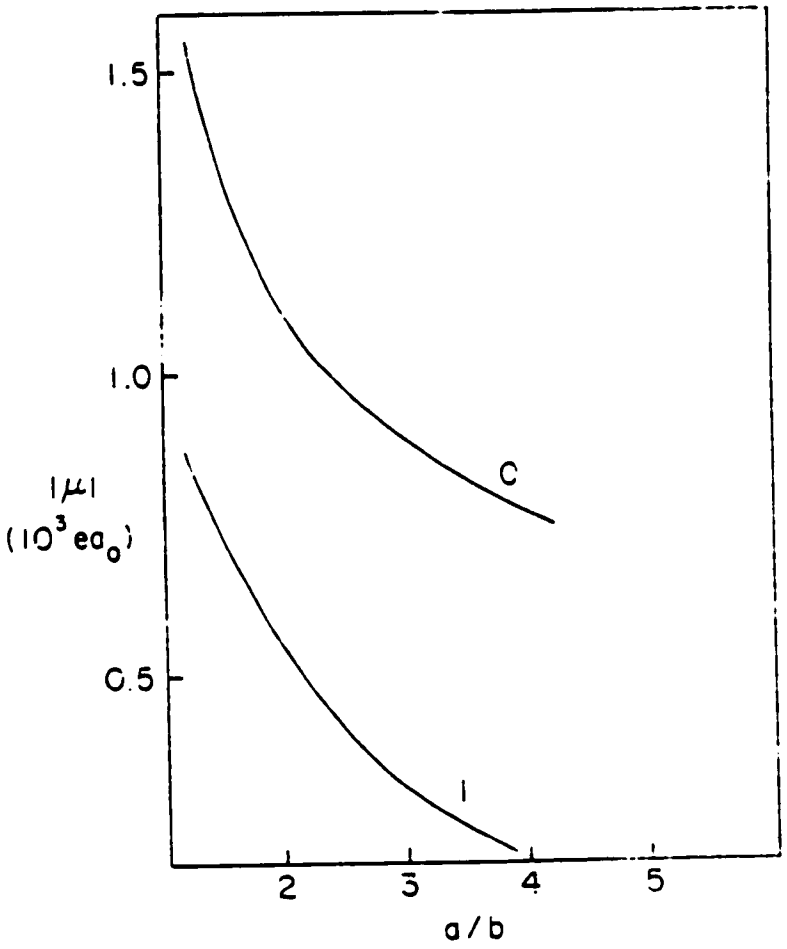

Fig. II.4

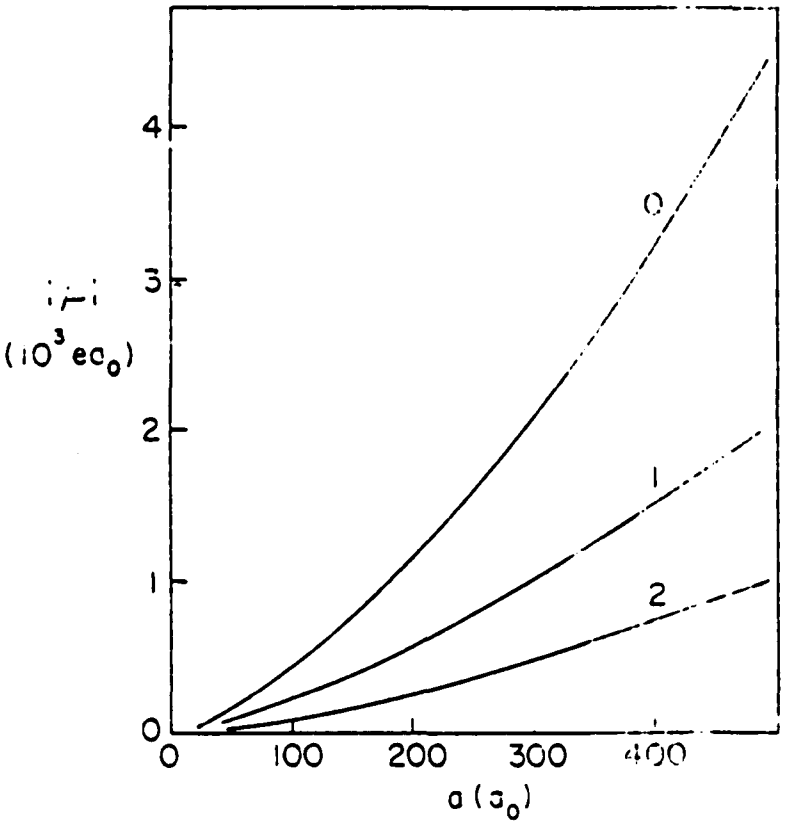

Fig. II.5

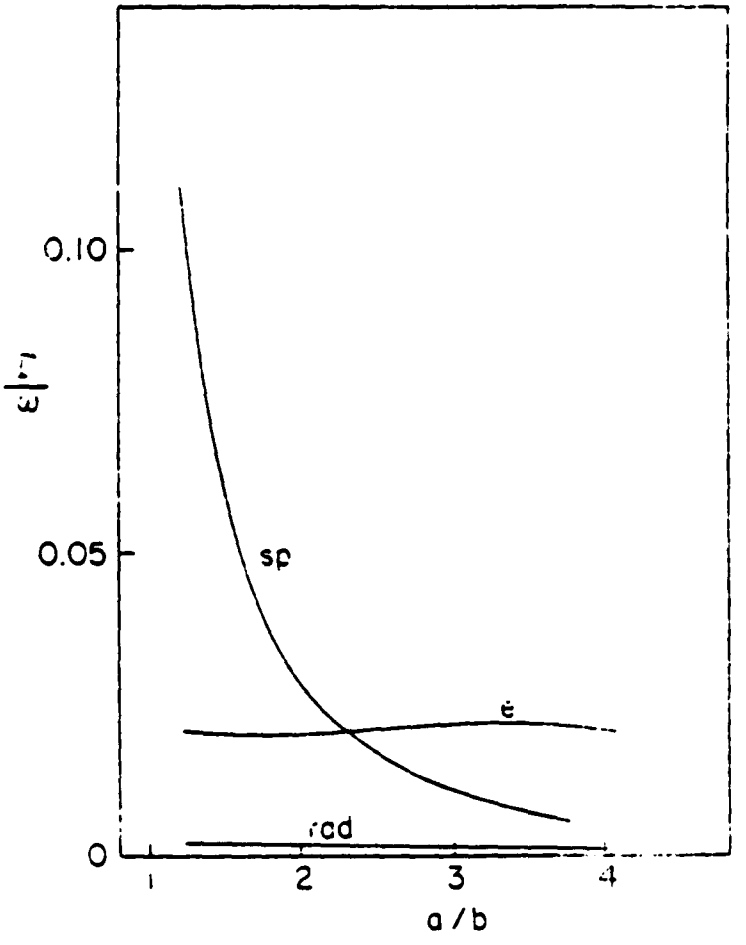

Fig. II.6

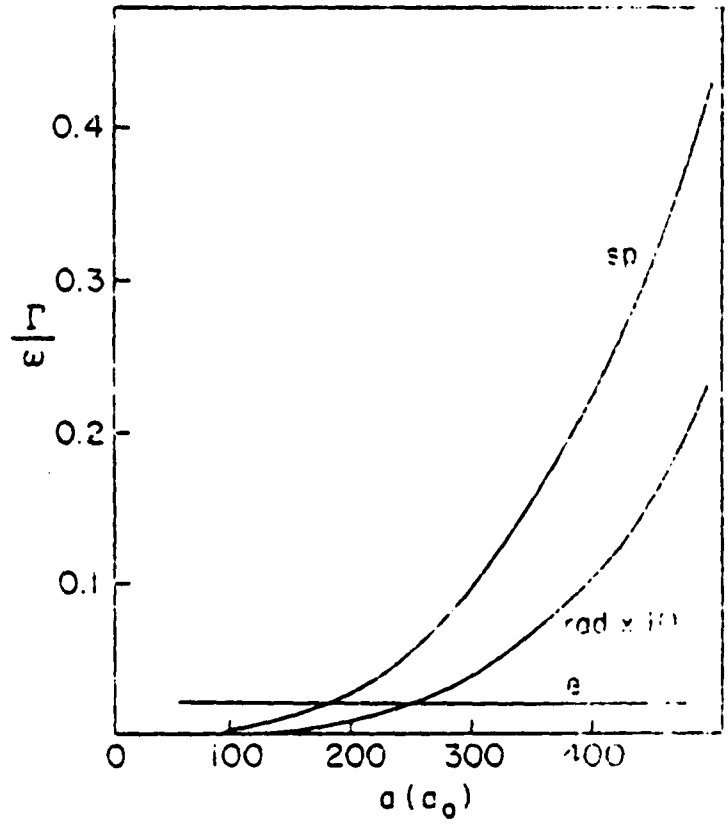

Fig. II.7

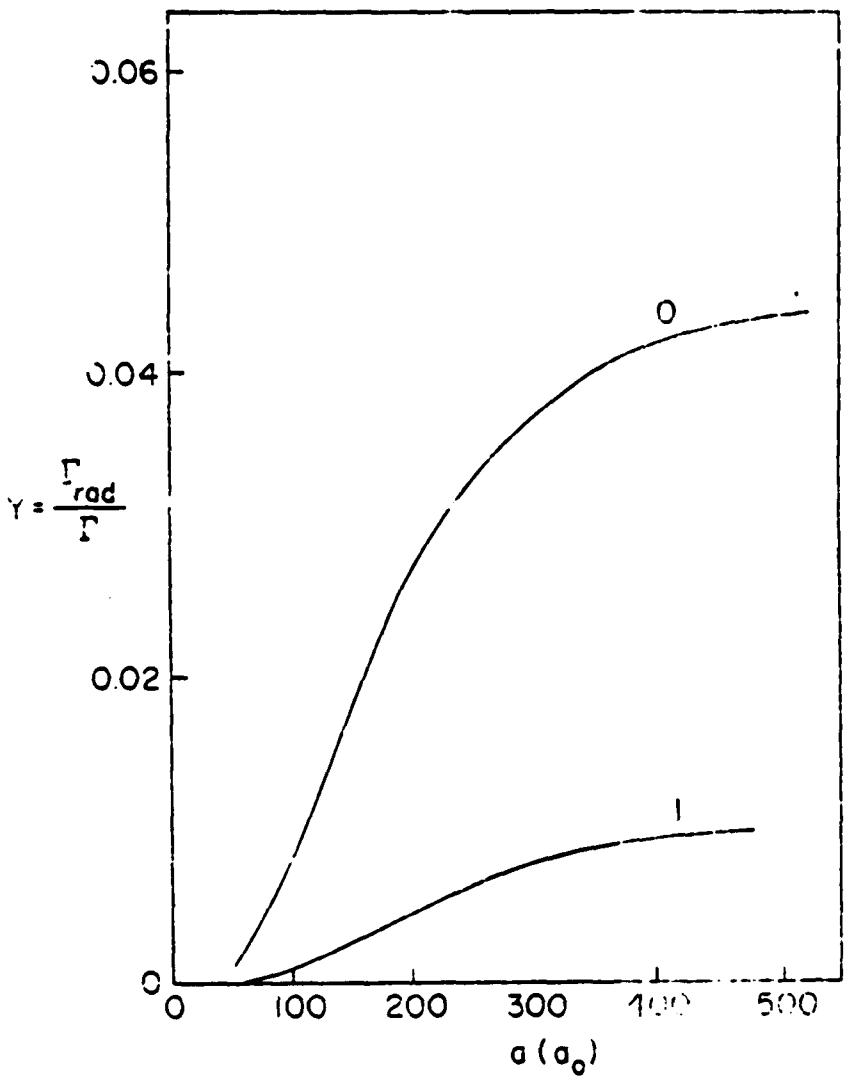
0.06
0.04
0.02
0
$\gamma = \frac{\Gamma_{rad}}{\Gamma}$
0
100
200
300
400
500
a (a_0)
0
1

Fig. II.8

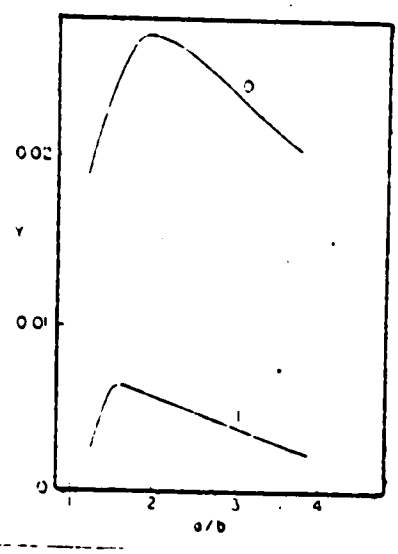

Fig. II.9

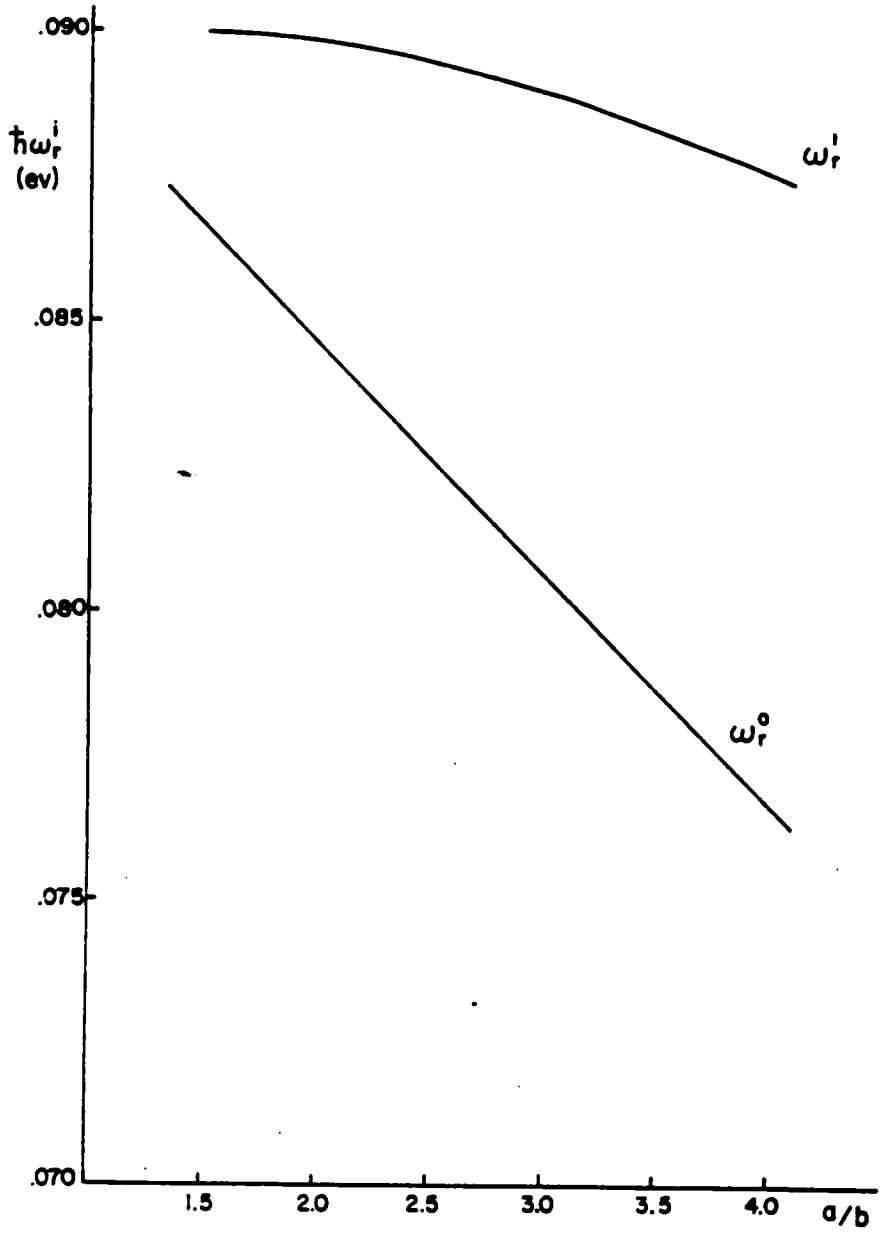

Fig. II.10

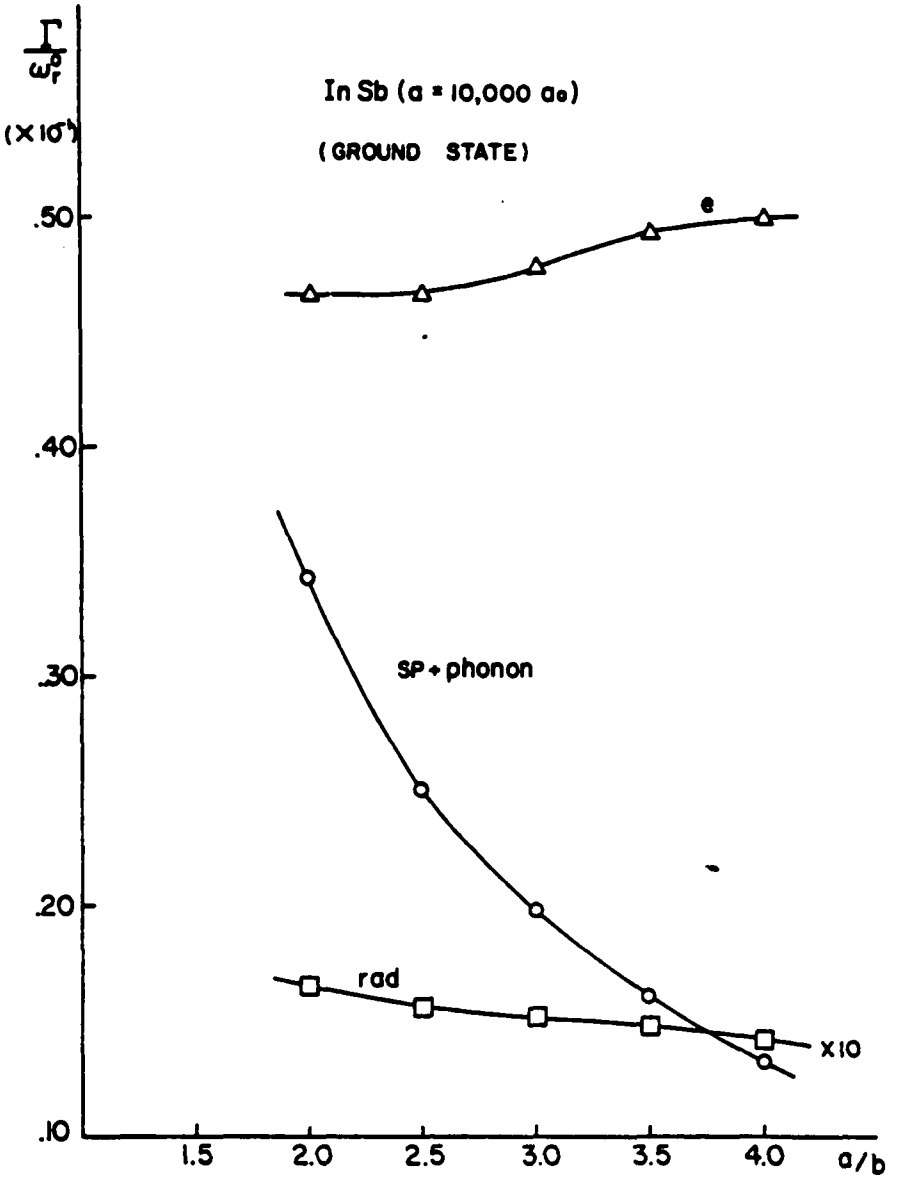
Γ/ω_r^0
(×10^-1)
In Sb (a = 10,000 a_0)
(GROUND STATE)
e
.50
.40
.30
.20
.10
SP + phonon
rad
x10
1.5
2.0
2.5
3.0
3.5
4.0
a/b

Fig. II.11

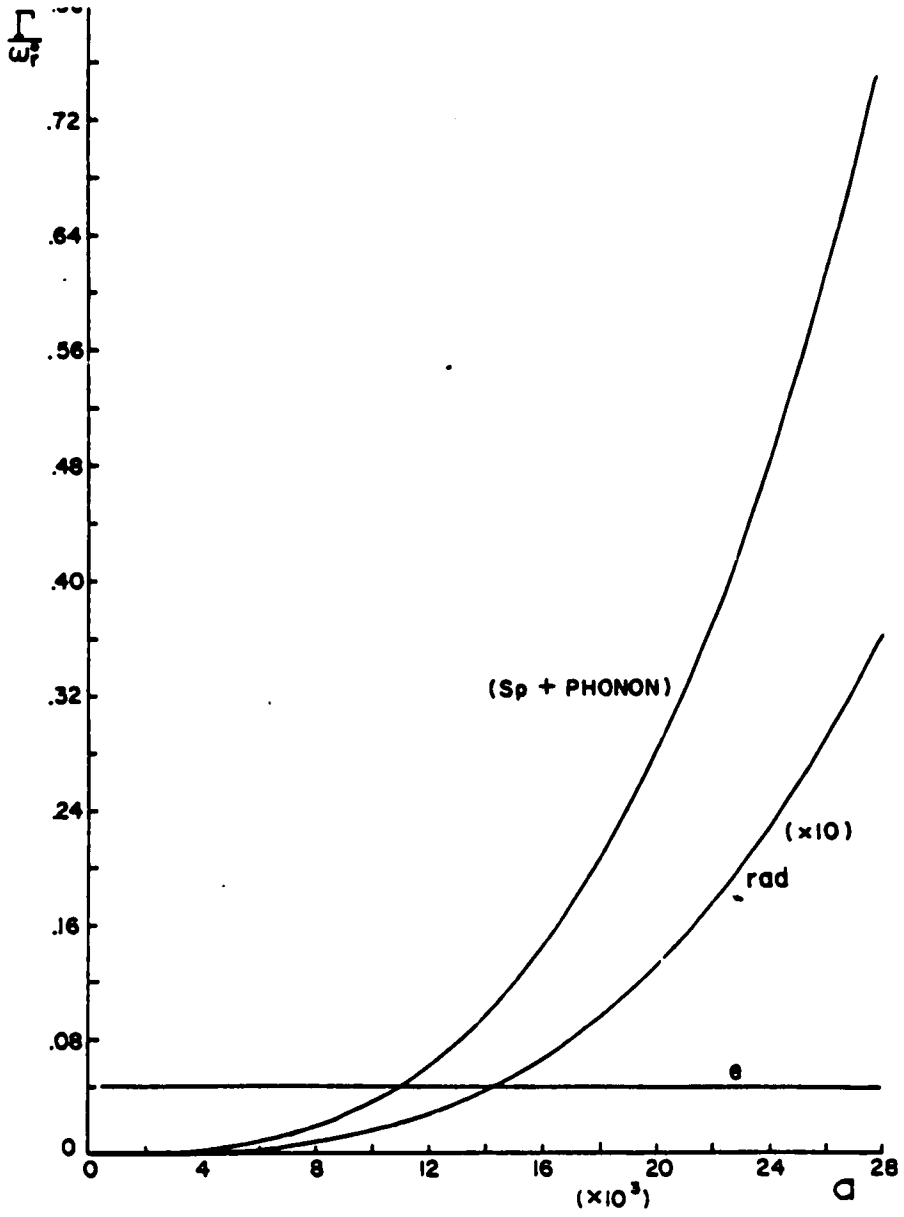
Γ/ω_r^3
.72
.64
.56
.48
.40
.32
.24
.16
.08
0
0
4
8
12
16
20
24
28
(×10^3)
a
(Sp + PHONON)
(×10)
rad
e

Fig. II.12

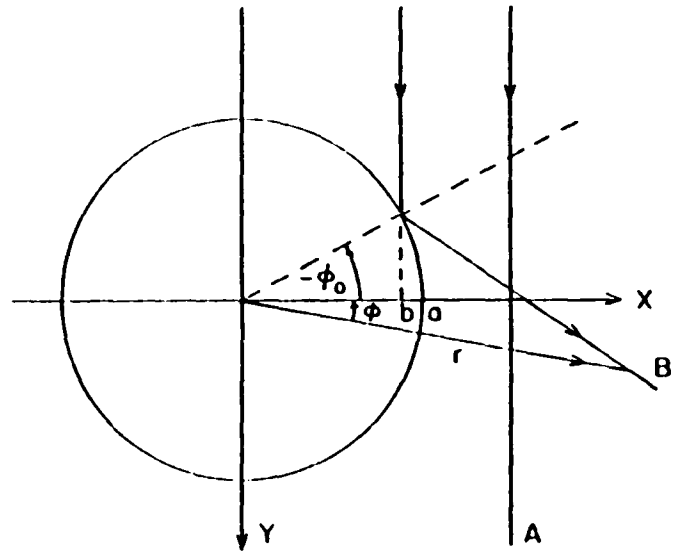

Fig. III.1

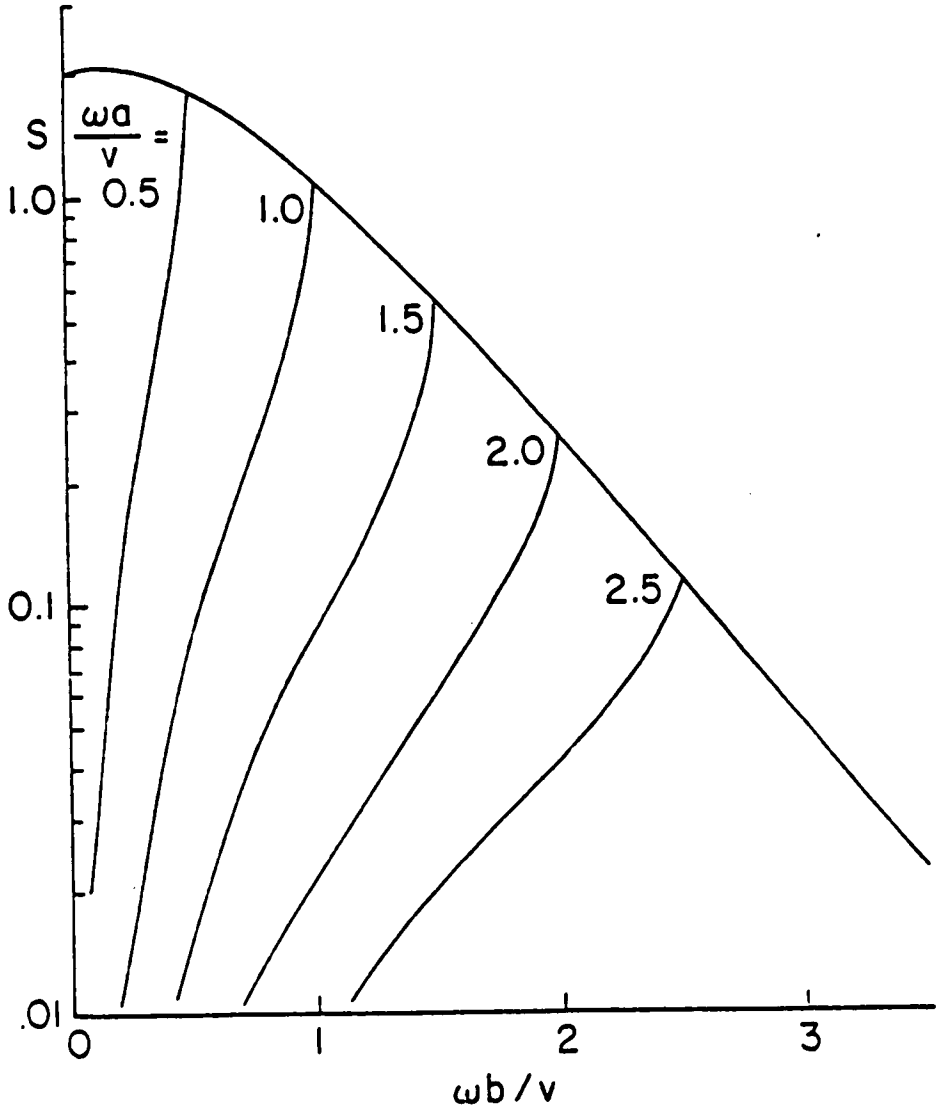

Fig. III.2

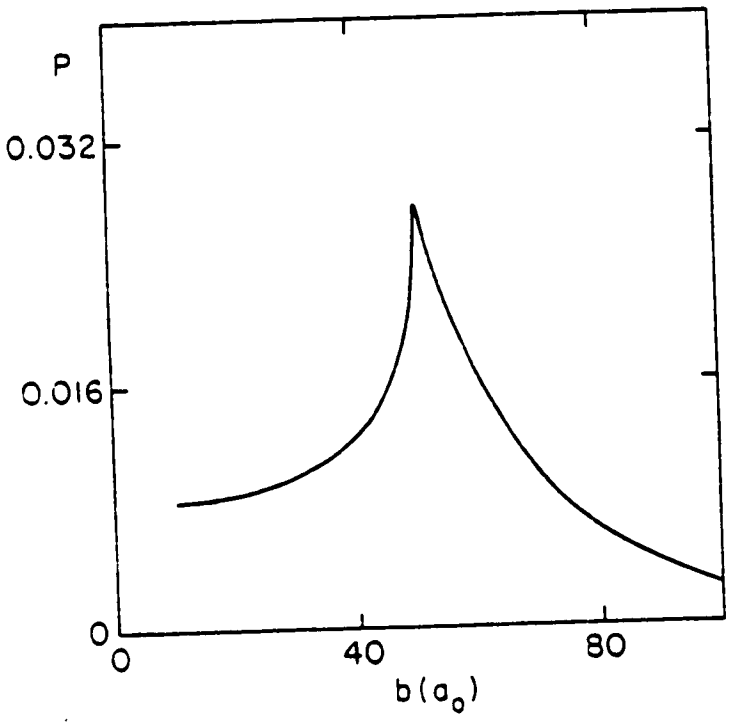

Fig. III.3

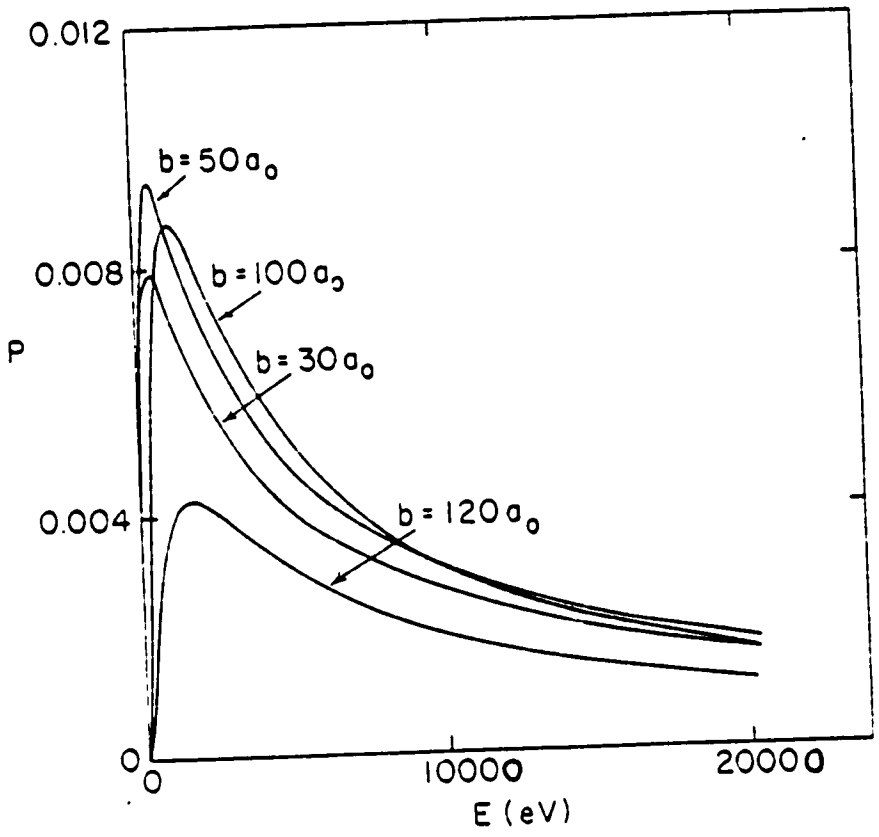
0.012
0.008
0.004
0
P
b = 50 a0
b = 100 a0
b = 30 a0
b = 120 a0
0
10000
20000
E (eV)

Fig. III.4

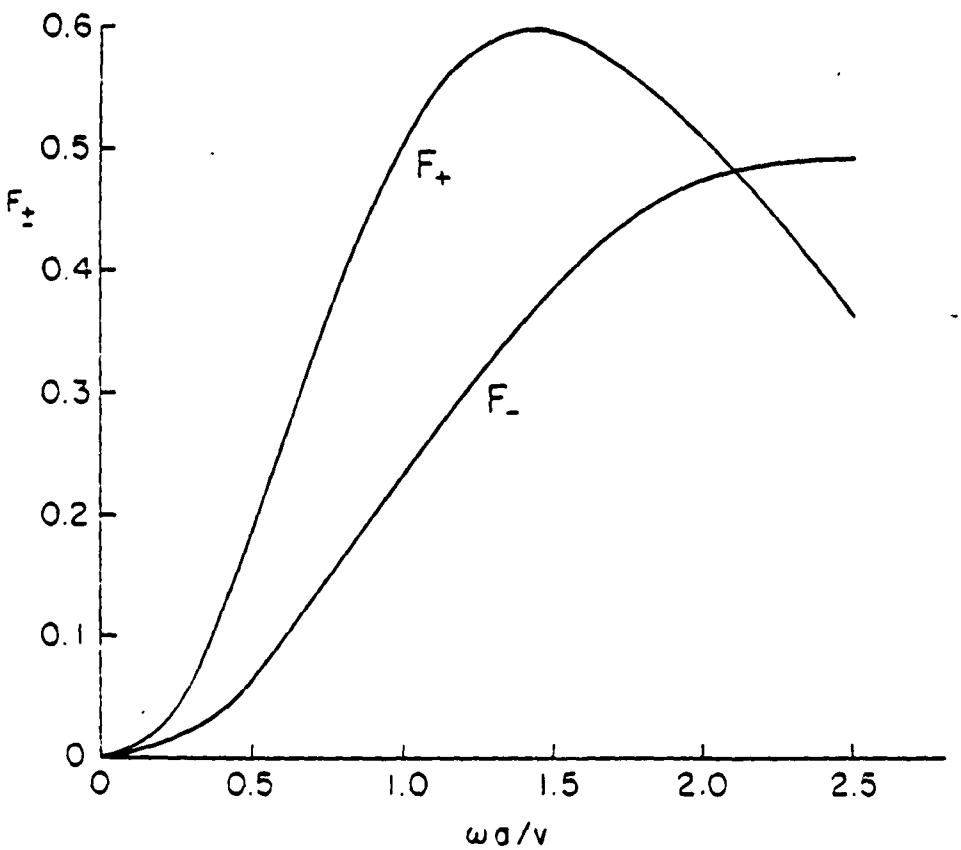

Fig. III.5

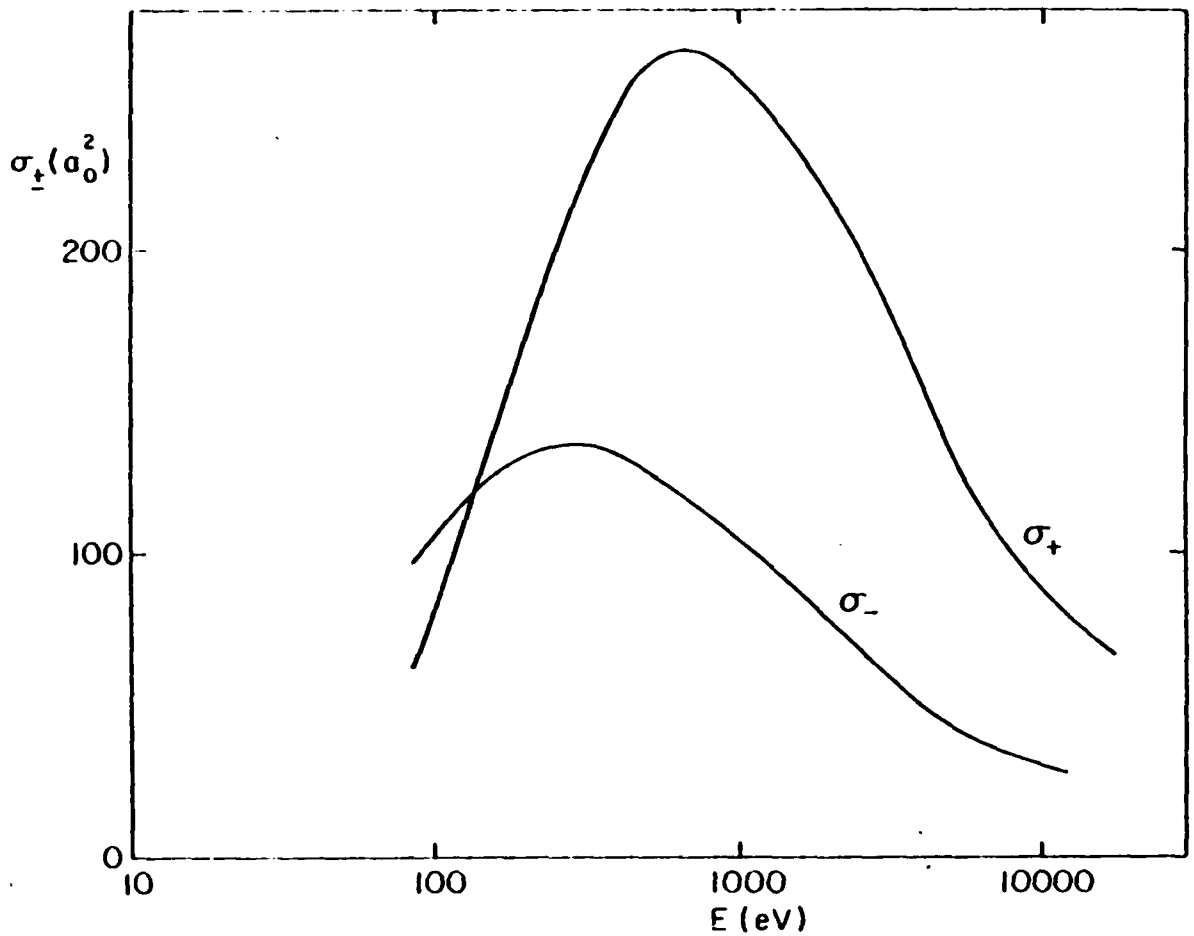

Fig. III.6

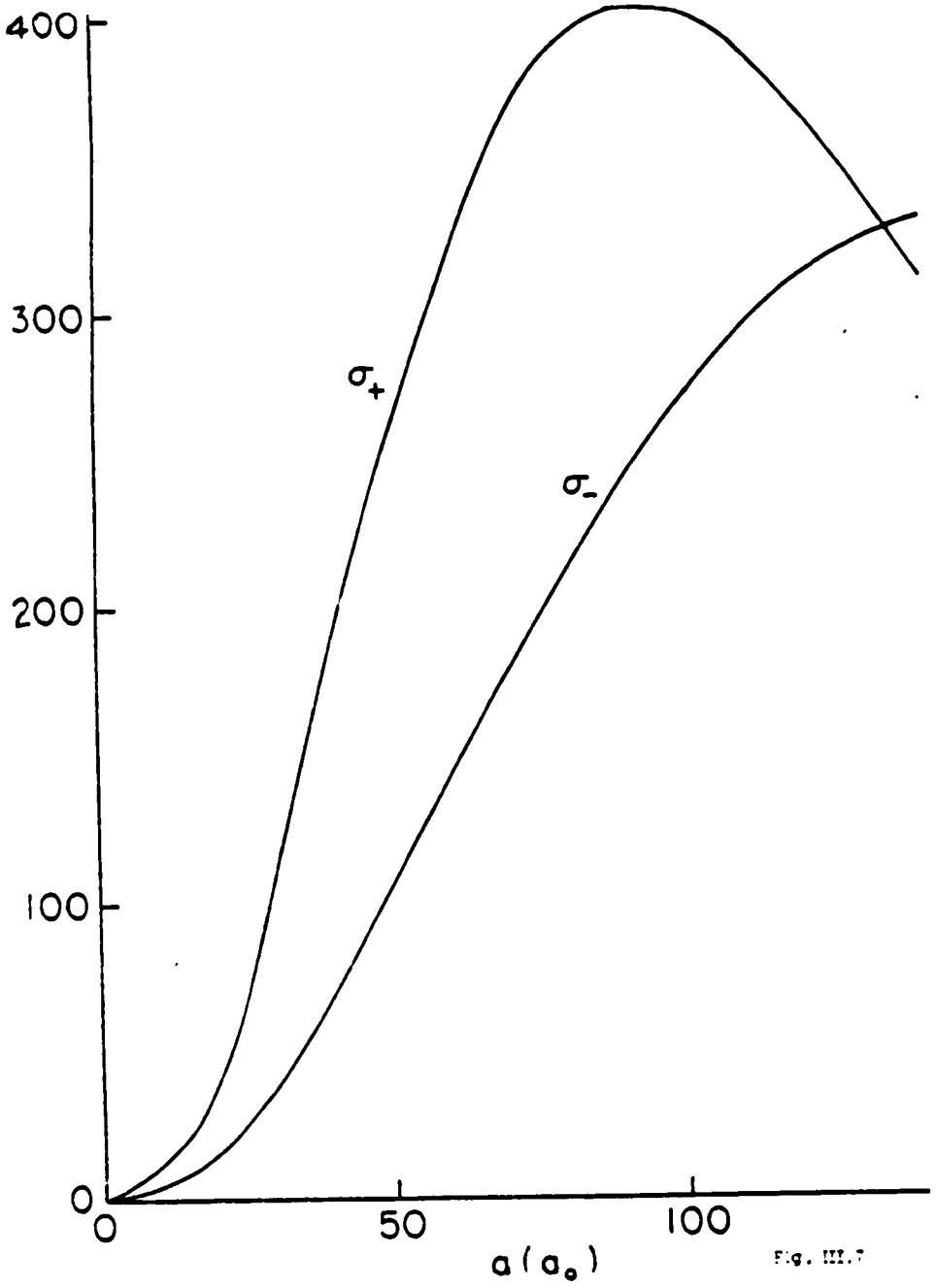

Fig. III.7

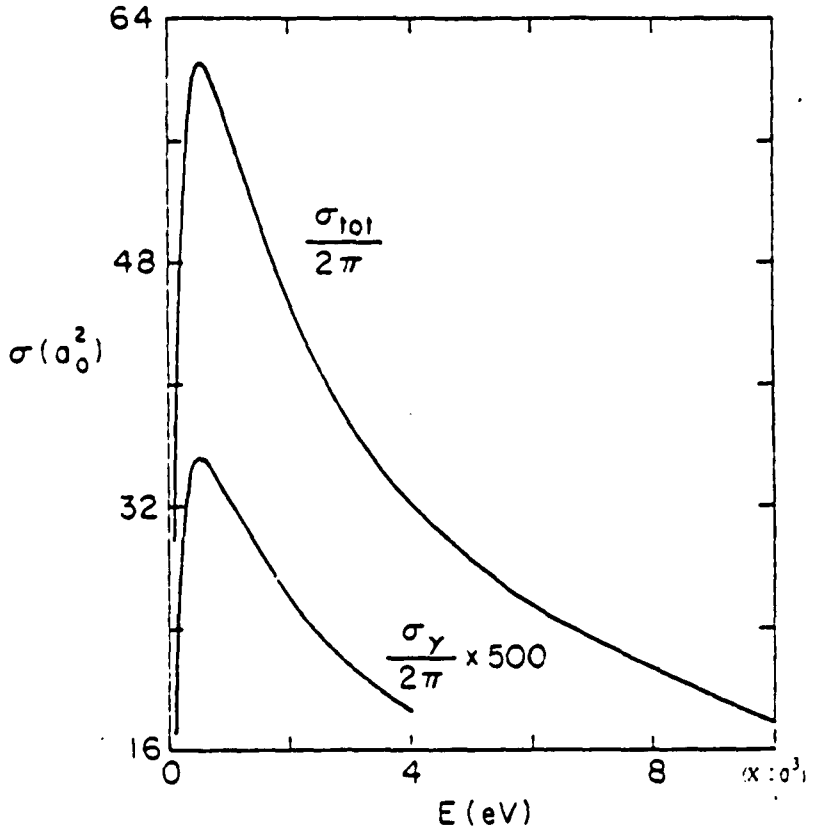
64
48
32
16
$\sigma(a_0^2)$
$\frac{\sigma_{tot}}{2\pi}$
$\frac{\sigma_\gamma}{2\pi}$ x 500
0
4
8
(x 10^3)
E (eV)

Fig. III.9

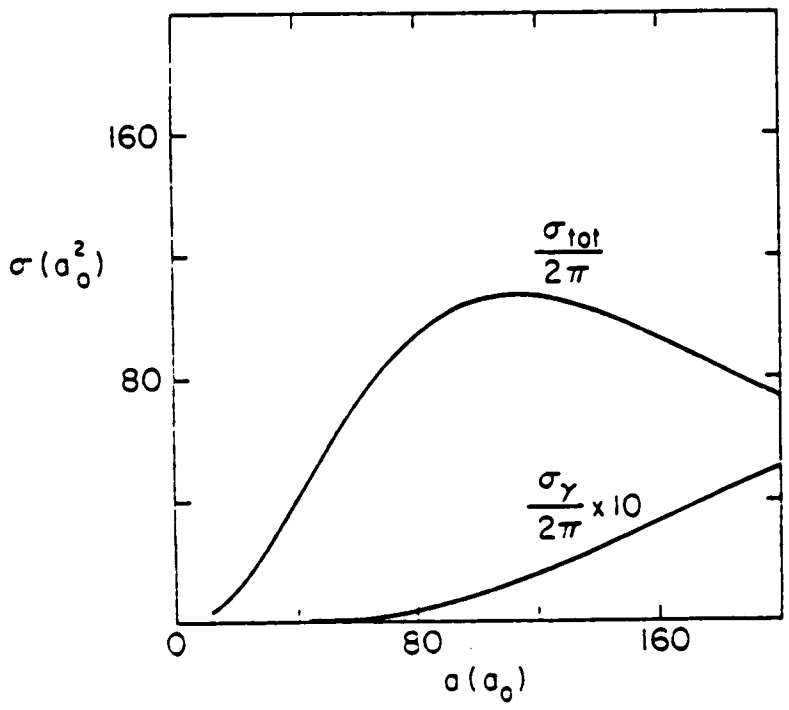
160
80
$\sigma(a_0^2)$
$\frac{\sigma_{tot}}{2\pi}$
$\frac{\sigma_\gamma}{2\pi} \times 10$
0
80
160
$a(a_0)$

Fig. III.9

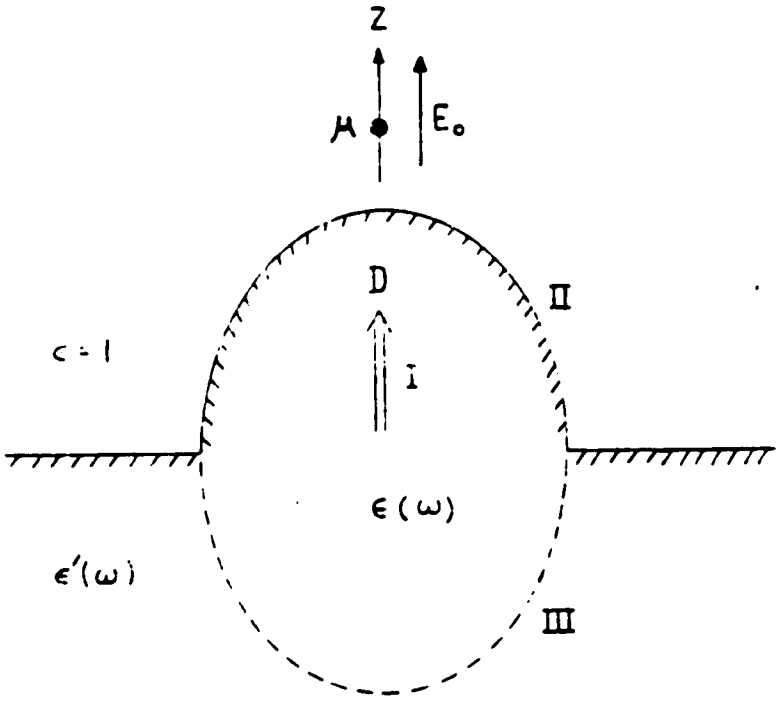

Fig.IV.1